UNCLASSIFIED

AD NUMBER
ADB024248
LIMITATION CHANGES
TO: **Approved for public release; distribution is unlimited.**
FROM: **Distribution authorized to U.S. Gov't. agencies only; Test and Evaluation; OCT 1977. Other requests shall be referred to Air Force Weapons Laboratory, Kirtland AFB, NM 87117.**
AUTHORITY
AFWL ltr, 7 Nov 1986

THIS PAGE IS UNCLASSIFIED

AD B024 248

AUTHORITY:
AFWL etc.,
7 NOV 86

AD-E200071

14 AFWL-TR-77-81

AFWL-TR-77-81

2

AD B024248

6

HAVE HOST CYLINDRICAL IN SITU TEST (CIST) DATA ANALYSIS AND MATERIAL MODEL REPORT.

9 Final Report,

10 Joseph H. Amend, III, Gilbert W. Ullrich, John M. Thomas

11 October 1977 12 108p.

Distribution limited to US Government agencies only because of test and evaluation of military systems (Oct 1977). Other requests for this document must be referred to AFWL (DES), Kirtland AFB, NM 87117.

This research was sponsored by the Defense Nuclear Agency under Subtask H35KAXSX355, Work Unit 14, MX Site Characterization.

18 SBIE 19 AD-E200071

Prepared for
Director
DEFENSE NUCLEAR AGENCY
Washington, DC 20305

and

SPACE AND MISSILE SYSTEMS ORGANIZATION
Los Angeles, CA 90009

AIR FORCE WEAPONS LABORATORY
Air Force Systems Command
Kirtland Air Force Base, NM 87117

AFWL-TR-77-81

This final report was prepared under Job Order WDMX0101 with the Air Force Weapons Laboratory, Kirtland Air Force Base, New Mexico. Captain Joseph H. Amend III (DES) was the Laboratory Project Officer-in-Charge.

This technical report has been reviewed and is approved for publication.

Joseph H. Amend III

JOSEPH H. AMEND III
Captain, USAF
Project Officer

GILBERT W. ULLRICH
Captain, USAF
Project Officer, Modeling & Analysis Br

John N Thomas

JOHN N. THOMAS
Project Officer
Modeling & Analysis Branch

Frank J. Leech

FRANK J. LEECH
Lt Colonel, USAF
Chief, Civil Engineering Research Division

FOR THE COMMANDER

Paul J. Daily

PAUL J. DAILY,
Colonel, USAF
Chief, Technology and Analysis Division

DO NOT RETURN THIS COPY. RETAIN OR DESTORY

UNCLASSIFIED

SECURITY CLASSIFICATION OF THIS PAGE (When Data Entered)

REPORT DOCUMENTATION PAGE

READ INSTRUCTIONS BEFORE COMPLETING FORM

1. REPORT NUMBER
AFWL-TR-77-81

2. GOVT ACCESSION NO.

3. RECIPIENT'S CATALOG NUMBER

4. TITLE (and Subtitle)
HAVE HOST CYLINDRICAL IN-SITU TEST (CIST) DATA ANALYSIS AND MATERIAL MODEL REPORT

5. TYPE OF REPORT & PERIOD COVERED
Final Report

6. PERFORMING ORG. REPORT NUMBER

7. AUTHOR(s)

Capt Joseph H. Amend, III
Capt Gilbert W. Ullrich
Mr John M. Thomas

8. CONTRACT OR GRANT NUMBER(s)
DNA-001-77-C-0037

9. PERFORMING ORGANIZATION NAME AND ADDRESS
Air Force Weapons Laboratory (DES)
Kirtland Air Force Base, NM 87117

10. PROGRAM ELEMENT, PROJECT, TASK AREA & WORK UNIT NUMBERS
62710H
WDMX0101

11. CONTROLLING OFFICE NAME AND ADDRESS
SAMSO
Los Angeles, CA 90009

Director
Defense Nuclear Agency
Washington. D.C. 20305

12. REPORT DATE
October 1977

13. NUMBER OF PAGES
112

14. MONITORING AGENCY NAME & ADDRESS (if different from Controlling Office)
Air Force Weapons Laboratory (DES)
Kirtland Air Force Base, NM 87117

15. SECURITY CLASS. (of this report)
UNCLASSIFIED

15a. DECLASSIFICATION/DOWNGRADING SCHEDULE

16. DISTRIBUTION STATEMENT (of this Report)

Distribution limited to US Government agencies only because of test and evaluation (October 1977). Other requests for this document must be referred to AFWL (DES), Kirtland Air Force Base, NM 87117.

17. DISTRIBUTION STATEMENT (of the abstract entered in Block 20, if different from Report)

18. SUPPLEMENTARY NOTES

This report was sponsored by the Defense Nuclear Agency under RDT&E RMSS Code B3440 77464 H35HAXSX355-14 H259 OD.

19. KEY WORDS (Continue on reverse side if necessary and identify by block number)

HAVE HOST
CIST
Pretest Prediction
AFTON
Soil Cementation
Material Models

20. ABSTRACT (Continue on reverse side if necessary and identify by block number)

CIST 18, conducted at the HAVE HOST Test Site south or Wellton, Arizona, is documented. This documentation begins with a brief description of the fielding of the test event and culminates with the in-situ material models presently being used in the HAVE HOST pretest predictions. Analysis of the data is accomplished and leads to several conclusions on the effect that soil cementation has on the test results. Acceleration, velocity and displacement time histories are found in Appendix A, along with comparisons between the actual data and present material models contained in Appendix B.

DD FORM 1 JAN 73 1473 EDITION OF 1 NOV 65 IS OBSOLETE

UNCLASSIFIED

SECURITY CLASSIFICATION OF THIS PAGE (When Data Entered)

Conversion factors for U.S. customary to metric (SI) units of measurement.

(Symbols of SI units given in parentheses)

To convert from	to	Multiply by
angstrom	meters (m)	1.000 000 X E -10
atmosphere (normal)	kilo pascal (kPa)	1.013 25 X E +2
bar	kilo pascal (kPa)	1.000 000 X E +2
barn	meter^2 (m^2)	1.000 000 X E -28
British thermal unit (thermochemical)	joule (J)	1.054 350 X E +3
calorie (thermochemical)	joule (J)	4.184 000
cal (thermochemical)/cm^2	mega joule/m^2 (MJ/m^2)	4.184 000 X E -2
curie	giga becquerel (GBq)*	3.700 000 X E +1
degree (angle)	radian (rad)	1.745 329 X E -2
degree Fahrenheit	degree kelvin (K)	$t_K = (t° f + 459.67)/1.8$
electron volt	joule (J)	1.602 19 X E -19
erg	joule (J)	1.000 000 X E -7
erg/second	watt (W)	1.000 000 X E -7
foot	meter (m)	3.048 000 X E -1
foot-pound-force	joule (J)	1.355 818
gallon (U.S. liquid)	meter^3 (m^3)	3.785 412 X E -3
inch	meter (m)	2.540 000 X E -2
jerk	joule (J)	1.000 000 X E +9
joule/kilogram (J/kg) (radiation dose absorbed)	Gray (Gy)**	1.000 000
kilotons	terajoules	4.183
kip (1000 lbf)	newton (N)	4.448 222 X E +3
kip/inch^2 (ksi)	kilo pascal (kPa)	6.894 757 X E +3
ktap	newton-second/m^2 (N-s/m^2)	1.000 000 X E +2
micron	meter (m)	1.000 000 X E -6
mil	meter (m)	2.540 000 X E -5
mile (international)	meter (m)	1.609 344 X E +3
ounce	kilogram (kg)	2.834 952 X E -2
pound-force (lbf avoirdupois)	newton (N)	4.448 222
pound-force inch	newton-meter (N•m)	1.129 848 X E -1
pound-force/inch	newton/meter (N/m)	1.751 268 X E +2
pound-force/foot^2	kilo pascal (kPa)	4.788 026 X E -2

Conversion factors for U.S. customary to metric (SI) units of measurement. (Continued)

(Symbols of SI units given in parentheses)

To convert from	to	Multiply by
pound-force/inch^2 (psi)	kilo pascal (kPa)	6.894 757
pound-mass (lbm avoirdupois)	kilogram (kg)	4.535 924 X E -1
pound-mass-foot^2 (moment of inertia)	kilogram-meter^2 (kg·m^2)	4.214 011 X E -2
pound-mass/foot^3	kilogram/meter^3 (kg/m^3)	1.601 846 X E +1
rad (radiation dose absorbed)	Gray (Gy)**	1.000 000 X E -2
roentgen	coulomb/kilogram (C/kg)	2.579 760 X E -4
shake	second (s)	1.000 000 X E -8
slug	kilogram (kg)	1.459 390 X E +1
torr (mm Hg, 0° C)	kilo pascal (kPa)	1.333 22 X E -1

*The becquerel (Bq) is the SI unit of radioactivity; 1 Bq = 1 event/s.

**The Gray (Gy) is the SI unit of absorbed radiation.

A more complete listing of conversions may be found in "Metric Practice Guide E 380-74," American Society for Testing and Materials.

TABLE OF CONTENTS

LIST OF ILLUSTRATIONS

LIST OF ILLUSTRATIONS (Continued)

LIST OF TABLES

SECTION 1
INTRODUCTION

The purpose of the Cylindrical In-Situ Test (CIST), developed in 1971, is to measure the dynamic response of geologic materials to a cylindrically symmetric high explosive shock input. This in-situ material properties test was developed at the Air Force Weapons Laboratory (AFWL) to eliminate some of the shortcomings inherent in the material sampling/laboratory testing approach to material property determination. A vertical cylindrical load geometry is used because of its unique capability for simultaneous loading of a number of near-surface horizontal layers. Resulting data are then used to determine the in-situ material properties of each layer.

In the past few years, extensive theoretical and experimental programs have been undertaken in an effort to quantify the response of strategic structures, sited in widely varying geologies, to various airblast and ground shock loadings. Characterization of this response depends on an adequate mathematical model of the material surrounding the structure; therefore, a prime requirement for determining the response of strategic structures to nuclear and high explosives blast loadings is an understanding of the response of the surrounding geologic materials to impulsive-type loads.

In order to obtain this dynamic response information, the CIST 18 experiment was detonated on the HAVE HOST Test Site, located on Luke Air Force Range, on 22 October 1976 (HAVE HOST being the name of the AFWL/SAMSO/DNA test series to validate MX protective structure concepts). The material models derived from the CIST data, along with laboratory data, will be used in the structural response and ground shock calculations for the HAVE HOST Test Series, and in the more general Multiple Aim Point ground shock prediction calculations.

In addition, the CIST 18 data yields important information concerning Multiple Aim Point geologies. Previous CISTs have been conducted on the Nevada Test Site (CISTs 5-7) (Ref. 1) and White Sands Missile Range (CISTs 15 and 16) (Ref. 2). These six CIST events provide valuable information on a wide range of materials that occur in the southwestern United States, ranging from saturated clays to dry sands to hard rock.

SECTION 2

TEST DESCRIPTION

The General Test Plan for the Cylindrical In-Situ Test (CIST), AFWL-TR-74-136 (Ref. 3), provides the general information on the fielding of CIST tests and, unless otherwise noted, no procedural deviations were made for CIST 18.

CIST 18 was located on the eastern boundary of the HAVE HOST Test Site (Figure 2.1), approximately 30 miles southeast of Yuma, Arizona, on the Luke Air Force Range. Figure 2.2 is a map of Arizona, giving the relative locations of Yuma and the HAVE HOST Test Site.

The major difference between the HAVE HOST CIST and previous CISTs is that two separate events, 18D and 18S, were detonated. The two CISTs were necessitated by the inability to find a single location that contained all the materials needed to characterize the HAVE HOST Test Site. These materials range from poorly to moderately cemented alluvium and highly jointed and fractured granite to highly jointed competent granite.

CIST 18D (deep), for which geology and instrumentation plan is given in Figure 2.3, was the original site, but inspection of the undisturbed samples indicated a lack of the poorly cemented surface material prevalent over much of the HAVE HOST Test Site. CIST 18S (shallow), shown in Figure 2.4, was located 150 feet northwest of 18D in a drainage channel where an abundance of poorly cemented alluvial material existed. A profile of the subsurface, interpreted from a refraction survey, on a line between the two CIST ground zeroes (GZ) is shown in Figure 2.5.

2.1 SITE GEOLOGY

The CIST 18 experiment was originally designed to test two different materials--a hard, jointed granite bedrock and a dry alluvium formed from the mechanical decomposition of the granite. Inspection of the undisturbed samples at the 18D GZ revealed three different types of silty sandy alluvium and two different types of granite.

The silty sand is present over the granite throughout the entire HAVE HOST Test Site, except where the granite outcrops. The only apparent physical difference in the alluvium is the amount of cementation present, and there is no

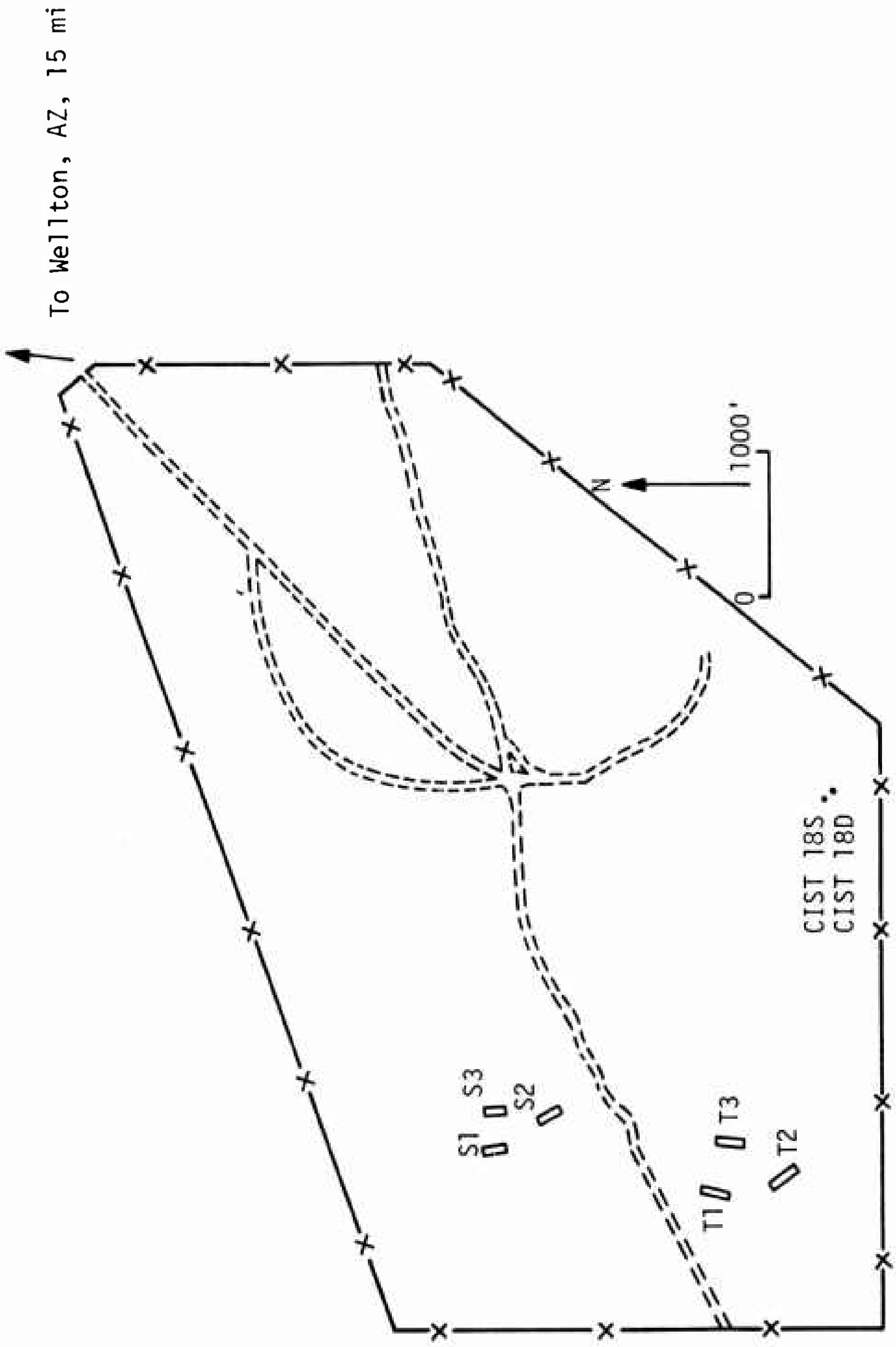

Figure 2.1. HAVE HOST test site.

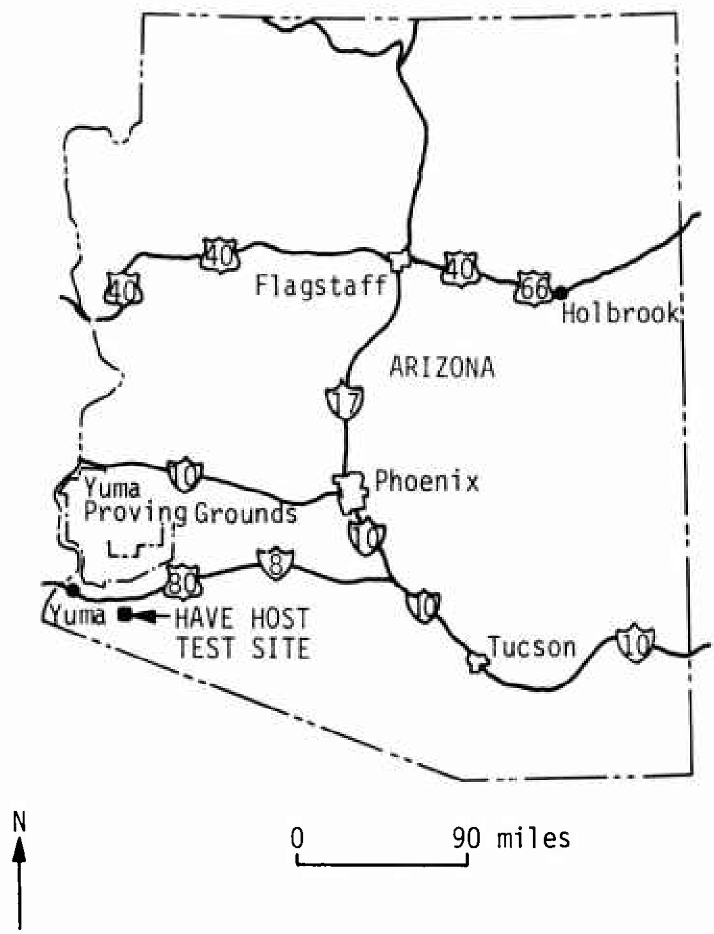

Figure 2.2. Arizona map with HAVE HOST test site located.

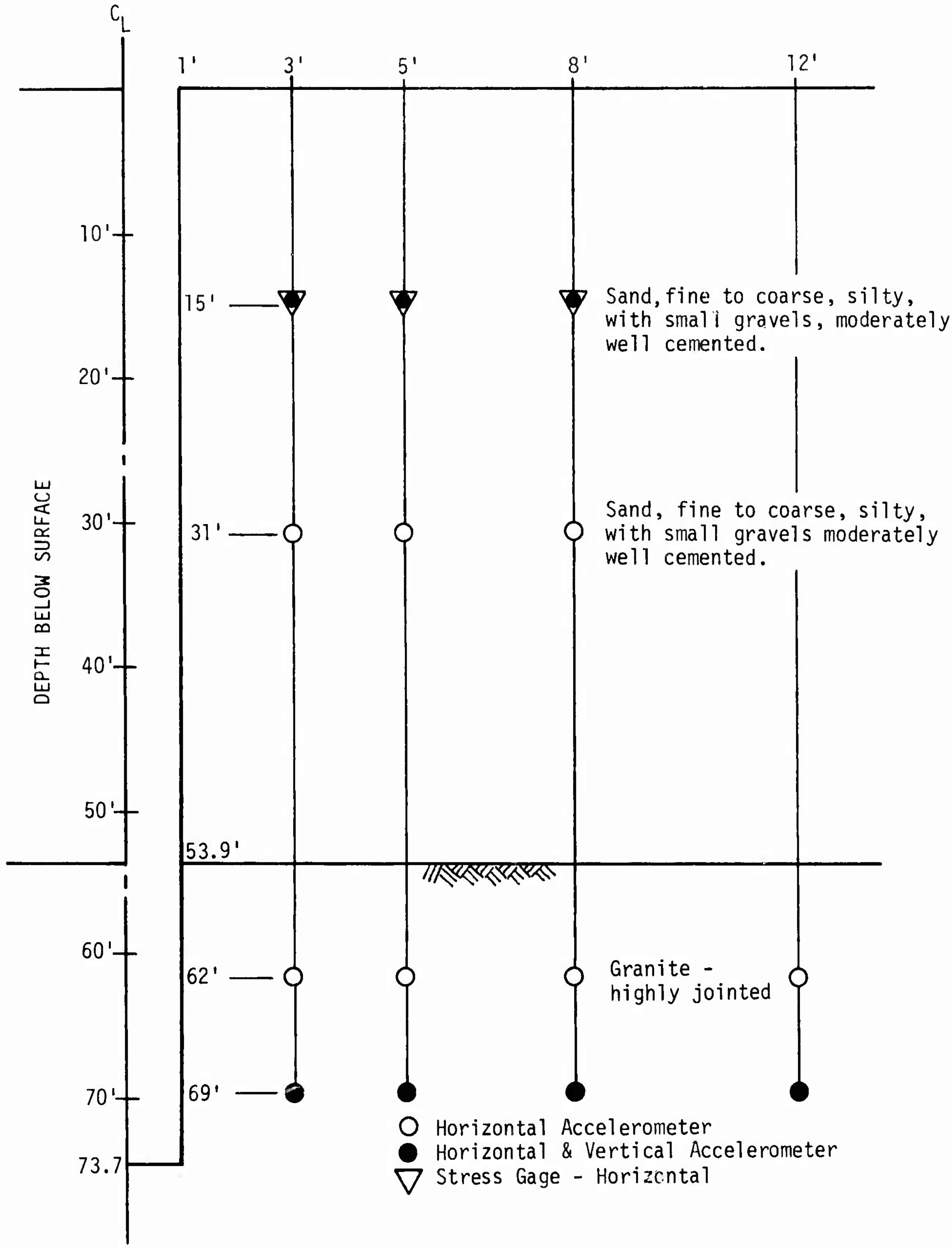

Figure 2.3. CIST 18D generalized geology and instrumentation plan.

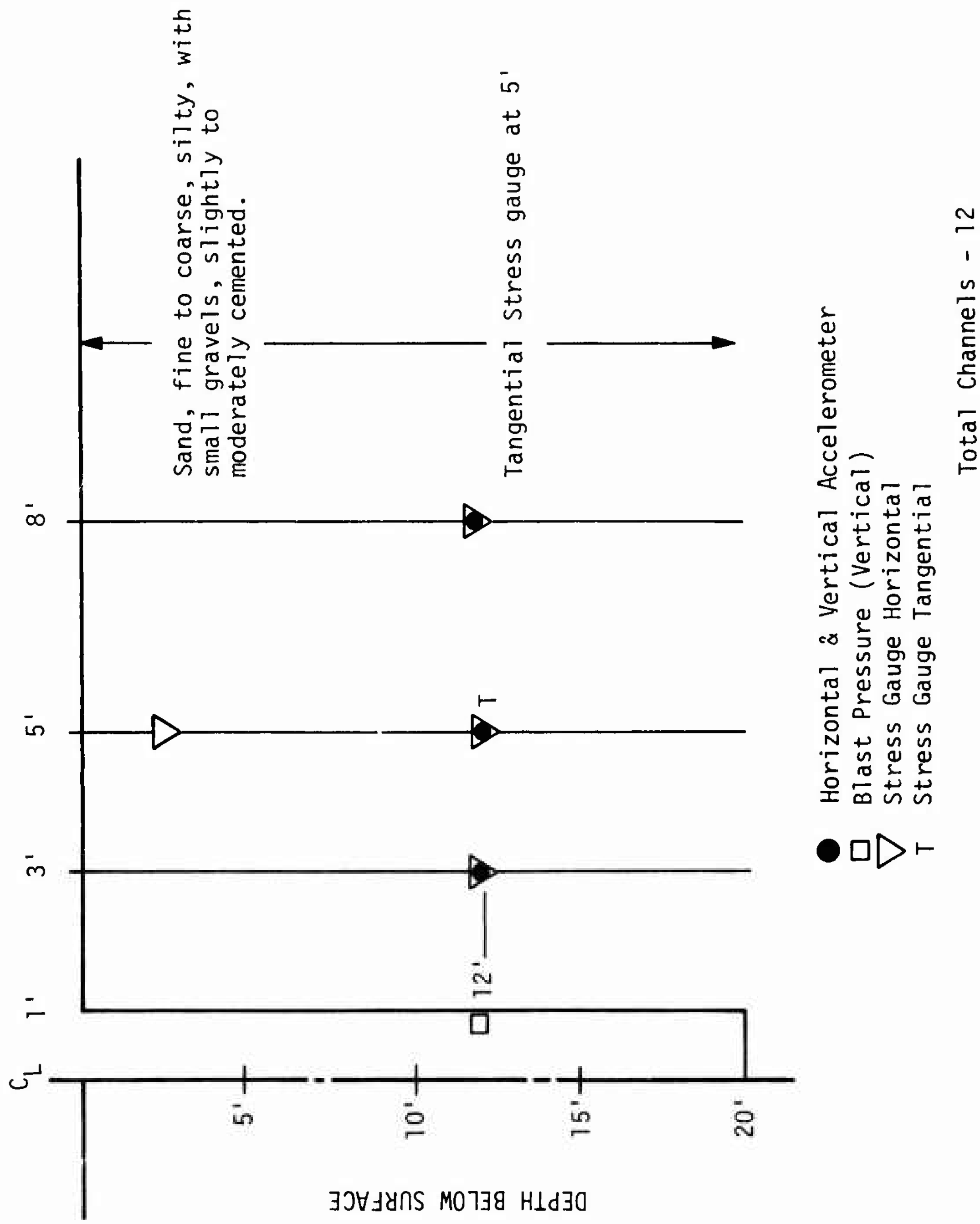

Figure 2.4. CIST 18S generalized geology and instrumentation plan.

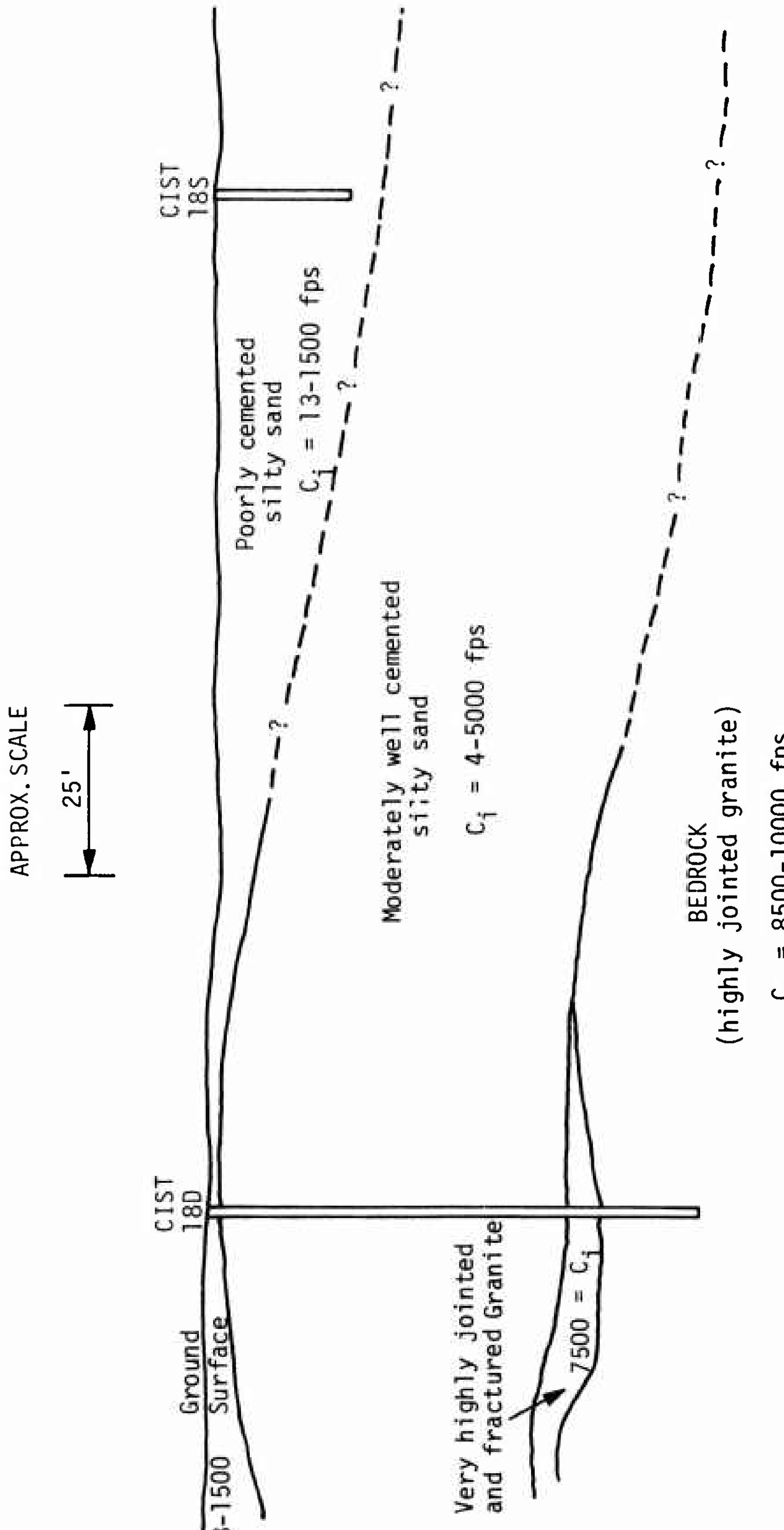

Figure 2.5. Geology cross section between CIST GZs.

trend of increasing cementation with depth. There is some evidence that the degree of cementation is reduced as the grain size of the alluvium increases.

The alluvium was logged as "sand, fine to coarse, silty with small pebbles." The pebbles were almost exclusively weathered granite. Once the alluvium had been disturbed, it was impossible to visually determine the depth or the location at which the sample originated. In general, three materials were found to exist; a slightly to moderately, moderately, and moderately to well cemented alluvium. For the purposes of this report, slightly cemented is defined as easily broken apart with the hands. Moderately cemented is defined as broken apart with the hands with some difficulty, and well cemented is defined as impossible to break apart with hands or broken apart with hands with great difficulty. One of the major purposes of CIST 18 was to determine the effect of these varying degrees of cementation on the material response.

In the 18D explosive hole, the soil extended to the granite bedrock at a depth of 53.9 feet, and the transition zone between the alluvium and the granite was very pronounced and easily identifiable. The granite was competent and highly jointed with a prominent north-south joint trend. The jointing was evident in the granite outcrop 100 meters east of the test site where the joint spacing was less then 3 inches. This close joint spacing caused difficulties in obtaining undisturbed rock cores. At certain depths in the granite, the method of coring (Longyear NQ wireline core barrel) pulverized the material so badly that samples longer that 1-1/2 inches were rare.

Inspection of the intact cores revealed numerous joints that were healed well enough so as not to separate on sampling. The difference in obtaining intact and fractured cores appeared to be the strength of the joint cementation. This observation also leads to the two different types of granite tested--highly fractured weakly cemented, and less-fractured stronger-cemented. As with the alluvium, no trend of increasing competency with depth was found, although this result is to be expected.

2.2 CIST 18D

The 18D explosive cavity was drilled to a depth of 73.7 feet. The hole was cased with a 24 inch steel culvert down to the alluvium/rock interface at 53.9 feet. A 22 inch explosive cavity was then drilled to 73.7 feet. The charge density of 5 pounds of detonating cord/linear foot of cavity remained constant in both the rock and alluvium.

Except for a few feet of surface material, the entire soil profile down to rock was moderately well cemented. The gauges at the 15.0 feet level were placed in moderately to well cemented alluvium, and the gauges at the 31.0 feet level were placed in moderately cemented alluvium. The gauges at the 62.0 feet level were in the most competent material available (highly jointed, competent granite).

2.3 CIST 18S

The shallow explosive cavity was 20.0 feet deep and lined with a 24 inch steel culvert. Except for a 1/2-foot hard crust, the first 3 feet of material were cohesionless. When drilling instrumentation holes through this material, bulbous cavities 3 to 4 feet in diameter were formed under the surface crust. This necessitated casing the first 4 to 5 feet to prevent fall-in. After the explosive cavity was augered, the 24 inch steel culvert was grouted in. The materials below this loose surface deposit were noticeably less cemented than in 18D and were logged as slightly to moderately cemented.

2.4 INSTRUMENTATION

The standard instrumentation packages, accelerometer canisters and stress gauge paddles were used in both 18D and 18S. However, placement techniques were modified to be compatible with the geologic materials to be tested.

With the exception of the 18D undisturbed rock cores and the section of the explosive cavity that was in granite, all the holes were drilled dry. The instrument holes were bored using compressed air as the drilling fluid, and the part of the explosive cavities in alluvium were excavated using a bucket auger. This was done to prevent water intrusion into the walls of the hole which might alter normal in-situ moisture contents and, therefore, seriously affect the data.

The procedure used in the excavation of the explosive cavity was as follows: A 27 inch bucket auger was used to remove the alluvial material down to the granite bedrock. A 24 inch steel casing was then placed in the cavity and grouted in. After the grout had hardened, the section of the explosive cavity in the rock was drilled using a 22 inch rock bit and drilling mud. The 22 inch bit was chosen as the largest bit that could be fit inside the culvert.

Figures 2.6 and 2.7 give the plan views of the 18S and 18D instrument holes. Table 1 gives the "As-Built" measurement list.

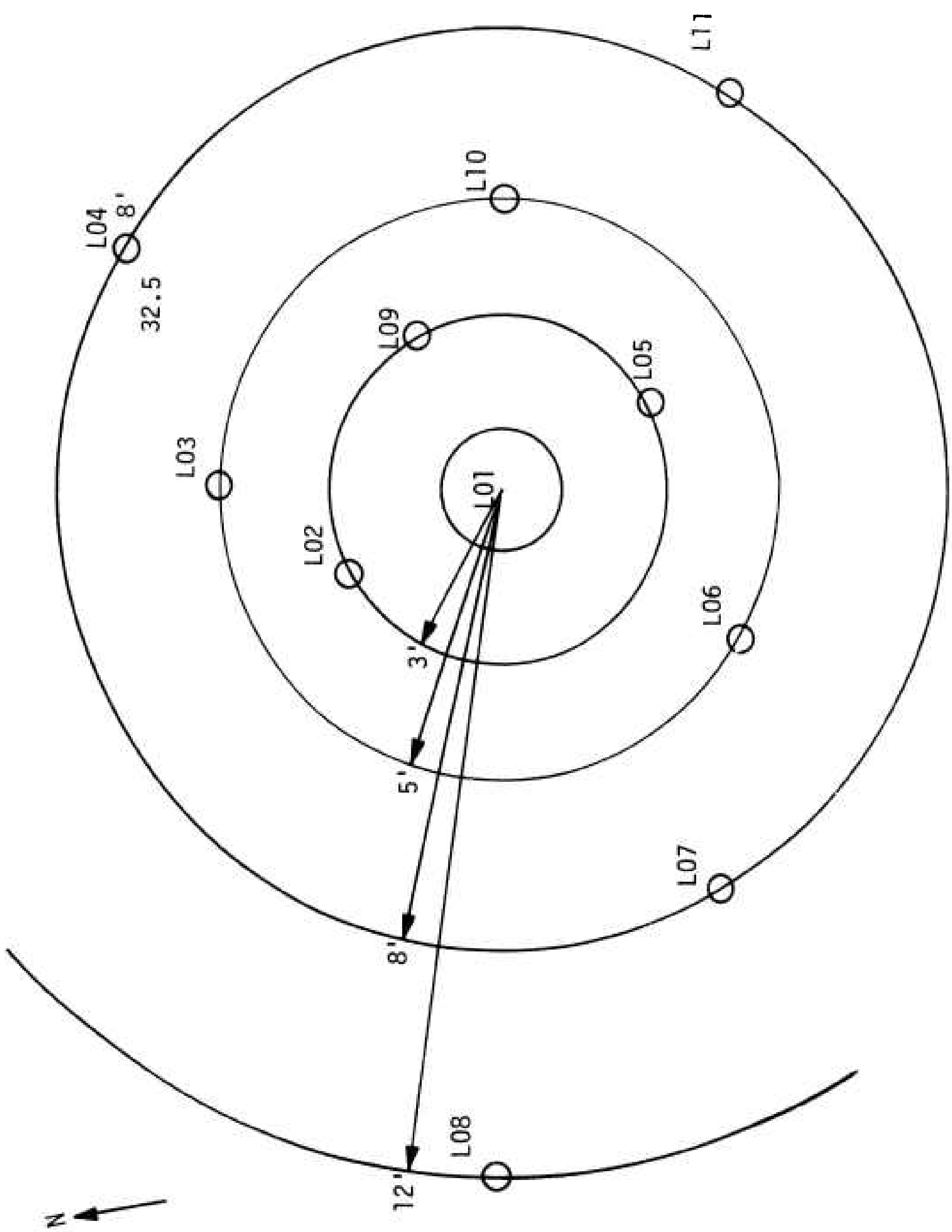

Figure 2.6. CIST 18D hole layout.

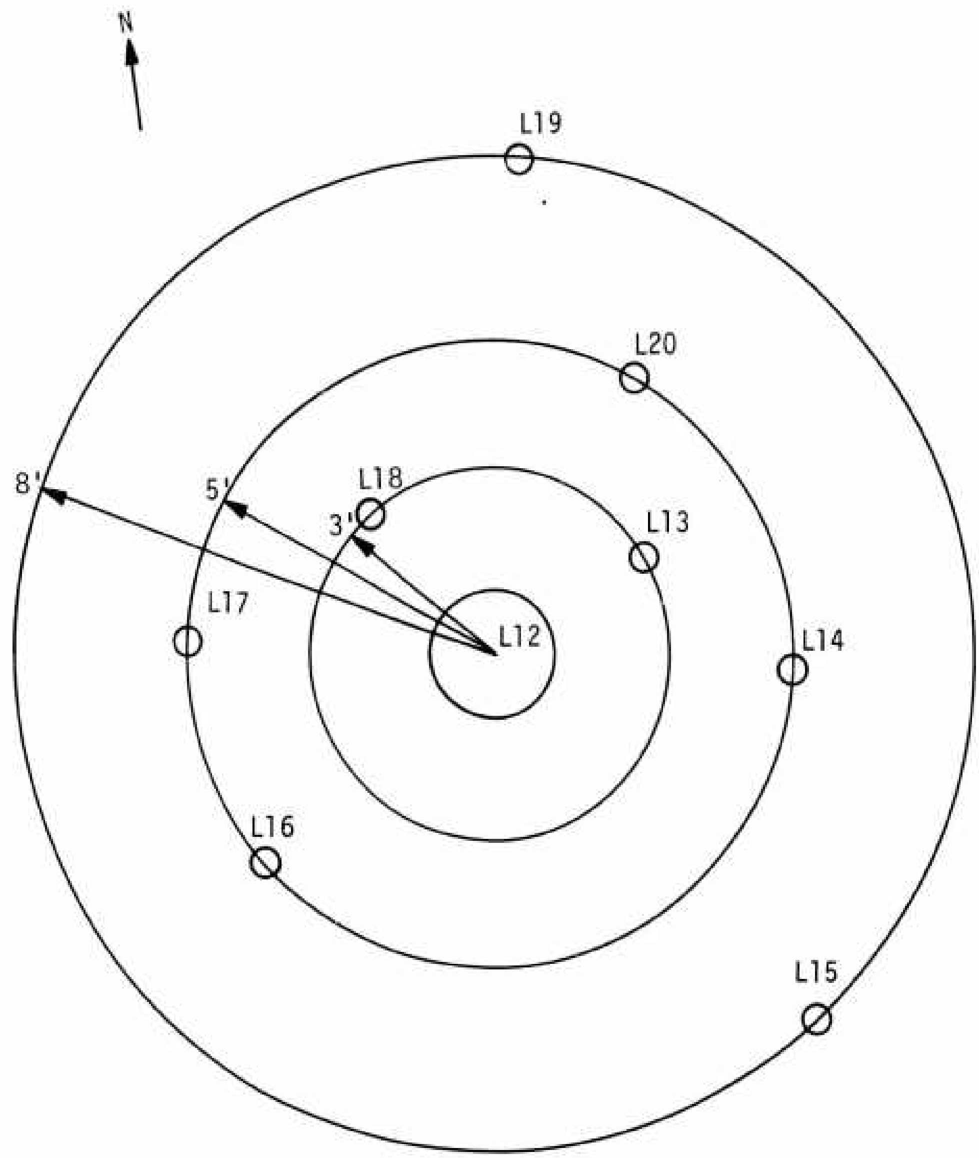

Figure 2.7. CIST 18S hole layout.

Table 2.1 CIST 18 Measurement List

Measurement Number	Measurement Designation	Gauge Range	Calibration
01	CIST-18S-F-E-L13-12.0-45-3.0-A-V	10,000 g's	2273.0 g's
02	CIST-18S-F-E-L13-12.0-45-3.0-A-H	10,000 g's	4936.9 g's
03	CIST-18S-F-E-L20-2.5-25-5.0-SE-H	2,000 psi	2934.6 psi
04	CIST-18S-F-E-L14-12.0-90-5.0-A-V	2,000 g's	697.2 g's
05	CIST-18S-F-E-L14-12.0-90-5.0-A-H	5,000 g's	1582.4 g's
06	CIST-18S-F-E-L17-12.0-270-5.0-SE-H	2,000 psi	1344.6 psi
07	CIST-18S-F-E-L15-12.0-135-8.0-A-V	2,000 g's	183.4 g's
08	CIST-18S-F-E-L15-12.0-135-8.0-A-H	2,000 g's	176.5 g's
09	CIST-18S-F-E-L19-12.0-0-8.0-SE-H	2,000 psi	384.6 psi
10	CIST-18D-F-E-L02-15.0-330-3.0-A-V	10,000 g's	2778.0 g's
11	CIST-18D-F-E-L02-15.0-330-3.0-A-H	10,000 g's	5014.8 g's
12	CIST-18D-F-E-L09-15.0-60-3.0-SE-H	2,000 psi	3046.6 psi
13	CIST-18D-F-E-L03-15.0-0-5.0-A-V	2,000 g's	711.8 g's
14	CIST-18D-F-E-L03-15.0-0-5.0-A-H	5,000 g's	1642.5 g's
15	CIST-18D-F-E-L10-15.0-90-5.0-SE-H	2,000 psi	1290.6 psi
16	CIST-18D-F-E-L04-15.0-30-8.0-A-V	2,000 g's	180.2 g's
17	CIST-18D-F-E-L04-15.0-30-8.0-A-H	2,000 g's	178.4 g's
18	CIST-18D-F-E-L11-15.0-120-8.0-SE-H	2,000 psi	408.9 psi
19	CIST-18S-F-E-L16-12.0-225-5.0-SE-T	2,000 psi	1259.1 psi
20	CIST-18S-F-E-L18-12.0-315-8.0-SE-H	2,000 psi	3006.3 psi
21	CIST-18D-F-E-L02-31.0-330-3.0-A-H	10,000 g's	4954.2 g's
22	CIST-18D-F-E-L05-62.0-150-3.0-A-H	30,000 g's	25259.6 g's
23	CIST-18D-F-E-L05-69.0-150-3.0-A-V	30,000 g's	11630.0 g's
24	CIST-18D-F-E-L05-69.0-150-3.0-A-H	30,000 g's	31111.1 g's
25	CIST-18D-F-E-L03-31.0-0-5.0-A-H	5,000 g's	1681.0 g's
26	CIST-18D-F-E-L06-62.0-210-5.0-A-H	10,000 g's	4822.0 g's
27	CIST-18D-F-E-L06-69.0-210-5.0-A-V	5,000 g's	2555.2 g's
28	CIST-18D-F-E-L06-69.0-210-5.0-A-H	20,000 g's	10330.0 g's
29	CIST-18D-F-E-L04-31.0-30-8.0-A-H	2,000 g's	177.4 g's
30	CIST-18D-F-E-L07-62.0-240-8.0-A-H	5,000 g's	1260.0 g's
31	CIST-18D-F-E-L07-69.0-240-8.0-A-V	2,000 g's	674.8 g's

Table 2.1 CIST 18 Measurement List (Continued)

Measurement Number	Measurement Designation	Gauge Range	Calibration
32	CIST-18D-F-E-L07-69.0-240-8.0-A-H	5,000 g's	2458.3 g's
33	CIST-18D-F-E-L08-62.0-270-12.0-A-H	2,000 g's	341.3 g's
34	CIST-18D-F-E-L08-69.0-270-12.0-A-V	2,000 g's	209.7 g's
35	CIST-18D-F-E-L08-69.0-270-12.0-A-H	2,000 g's	698.4 g's
36	CIST-18D-F-E-L12-12.0-0-1.0-CP-V	10,000 psi	9813.9 psi

All channels redundantly recorded, except for MN 10,16.

SECTION 3

DATA AND ANALYSIS

Figure 3.1 is a plot of peak horizontal particle acceleration versus range for all the CIST 18 alluvium layers (both 18S and 18D). From this plot, the expected material response due to cementation effects is not obvious. These values plot within the scatter of the CIST 5 (Area 10, NTS) alluvial data. The predictions for the alluvial response were based on the CIST 16 (Queen 15 Area WSMR) and were adequate.

A plot of maximum horizontal velocity versus range (Figure 3.2) shows virtually no difference in the peak velocities of the three layers. This result reinforces the previously stated observation: Cementation effects had a negligible effect on maximum values.

Figure 3.3 is a plot of all the dry, sandy alluvium CIST data. These data consist of CIST 5 (silty sands), CIST 16 (clayey, silty sands) and CIST 18 (silty sands). It is seen that the CISTs 5 and 18 peak velocity response is about the same, and the CIST 16 dry alluvium data can be used as an upper bound of all MAP dry, sandy alluvium data collected to date.

An evaluation of the "one-dimensionality" of the alluvium data is accomplished in a table of the ratio of peak vertical particle velocity to peak horizontal particle velocity for all depths and ranges in the CIST 18 experiment.

	3'	5'	8'
18D - 15' depth	0.093	0.123	0.018
18S - 12' depth	0.023	0.049	0.026

Because ratios are on the order of 0.1 or less, we feel that the material model development can be treated as a one-dimensional problem.

The actual rock response was about an order of magnitude below the pretest prediction, as shown in a plot of peak horizontal acceleration versus range for the jointed granite (Figure 3.4). This over-prediction is attributed to two factors; the conservative method of prediction and an underestimation of the in-situ jointing and fracture conditions of the granite. The conservative method of prediction was dictated because there were no hard rock CIST data prior to

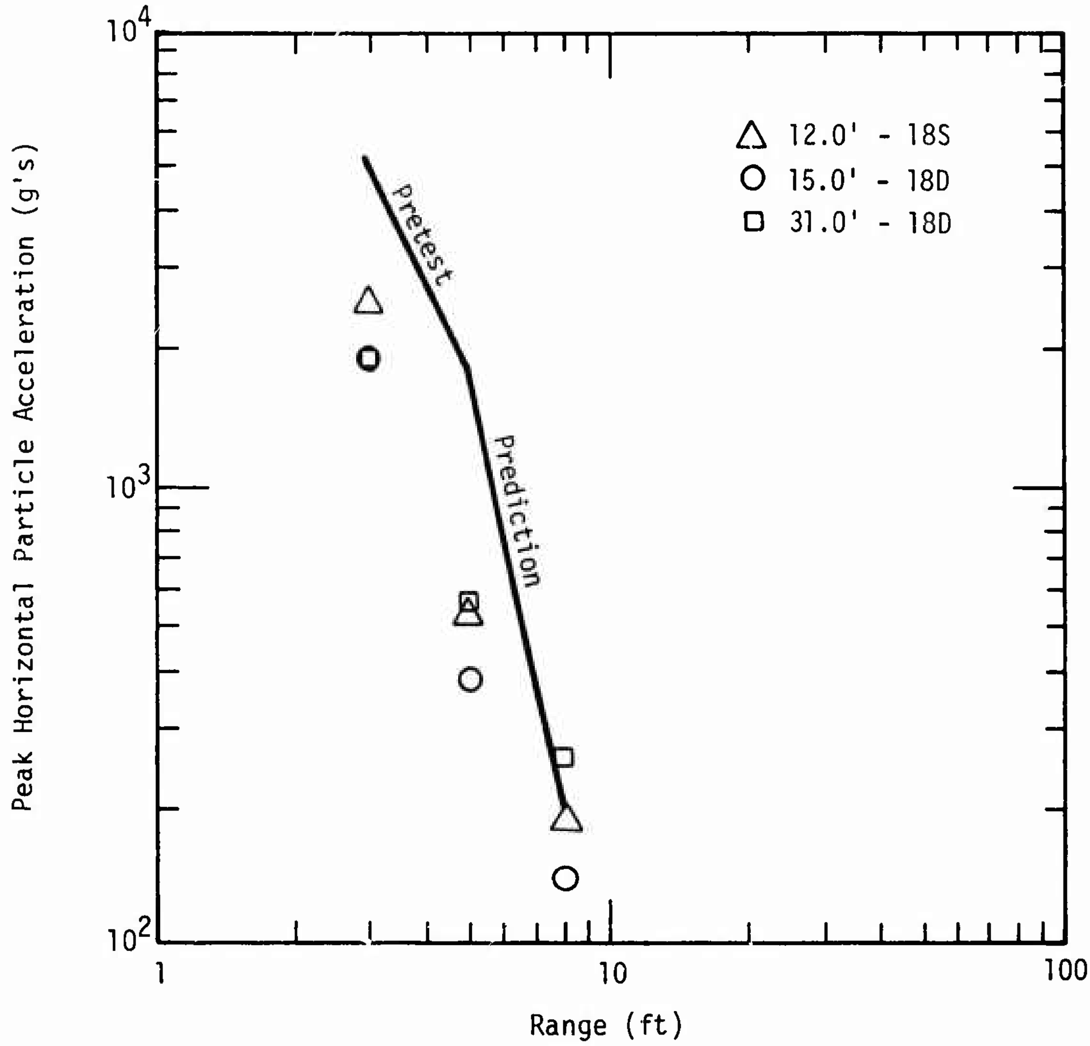

Figure 3.1. Plot of peak horizontal particle acceleration versus range for CIST 18 alluvium.

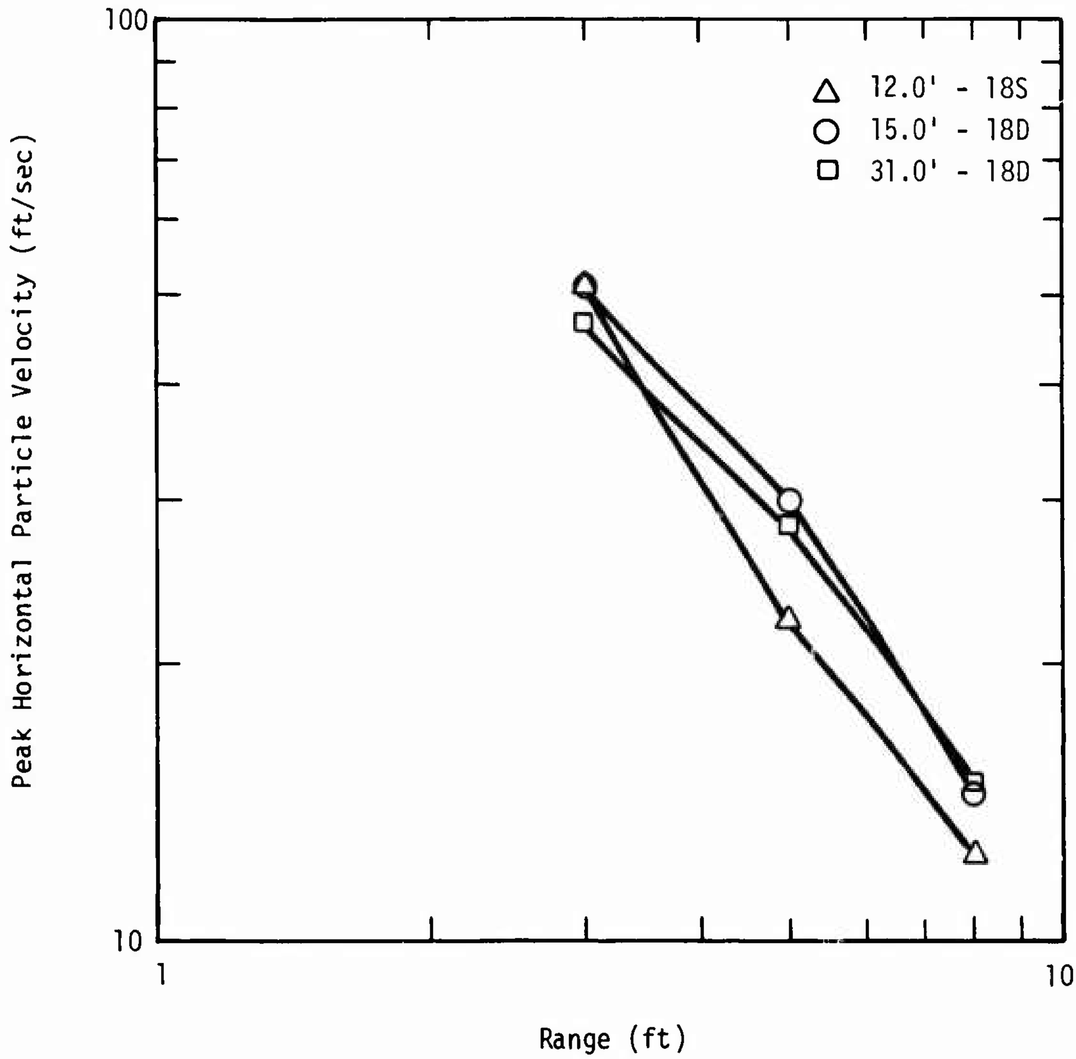

Figure 3.2. Plot of peak horizontal particle velocity versus range for CIST 18 alluvium.

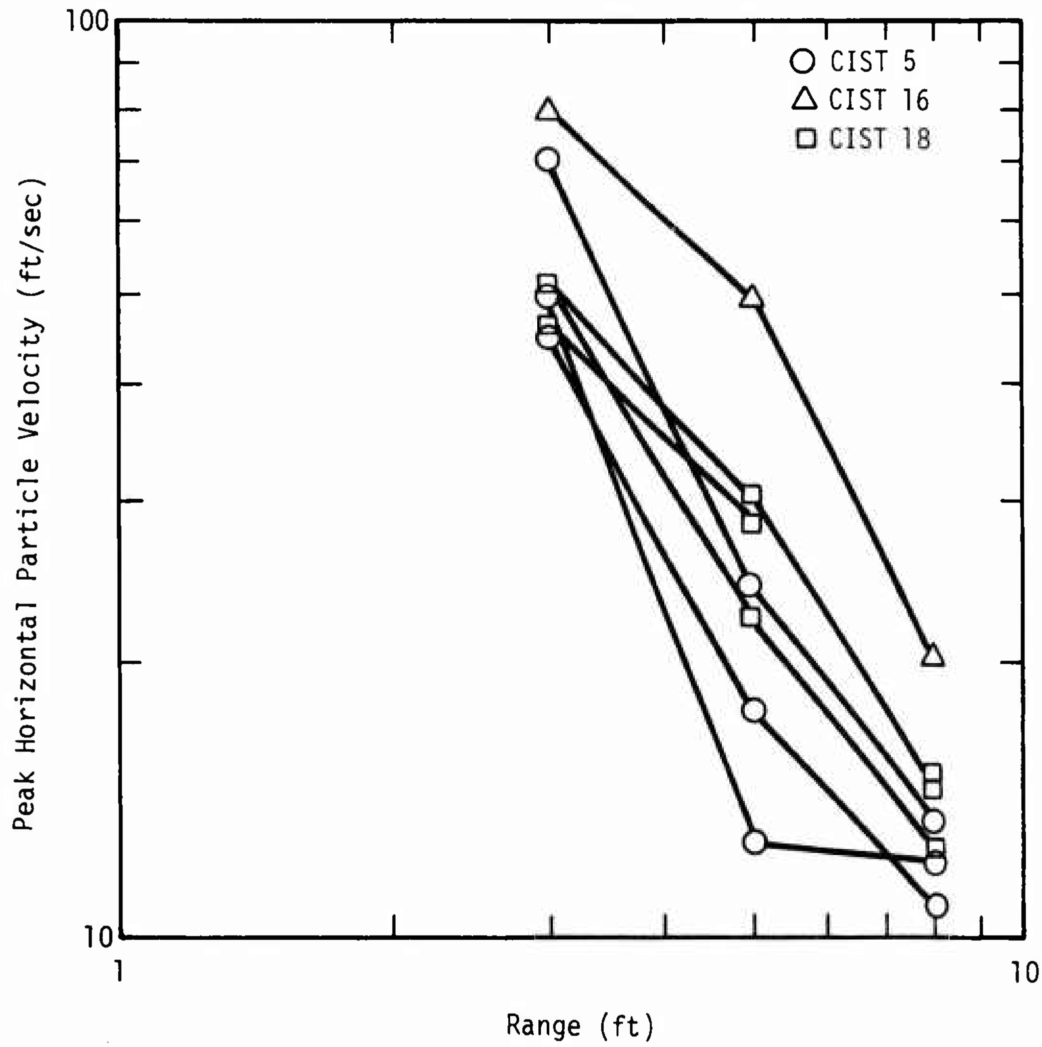

Figure 3.3. Plot of peak horizontal particle velocity versus range for MX sandy dry alluvium.

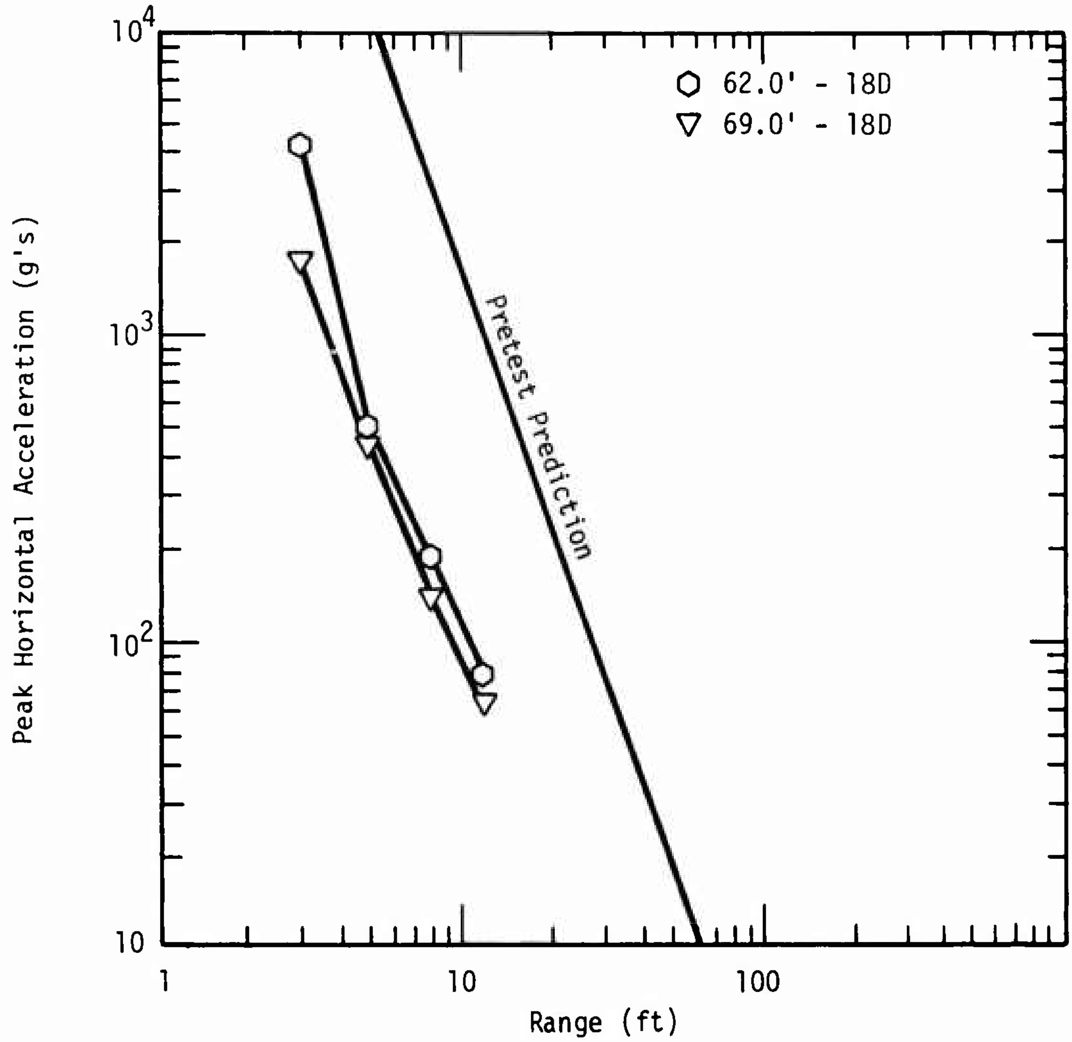

Figure 3.4. Plot of peak horizontal acceleration versus range for CIST 18 granite.

CIST 18, and such data were a primary goal of CIST 18. Consequently, to insure that data were obtained, the predictions were deliberately conservative. In addition, two different sets of gauge ranges were used in the two different rock layers and redundant recordings of all measurements were made. The granite response predictions were based on the DATEX II granite (Ref. 4) (Cedar City tonalite). The seismic velocity of this material is 11,000 feet/second, as compared to the 9,300 feet/second HAVE HOST granite. The matrix structure of the DATEX II granite is weaker that HAVE HOST; however, the DATEX II joint spacing is on the order of 1 to 3 feet, whereas, the HAVE HOST joint spacing is about 3 inches. In addition, the extensive fracturing that is common at HAVE HOST is absent at the DATEX test site, making the tonalite, in a macroscopic sense, much more competent than the HAVE HOST granite. The jointing and fracturing of the rock would tend to filter out high frequency response, as the CIST 18 granite data illustrate, and greatly increase the spatial attenuation that would occur. In addition, DATEX II was a plane wave simulation, and CIST tests are a cylindrical wave simulation making scaling from one to the other extremely difficult.

A plot of soil stress data versus range (Figure 3.5) indicates the anomalous nature of the soil stress measurements. Some of the gauges appear to have over registered. Possible causes are faulty placement techniques or the soil grain-gauge contact. With sandy materials, a nonuniform soil contact across the gauge face is possible. If this happens, very high point stresses could develop and make the gauge reading erroneous. As further evidence, the $\rho C_p V$ calculations assuming a density (ρ) of 115 pounds/feet^3 and loading wave speed (C_p) = 800 feet/second are a lower bound to the stress data. There were also instrumentation difficulties that have not been resolved, i.e., calibration levels of several of the 18S gauges that cast further doubt on the validity of the measurements. These problems have prompted the fielding of a Placement Evaluation Technique (PET) test in February 1977 at the HAVE HOST Test Site. Until the calibration problems are resolved and the PET test data analyzed, the stress data should be considered unusable or highly suspect.

The time of arrival (TOA) versus range are displayed in Figure 3.6. These data were computed from the first motion of the accelerometers. The seismic velocities of the alluvium layers are 2000, 3200 and 3500 feet/second for 18D, 15 feet; 18S, 12 feet; and 18D, 31 feet, respectively. It seems that the initial assumption of 18S being less cemented is not supported by the TOA data. The

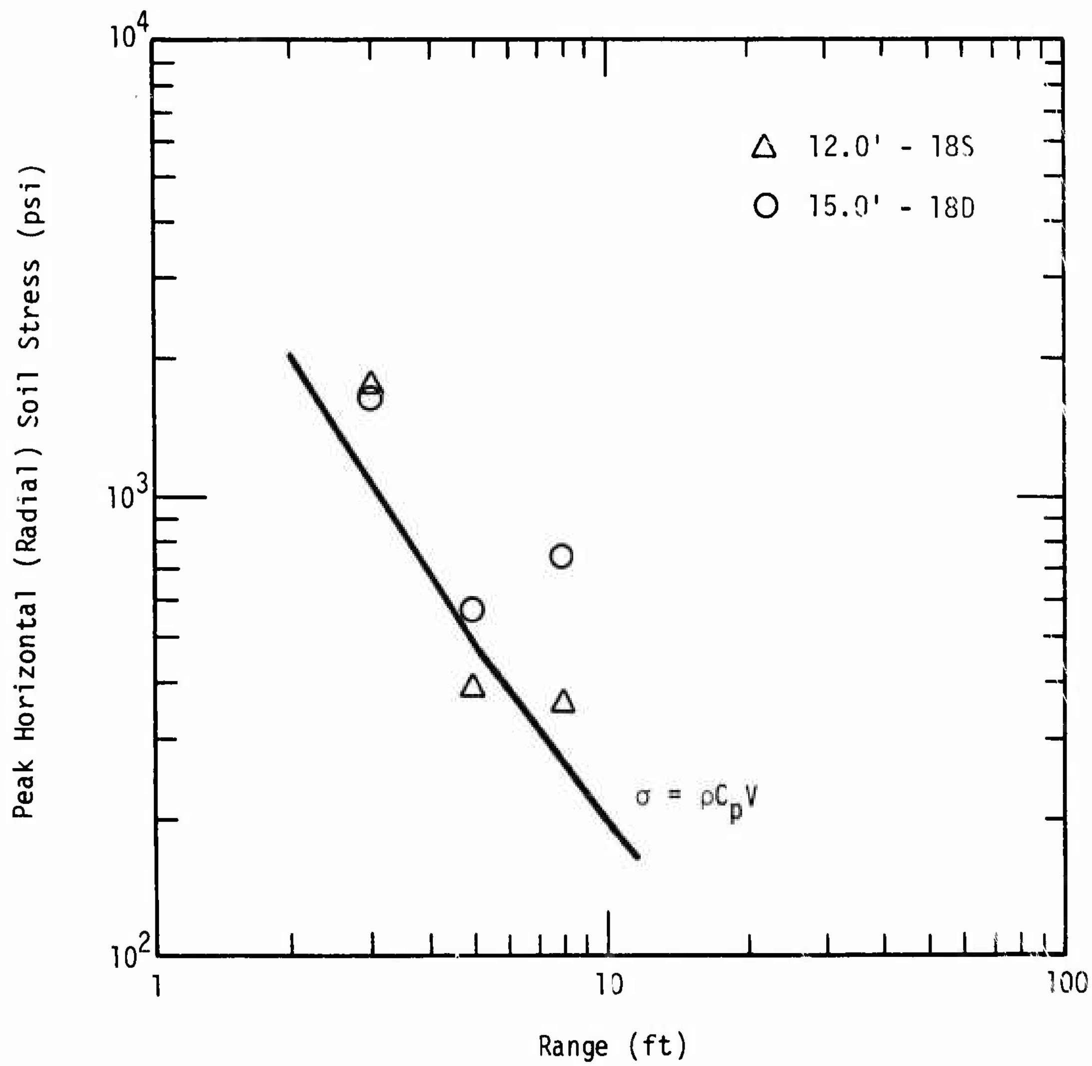

Figure 3.5. Plot of peak horizontal soil stress versus range for CIST 18 alluvium.

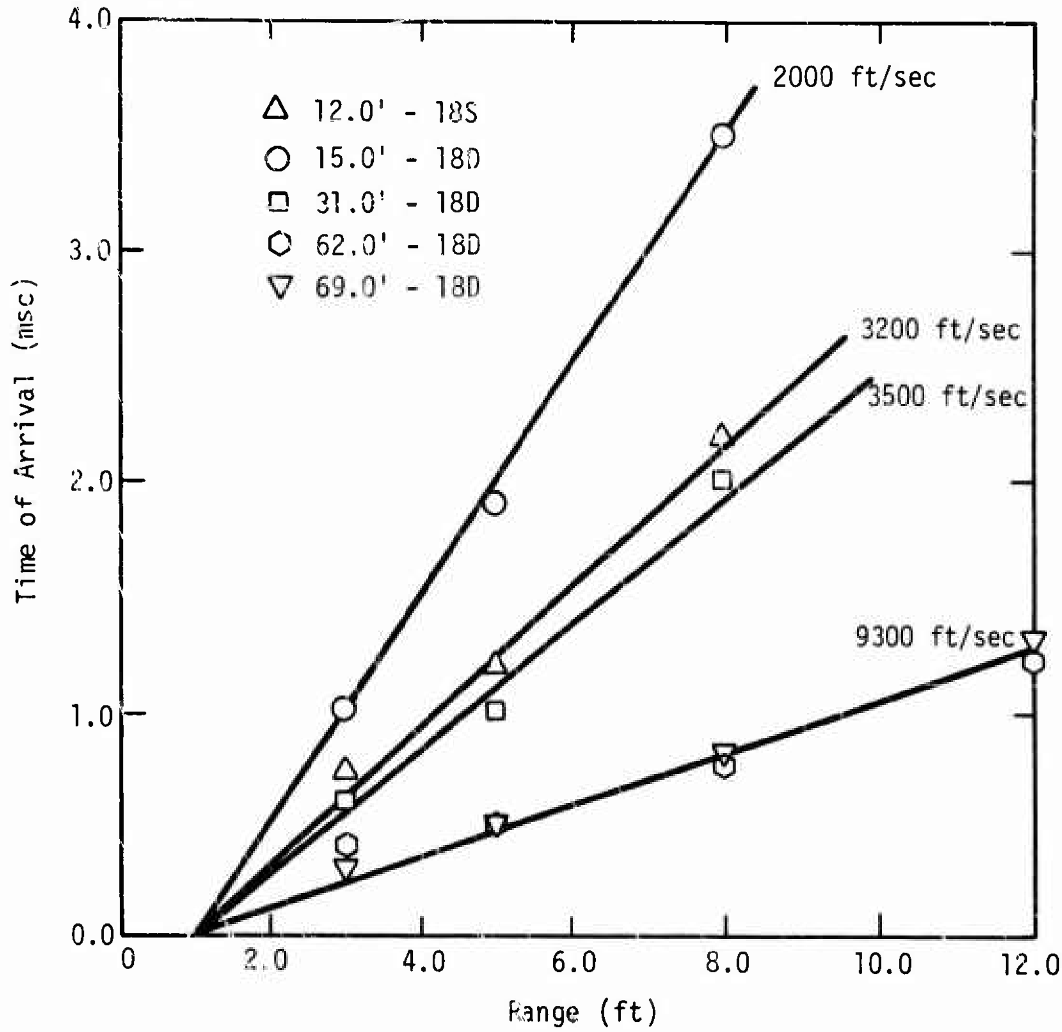

Figure 3.6. Plot of time of arrival versus range for CIST 18.

seismic velocity is a possible indication of the alluvial cementation, and it now appears logical to assume that the present surface water drainage channels at the HAVE HOST Test Site are not necessarily in the same position as they were in earlier geologic times when the subsurface materials were deposited.

It appears that soil cementation is a function of two distinct parameters; in-situ grain size and age of deposition. The controlling factor in the grain size appears to be the gradation of the fines (materials <0.076 mm particle diameter). More cementation is present when the fines are silty in nature, and less cementation is present when the sands are clean (i.e., very little silt). This observation is consistent with other areas and is probably due to the lower permeability of the silty sands causing slower ground water movement allowing more deposition of cement of the numerous grain contacts.

The effect of age of deposition is fairly obvious--the younger the material, the less cementation present. However, these two phenomena are interactive and are likely to be more complex than the simplistic discussion would indicate. The mechanics of soil cementation is not yet clearly understood, and the subject is still under investigation.

The seismic velocity of the granite, as determined from acceleration TOAs, is approximately 9300 feet/second. This value is in general agreement with the visual classification of the granite as highly jointed and fractured. This value for seismic velocity is also consistent with the results of the seismic refraction work conducted on the HAVE HOST Test Site.

A plot of the time to peak velocity versus distance (Figure 3.7) shows that the amount of cementation has little effect on the propagation velocity of the peak particle velocity (~ 800 feet/second). The 18S and 31.0 feet 18D loading wave velocities are identical; the 15.0 feet 18D velocities are noticeably slower. This reinforces the observation from Figures 3.5 and 3.6 that the maximum material response was not a function of the amount of cementation present in these alluvial materials. Preliminary grain size analysis (Ref. 5) indicates that the materials grade finer with depth. The 31.0 feet (18D) gauges were placed in 25 percent more fines that the 12.0 feet (18S) gauges. At this time, the effect of the grain size distribution on material response is not evident. This situation should clear up when more laboratory test data become available. Further analysis of the TOA and time to peak velocity data indicates the ratio of propagation velocity to seismic velocity, commonly assumed to be 1/2 as an initial guess, does not hold in this case. A ratio of 1/3 to 1/4 would be much

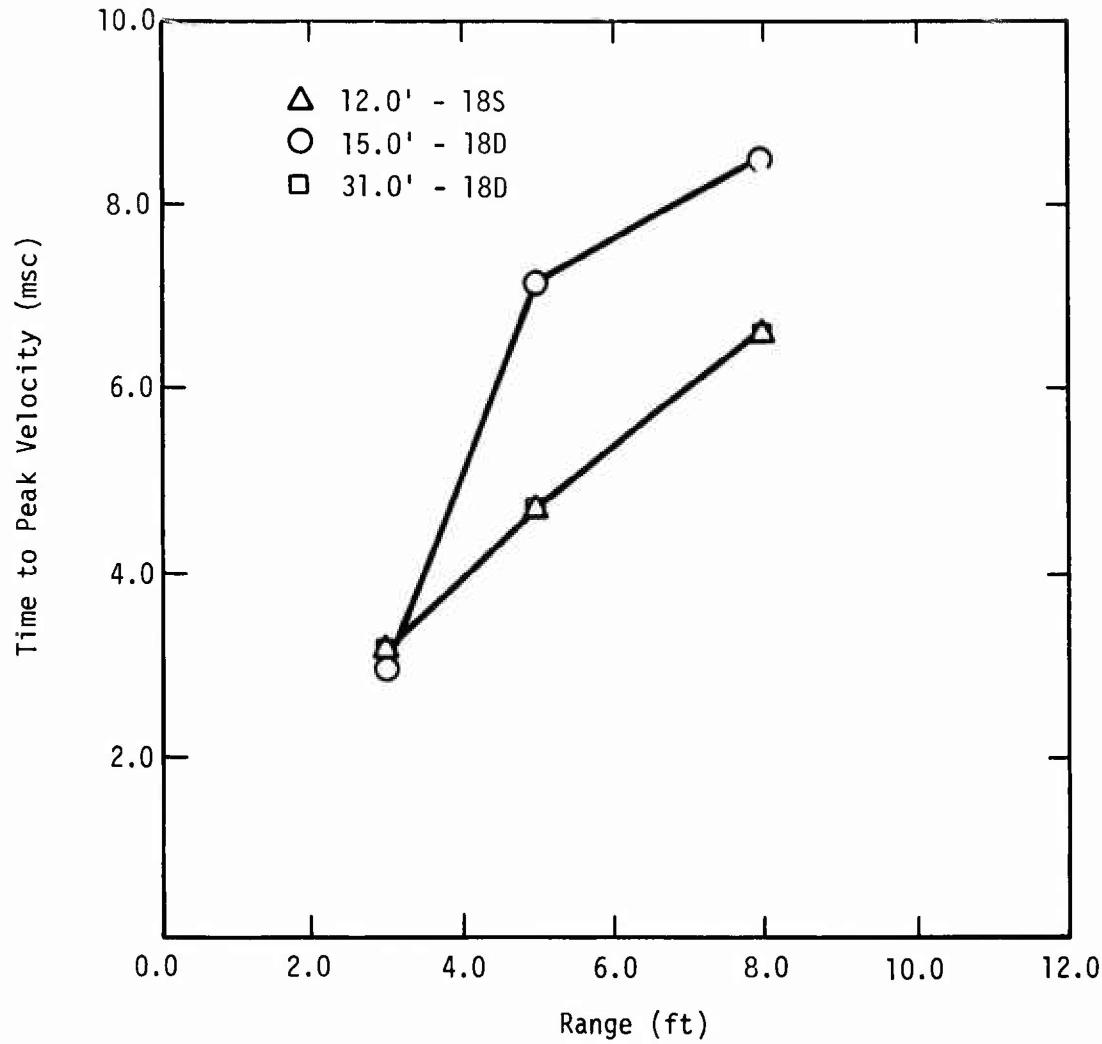

Figure 3.7. Time to peak velocity versus range for CIST 18 alluvium.

more accurate. This difference can noticeably affect ground motion predictions made for this material.

SECTION 4
MATERIAL MODEL DEVELOPMENT

The primary purpose of the CIST 18 experiment was to measure the dynamic response of in-situ materials for the development of parameters in material models that could be used in HAVE HOST and MAP calculational efforts. These models will serve as inputs for the ground shock and structural dynamics soil island calculations that will accompany the HAVE HOST field test.

We cannot overemphasize that material modeling is a continuing process, and the model presented in this report is one that is available at this time (January 1977). This model is by no means intended to be the final HAVE HOST model.

The model parameters were developed using AFTON (a 2-D finite difference code) and WONDY IV (a 1-D finite difference code). AFTON was used principally because of greater familiarity with the code and more flexibility of its use. WONDY IV was used in the parametric studies that were performed to determine the specific effect of individual parameter variations.

The discussion of the material model is divided into the hydrostatic component and the deviatoric models.

4.1 HYDROSTATIC MODEL

The hydrostatic model contains both density and energy components. First the density components are described and then the energy-dependent terms are added.

The pressure-density relation, Figure 4.1, is described as the function

$$P_H = f\ (\mu,\mu^*) \tag{1}$$

where $\mu = \frac{\rho-\rho_o}{\rho_o}$, ρ_o is the initial material density, and μ^* is the minimum of μ_3 (a material parameter) and the maximum μ experienced by the material. For μ greater than μ_3, the hydrostatic pressure is described by the relation

$$P_H = P_3+K_m(\mu-\mu_3) - (K_m-K_z)\mu s[1-A_e] \tag{2}$$

where $$A_e = \exp\ [-(\mu-\mu_3)/\mu s],$$

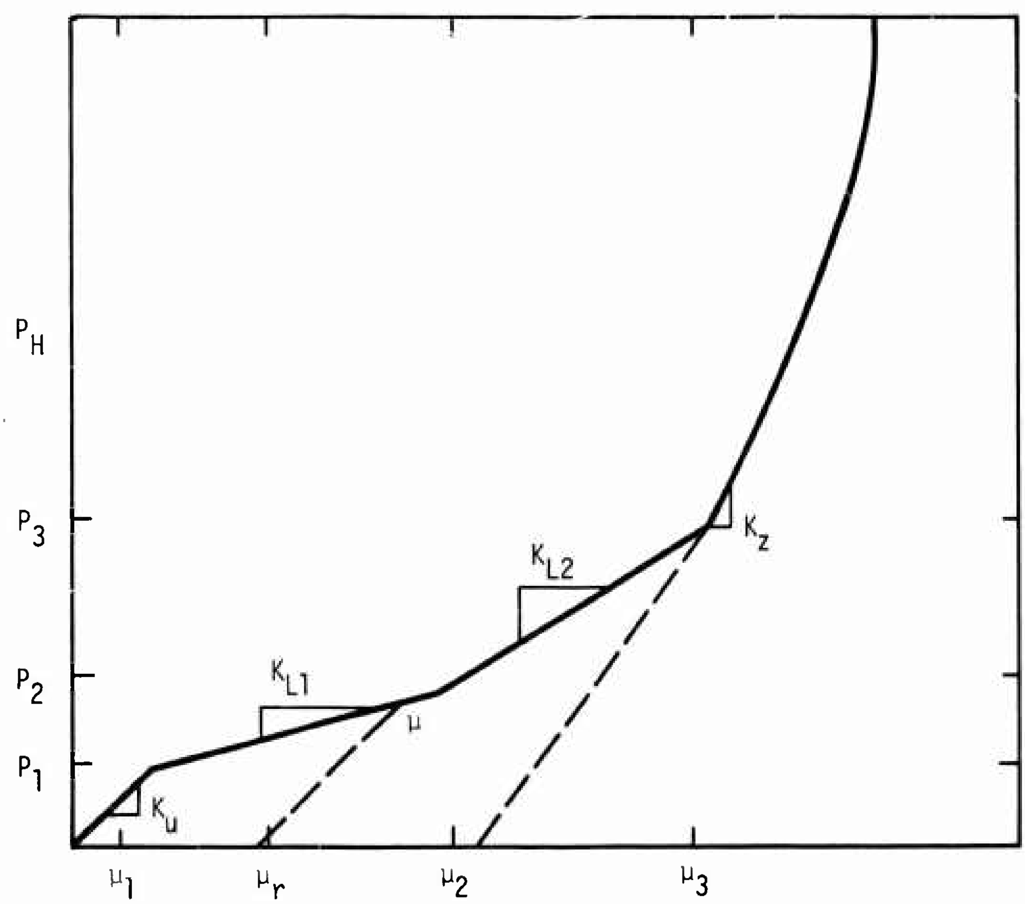

Figure 4.1. Schematic of the hydrostatic pressure-density relation.

P_3 is the hydrostatic pressure at μ_3,

$$K_z = C_z \cdot \frac{\rho_o}{3} \cdot \frac{(1+\nu_u)}{(1-\nu_u)} \tag{3}$$

and K_m, μ_s, C_z, and ν_u are material parameters. In particular, ν_u is the unloading Poisson's ratio. For the condition μ less than μ_3, the hydrostatic-pressure relations are divided into loading and unloading relations.

The loading relations are used when μ is greater than or equal to μ^* and are defined by three relations. For $\mu \leq \mu_1$, the relation is

$$P_H = K_u \mu \tag{4}$$

where

$$K_u = C_u^2 \cdot \frac{\rho_o}{3} \cdot \frac{1+\nu_u}{1-\nu_u} \tag{5}$$

$$\mu_1 = P_1/K_u$$

with P_1 and C_u material parameters. In particular C_u is the seismic velocity. For $\mu_1 < \mu \leq \mu_2$, the relation is

$$P_H = P_1 + K_{L_1}(\mu - \mu_1) \tag{6}$$

where

$$K_{L_1} = C_{L_1}^2 \cdot \frac{\rho_o}{3} \cdot \frac{1+\nu_L}{1-\nu_L} \tag{7}$$

$$\mu_2 = \mu_1 + (P_2 - P_1)/K_{L_1}$$

with P_2, C_{L_1}, and ν_L material parameters. In particular, ν_L is the loading Poisson's ratio. For $\mu_2 < \mu \leq \mu_3$, the relation is

$$P_H = P_2 + K_{L_2}(\mu - \mu_2) \tag{8}$$

where

$$K_{L_2} = C_{L_2}^2 \cdot \frac{\rho_o}{3} \cdot \frac{1+\nu_L}{1-\nu_L}$$

with C_{L2} a material parameter.

The unloading relation is used when μ is less than μ^*. The relation is defined as a function of the hydrostatic pressure, P_{HL}, calculated by substituting μ^* for μ in relations (4), (6), or (8), and the value of μ. The relation is

$$P_H = P_{HL} - K_u(\mu^* - \mu) \tag{9}$$

for

$$\mu_r \leq \mu < \mu^*$$

where

$$\mu_r = (K_u\mu^* - P_{HL})/K_u \tag{10}$$

For

$$\mu < \mu_r,\ P_H \text{ is max} \begin{Bmatrix} K_u\ (\mu-\mu_r) \\ -L_H + T_1 - (T_2 - T_1) \cdot F_f \end{Bmatrix}$$

where L_H is the local lithostatic load and T_1, T_2 and F_f are defined in Sect. 4.2.

Two energy-dependent expressions are used, depending on the relation of μ to μ_r. For $\mu \geq \mu_r$, the relation is

$$P = P_H + \Gamma\rho e \tag{11}$$

where

$$\Gamma = A + \frac{B}{\frac{e}{\eta^2 e_o} + 1}$$

$$\eta = \frac{\rho}{\rho_o}$$

e is the specific internal energy and A, B, and e_o are material parameters. For $\mu < \mu_r$, the relation is

$$P = \rho\gamma' e' + P_H \tag{12}$$

$$\rho = \rho_o(\mu + 1)$$

$$\rho_r = \rho_o(\mu_r + 1)$$

$$\eta_r = \rho/\rho_r$$

$$\gamma' = A + (\Gamma - A)(\eta_r)^{1/2}$$

$$e' = e - e_s\,[1 - \exp\,(\phi)]$$

$$\phi = N\,(1 - 1/\eta_r)/\eta_r$$

$$N = \frac{K_u}{\rho_r \Gamma e_s}$$

with e_s a material parameter.

4.2 DEVIATORIC STRESS MODEL

The deviatoric-stress relations are calculated using an elastic-plastic analysis with a nonassociative flow rule for alluvium and an associative flow rule for rock. The shear modulus, G, is calculated by the relation

$$G = \min\,(K \cdot \Delta, G_m) \tag{13}$$

where

$$G_m = K_z \cdot \frac{3}{2} \cdot \frac{(1-2\nu_u)}{(1+\nu_u)}$$

K is the appropriate K for the loading condition and

$$\Delta = \begin{cases} \dfrac{3}{2}\,\dfrac{1-2\nu_L}{1+\nu_L} & \text{for } \mu \geq \mu^* \\[2ex] \dfrac{3}{2}\,\dfrac{1-2\nu_u}{1+\nu_u} & \text{for } \mu < \mu^* \end{cases}$$

The yield conditions, Figure 4.2, are functions of both total hydrostatic pressure, with compressive-stress positive, and specific energy. The two yield relations are expressed as follows:

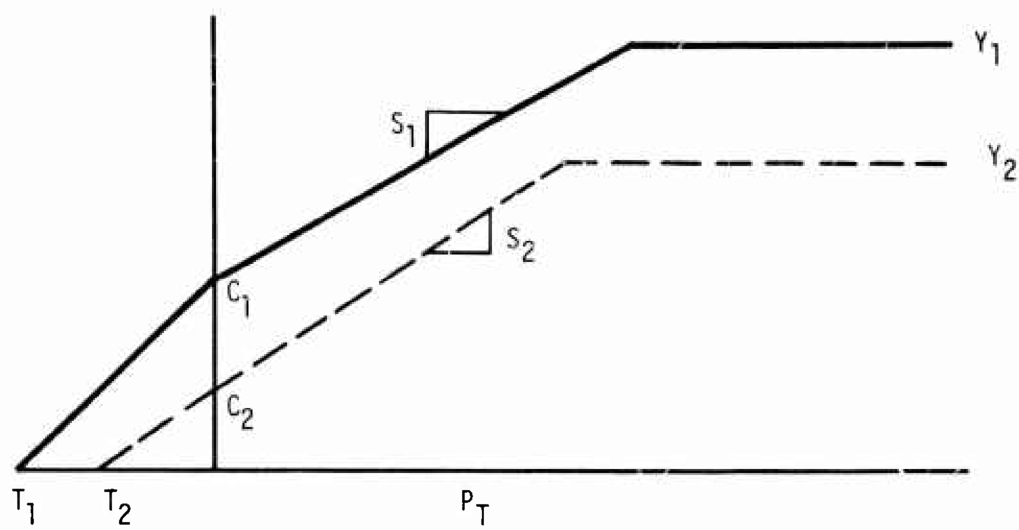

Figure 4.2. Schematic of the yield condition versus pressure relation.

$$Y_i' = \begin{cases} \max\ [o, C_i\ (1 - \frac{Pi}{Ti})]\ \text{for}\ P_T < 0 \\ \min\ [C_i + S_i P_T,\ Y_i]\ \ \text{for}\ P_T \geq 0 \end{cases} \quad (14)$$

where $P_T = P + L_H$

and i = 1 is the initial yield-condition, i = 2 is the residual yield-condition, and T_i, C_i, S_i, and Y_i are material parameters. The nonenergy-dependent yield relation for any zone is then calculated with

$$Y' = Y_1' + (Y_2' - Y_1') .\ F_f \quad (15)$$

where $$F_f = \min\ (0.04\ N_f,\ 1)$$

and N_f is the number of calculational cycles of plastic flow for each zone. Also, if zero is ever calculated from the use of relations (14) and (15) or if e is ever greater than e_s, then F_f is set to 1. The energy dependence of the yield condition is then calculated with the expression

$$Y = \max\ [0,\ Y' \cdot (1 - \frac{e}{e_s})] \quad (16)$$

The material parameters for the CIST-18S and all depths, except the 69-foot depth in CIST-18D, are given in Table 4.1. The 69-foot depth was not included because the material was the same as the 62-foot depth. Since the tests did not extensively exercise material above 3,000 psi, any parameters that are important only above that stress level are not based on the CIST data. These parameters (which include C_z, μ_3, μ_s, K_m, A, B, e_o, e_s, Y_1, and Y_2) were assigned values based on (1) a desire to be generic in nature, (2) previous experience that they are consistent with high pressure data, and (3) consistency with certain simple relations. Where those values are important, extreme caution should be used, and other sources must be consulted. Also, even for the parameters within the stress range of interest, final agreement with CIST data (Appendix B) has not been reached. Therefore, changes in those parameters or material model forms may occur.

Table 4.1 HAVE HOST material models

Parameter	Units	18S	18D		
Depth	feet	12	15	31	62 - 69
Mat type		alluvium	alluvium	alluvium	Rock
ρ_o	gm/cc	1.85	1.85	1.85	2.5
ν_L		0.3	0.3	0.3	0.23
ν_u		0.3	0.3	0.3	0.23
C_{L1}	feet/second	1500	1400	2000	8500
C_{L2}	feet/second	1200	1000	1400	8500
C_u	feet/second	1800	1800	2000	8500
C_z	feet/second	1800	1800	2000	8500
P_1	psi	18	0	0	10.00
P_2	psi	200	125.00	125.00	100.00
μ_3		0.17	0.17	0.17	0.04
μ_s		0.25	0.25	0.25	0.25
K_m	psi	E7	E7	E7	E7
A		0.5	0.5	0.5	0.5
B		1.3	1.3	1.3	1.3
e_o	cgs	E9	E9	E9	E9
e_s	cgs	E11	E11	E11	E11
T_1	psi	0	-10.00	-10.00	-5.00
C_1	psi	0	10.00	10.00	5.00
S_1		0.6	0.6	0.6	1.00
Y_1	psi	4000	4000	4000	15000
T_2	psi	0	0	0	0
C_2	psi	0	0	0	0
S_2	psi	0.6	0.6	0.6	1.00
Y_2	psi	4000	4000	4000	15000

Figures 4.3 through 4.6 are comparisons of the 3, 5, and 8 feet experimental data and AFTON calculations using the material models given in Table 4.1. A similar comparison for 12 feet range is shown in Figure 4.7. More detailed comparisons are found in Appendix B.

Comparison of the experimental and calculated data points out several deficiencies in the model currently used at AFWL. This model is known as the engineering model. The present AFWL computer codes (AFTON and WONDY IV) do not replicate the smooth peaks in the velocity waveforms for dry materials. (This appears to be a shortcoming of the engineering model rather than a shortcoming of the codes.) The engineering model works with varying degrees of success for different materials. In dry sandy alluvium, the deficiencies are apparent (Figure 4.3).

In dry sandy alluvium, the engineering model cannot completely match the data at the gauge ranges in the CIST (3, 5, and 8 feet). The usual result would be to undershoot the data at 3 feet and overshoot the data at 8 feet. These deficiencies may be caused by strain rate effects present in these materials that cannot be taken into account with the engineering model. At this point in time, it is not apparent that any other material model can adequately model this material either. This point reemphasized the need to develop material models that can adequately quantify material response for the wide variety of materials encountered in MX geologies.

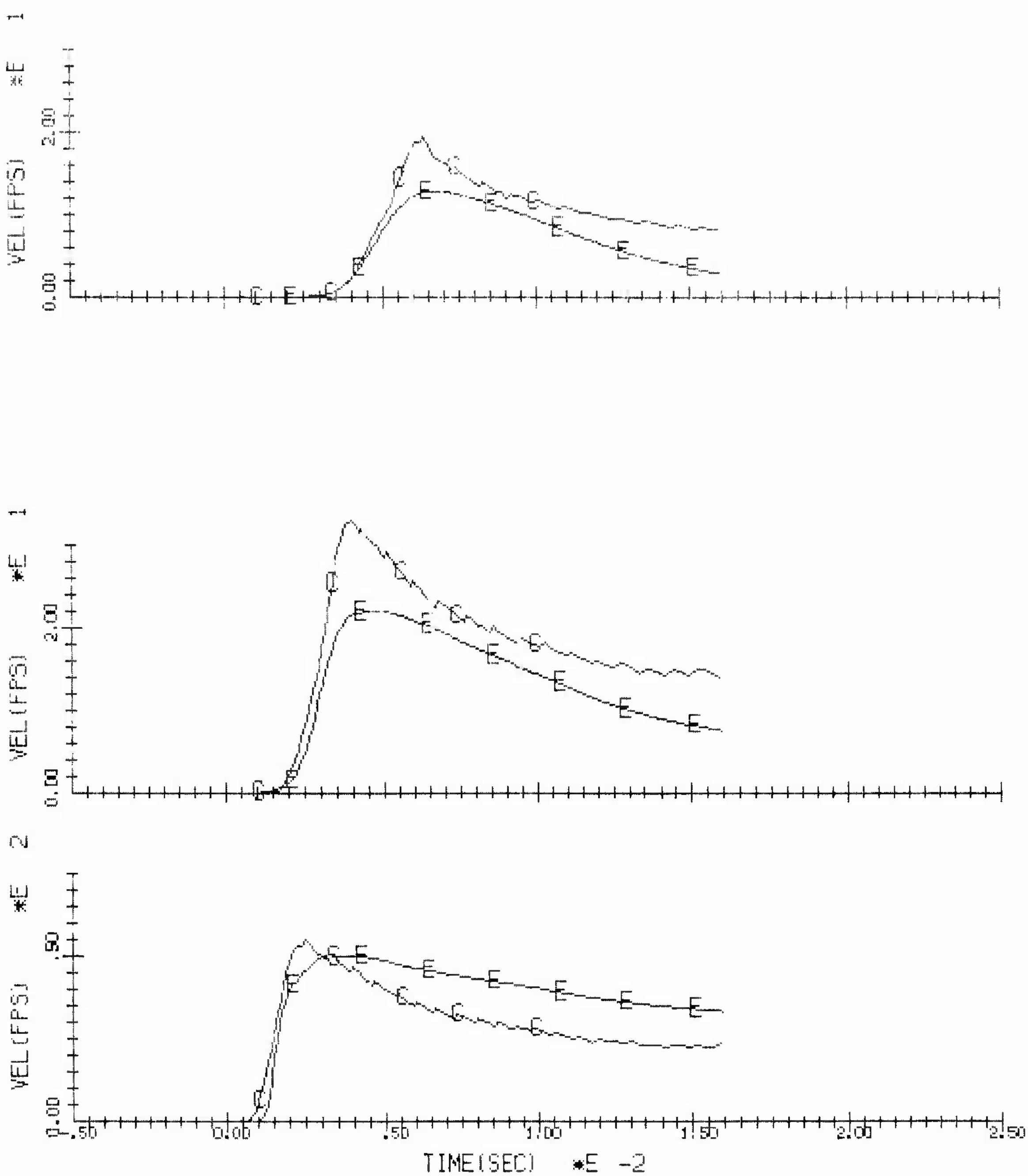

Figure 4.3. Comparison of experimental data and AFTON calculation for CIST 18S.

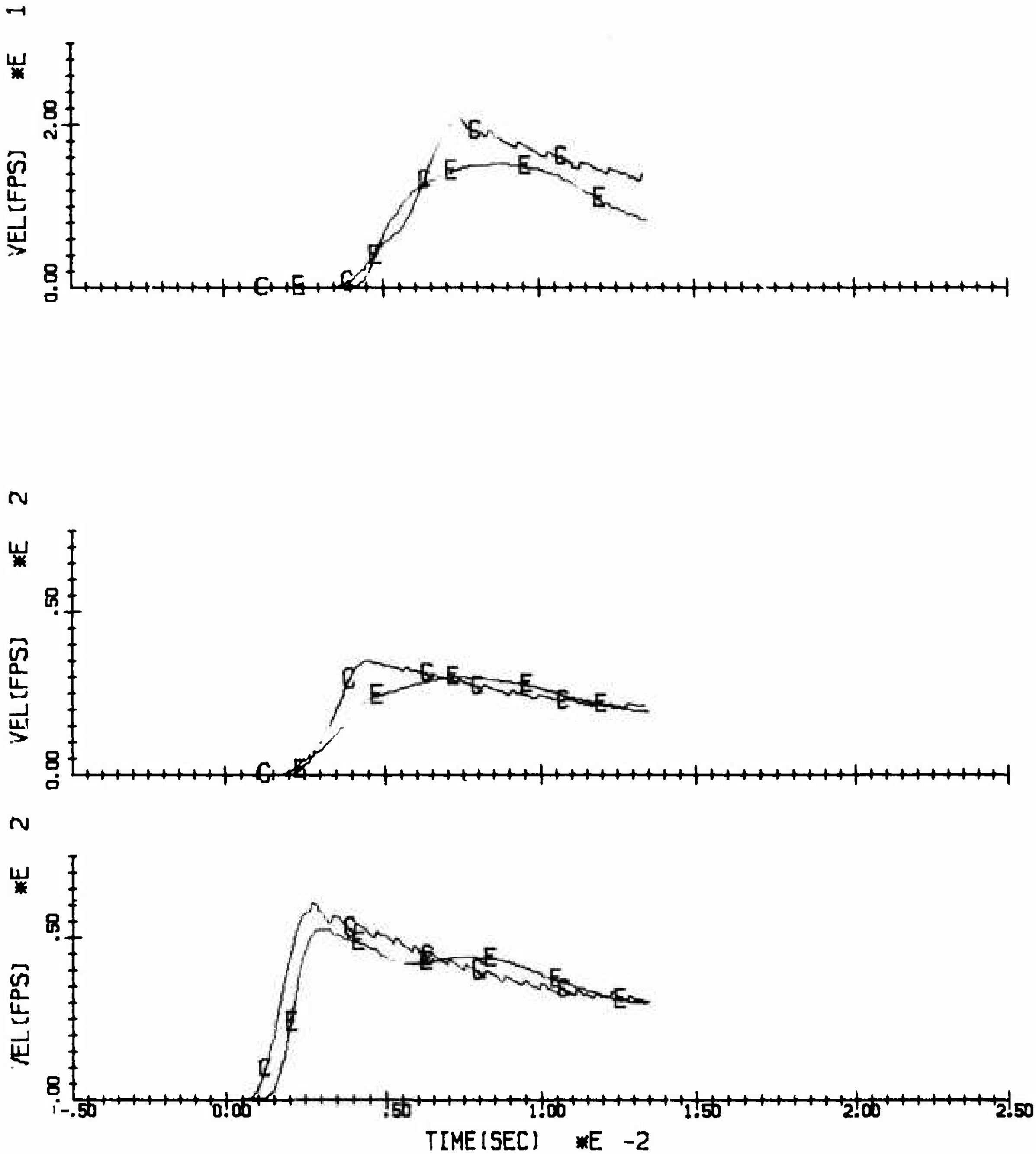

Figure 4.4. Comparison of experimental data and AFTON calculation for 15' depth in CIST 18D.

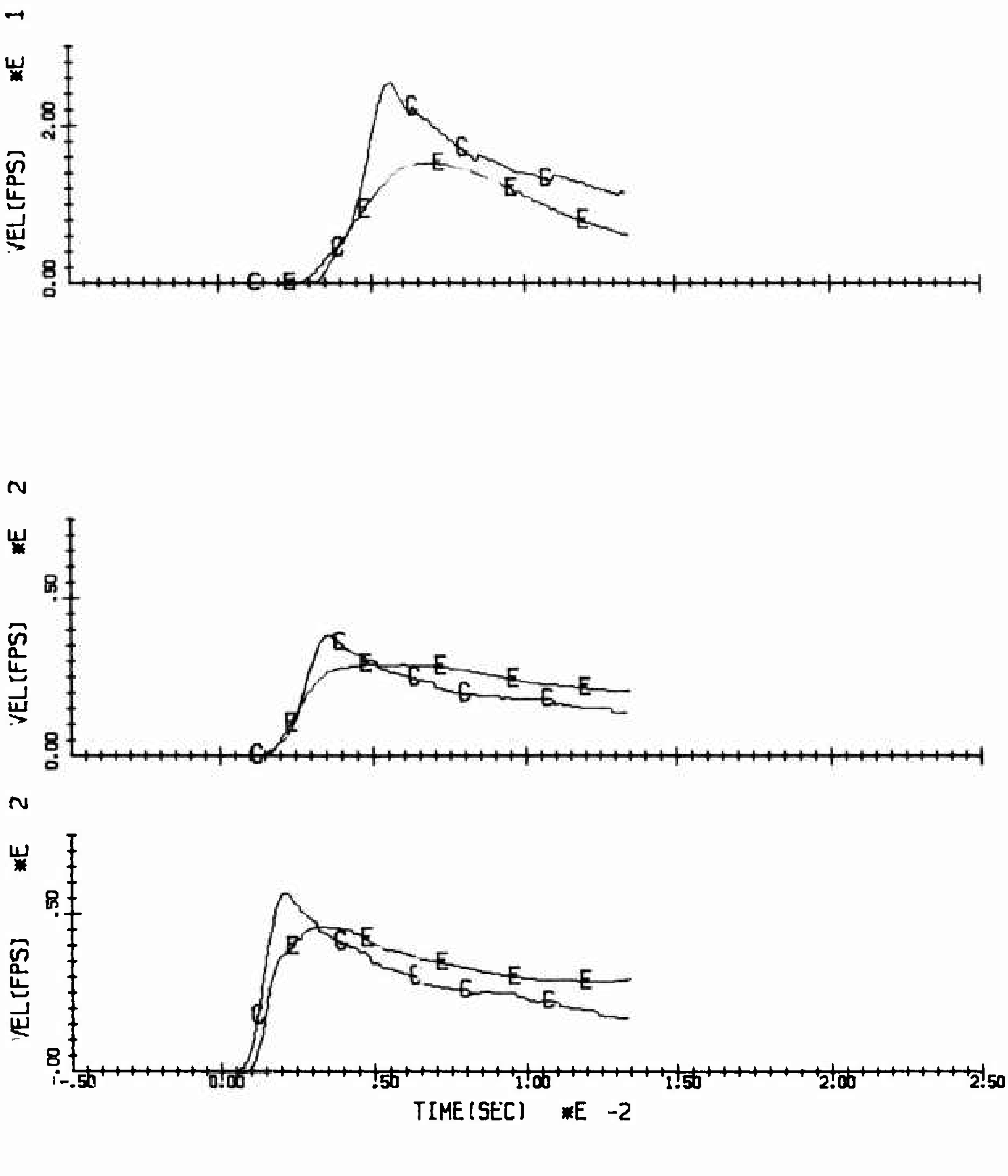

Figure 4.5. Comparison of experimental data and AFTON calculation for 31' depth in CIST 18D.

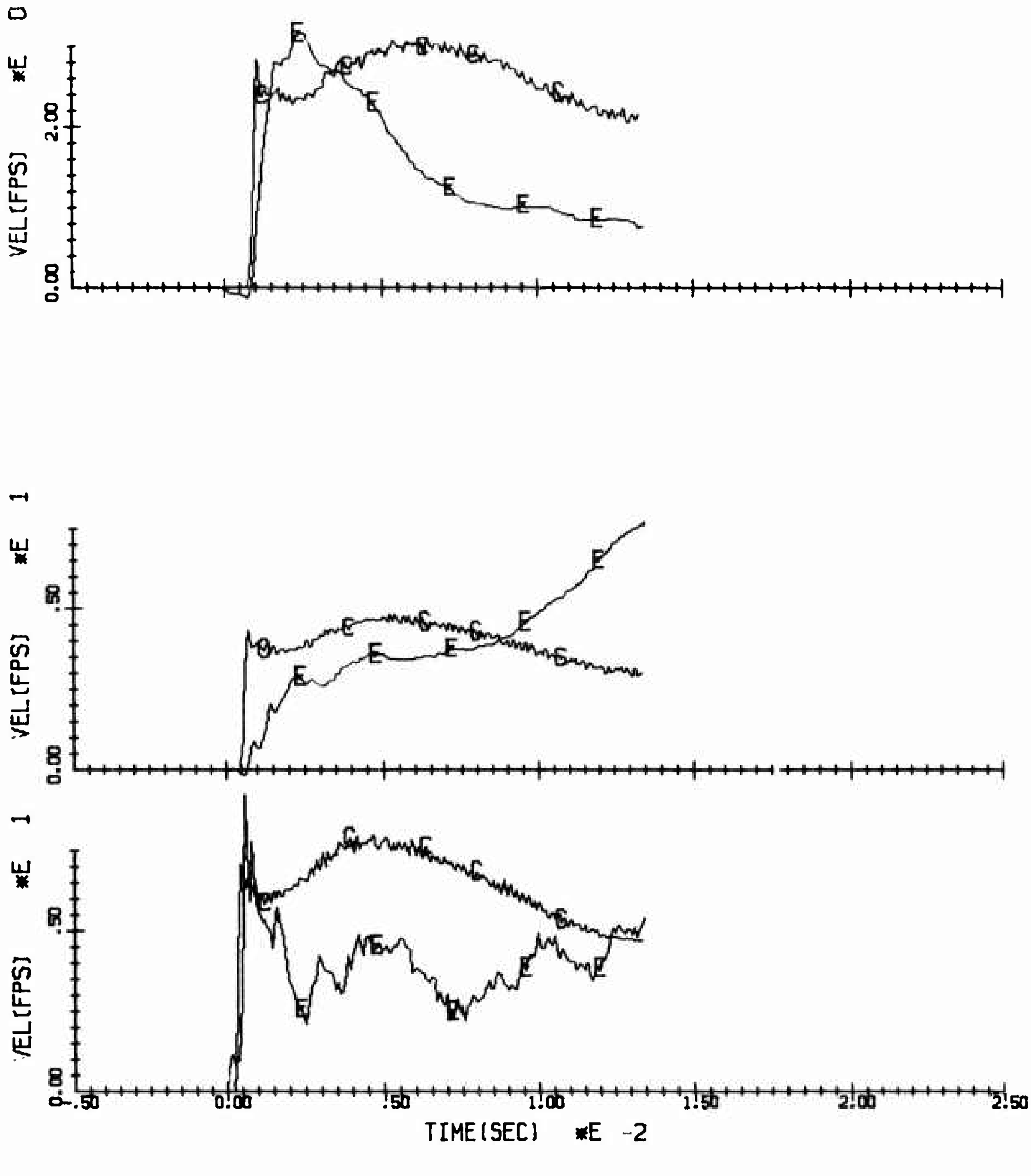

Figure 4.6. Comparison of experimental data and AFTON calculation for 62' depth in CIST 18D.

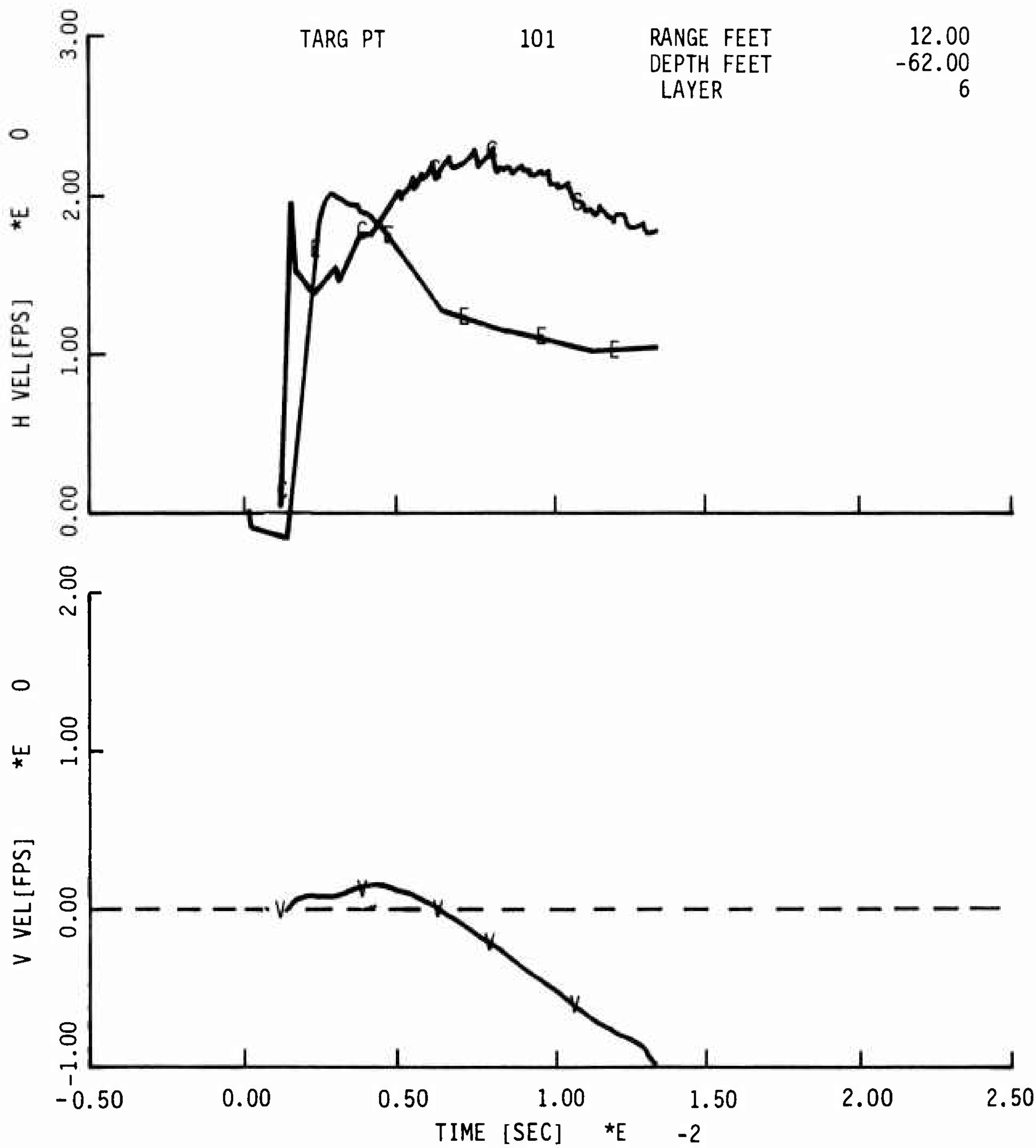

Figure 4.7. Comparison of experimental data and AFTON calculation for 12' range and 62' depth.

SECTION 5

CONCLUSIONS

Listed below is a summary of the data recovery for CIST 18.

	# Accel Msmts (% Data Recovery)	# Stress Msmts (% Data Recovery)
Alluvium	15 (100)	8 (100)
Rock	12 (100)	None recorded
TOTAL:	27 (100)	8 (100)

It can be seen that there was 100 percent data recovery. Based on the percentage and quality of data recovered, CIST 18 was a completely successful experiment. However, the data, wnen compared to the material model calculations, point out apparent inadequacies in the engineering model. This problem is currently being addressed at AFWL/DES.

Based on the data, several conclusions can be drawn from the data analysis:

(1) Seismic velocity is a function of soil cementation.

(2) The propagation velocity of the peak particle velocity is independent of soil cementation.

(3) The maximum alluvial response to CIST type loadings is independent of soil cementation.

This experiment has yielded a great deal of information on the material properties of sandy alluvium. However, much work remains to be accomplished, particularly in the development of a material model to adequately characterize the response of these materials.

REFERENCES

1. Davis, Stephen E., Nevada Test Site CIST Events Data, AFWL-TR-74-131, Air Force Weapons Laboratory, Kirtland AFB, New Mexico, May 1974.
2. Amend, Joseph H., Cylindrical In-Situ Tests at Selected Nuclear and High Explosive Test Sites, AFWL-TR-76-209, Air Force Weapons Laboratory, Kirtland AFB, New Mexico, January 1977.
3. Davis, Stephen E., General Test Plan for the Cylindrical In-Situ Test, AFWL-TR-74-136, Air Force Weapons Laboratory, Kirtland AFB, New Mexico, June 1974.
4. Calhoun, Delmar and Stephenson, Dale, Constitutive Rock Properties for the HANDEC II Site, AFWL-TR-69-110, Air Force Weapons Laboratory, Kirtland AFB, New Mexico, December 1969.
5. Jackson, Ed, "Preliminary CIST 18 Grain Size Analysis," letter reprint from WES to AFWL, January 1977.

APPENDIX A

ACCELERATION, VELOCITY AND DISPLACEMENT TIME HISTORIES

Plots are arranged in order of increasing range (3, 5, 8, and 12 feet, respectively). Horizontal data for a given location are followed by vertical data if available. Whenever available, redundant recordings are given in lieu of primary recordings. The redundant recordings were calibrated at 80 percent band edge, and the primary recordings were calibrated at 40 percent band edge; hence, tne redundant recordings signal to noise ratio is much improved.

A.1 MEASUREMENT IDENTIFICATION

Each data trace is identified at its top center by a measurement designation number. The measurement designation number consists of eight alpna-numeric designators in the following form:

X - X - XXX - XX.X - XXX - X.X - XX - X

1 2 3 4 5 6 7 8

a. The first character indicates the organization that established the measurement required:

F - AFWL (Free-Field) (DES-G)

b. The second character denotes the method of data acquisition:

E - Electronic

c. The third set of characters indicates the plan location of the free-field measurement. L01 refers to hole number one (hole layouts are given in Figures 2.6 and 2.7).

d. The fourth set of characters indicates the depth (in feet) of the transducer below the surface.

e. The fifth designator indicates the azimuth, in degrees from North (0°), of the radial on which the measurement is made.

f. The sixth set of characters indicates the radial distance in feet from GZ to the center of the transducer.

g. The seventh set of characters specifies the type of measurement being made (as shown below).

A - Acceleration

CP - Cavity Pressure

SE - Soil Stress

h. The last set of characters indicates the orientation of the sensing axis of the transducer:

V - Vertical

H - Horizontal Radial

T - Horizontal Transverse

Following the measurement designation number are the tape number, track number, and measurement number. These three numbers appear to the right of the measurement designation number and are separated by a slash (/) and an asterick (*). The first is the tape machine number; the second is the track number, and the third is the measurement number.

Figure A.1 illustrates the azimuth, range, and sensing axis of the free-field transducers. A sample of the labeling system is given in Figure A.2. Table 2.1 presents the CIST measurement list and calibration values.

A.2 DATA PLOTS

The time histories presented in the appendix are edited data. The only posttest data correction that has been made is that cable breaks were truncated. This was done so the first and secord integral time histories scaling would not be driven by the cable breaks. Data correction is planned in the near future. It appears at this time that there are no drastic early time (first 25 msc) corrections to be made.

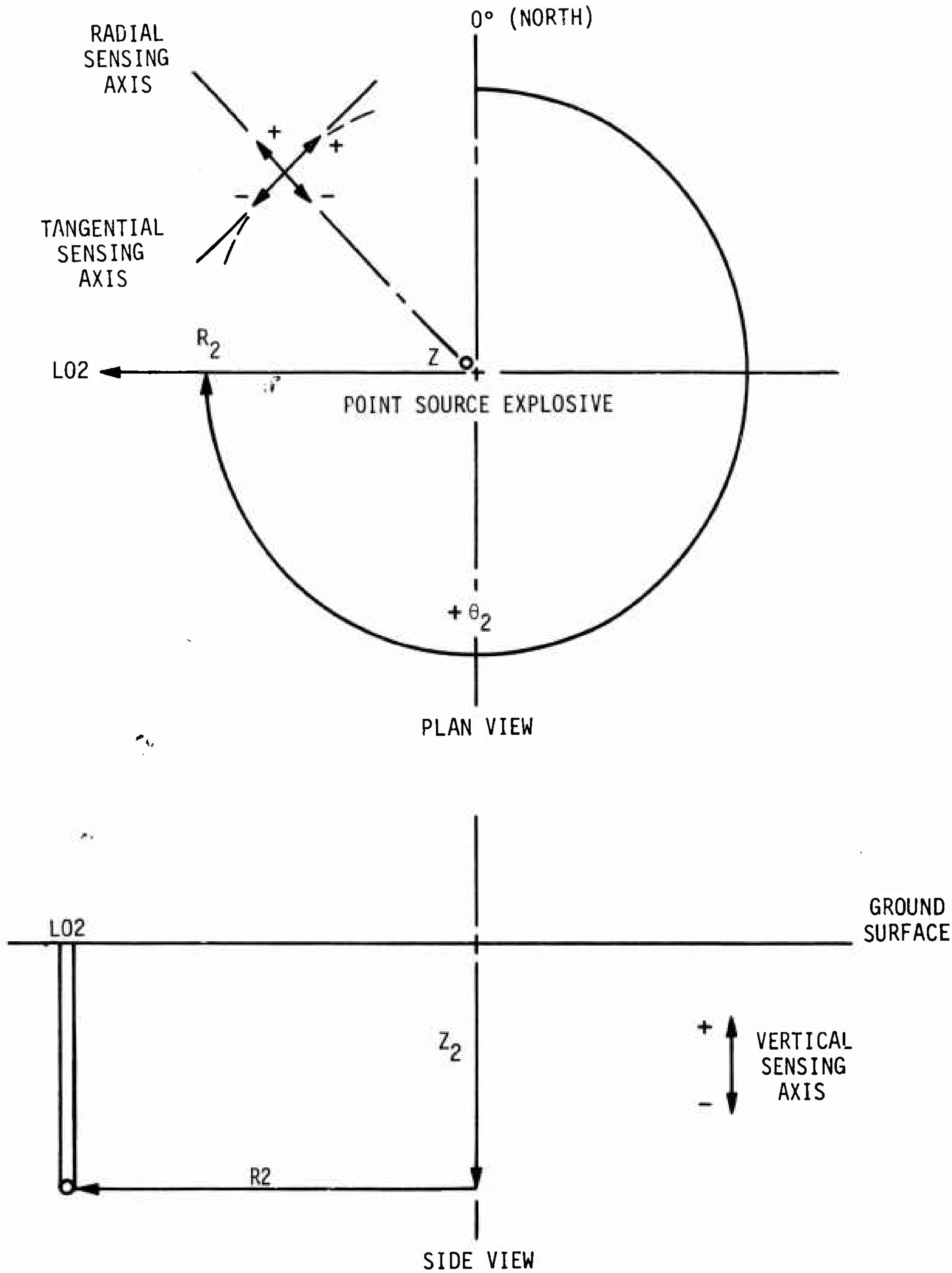

Figure A.1. Definition of azimuth, range, depth, and sensing axis.

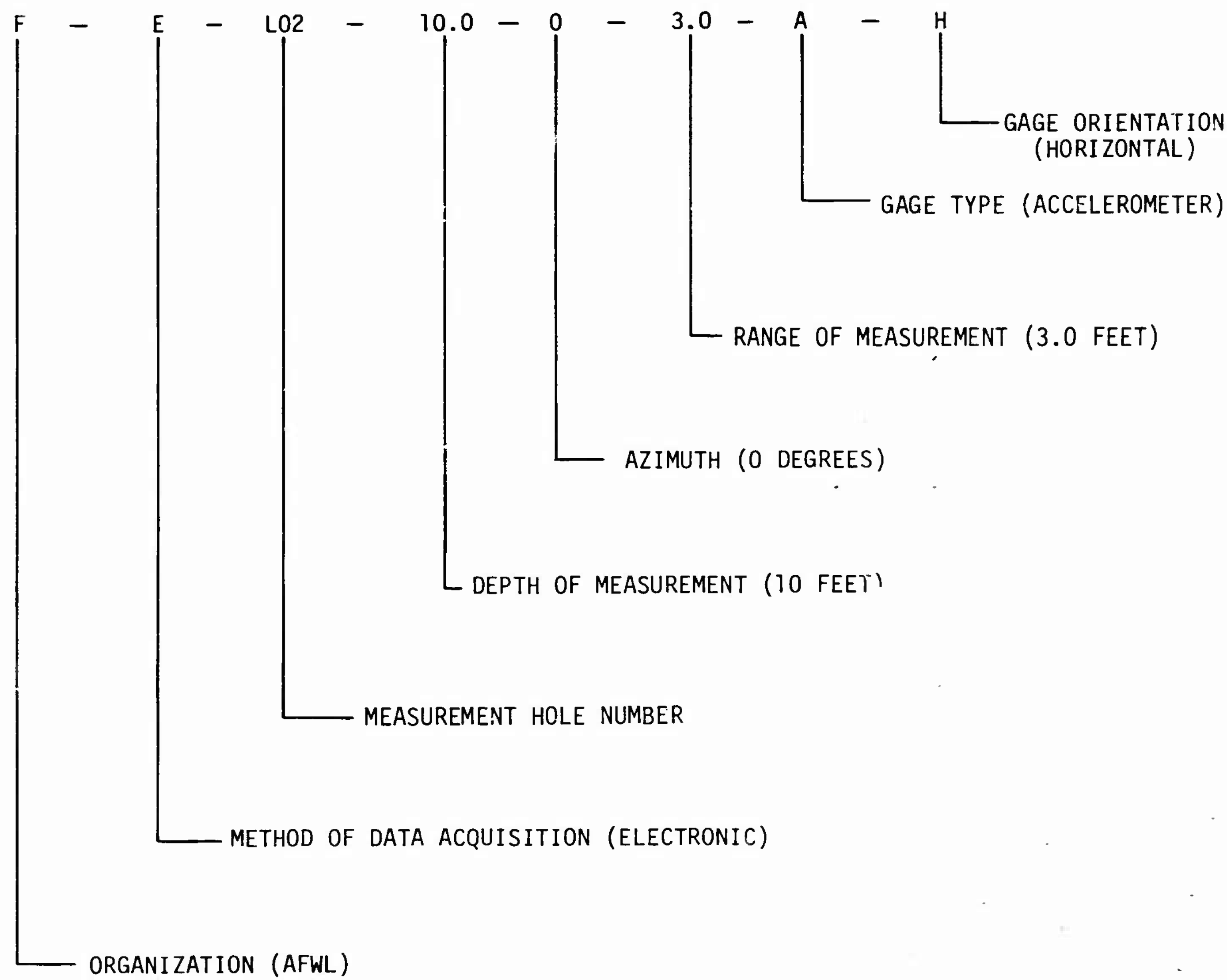

Figure A.2. Sample of record labeling system.

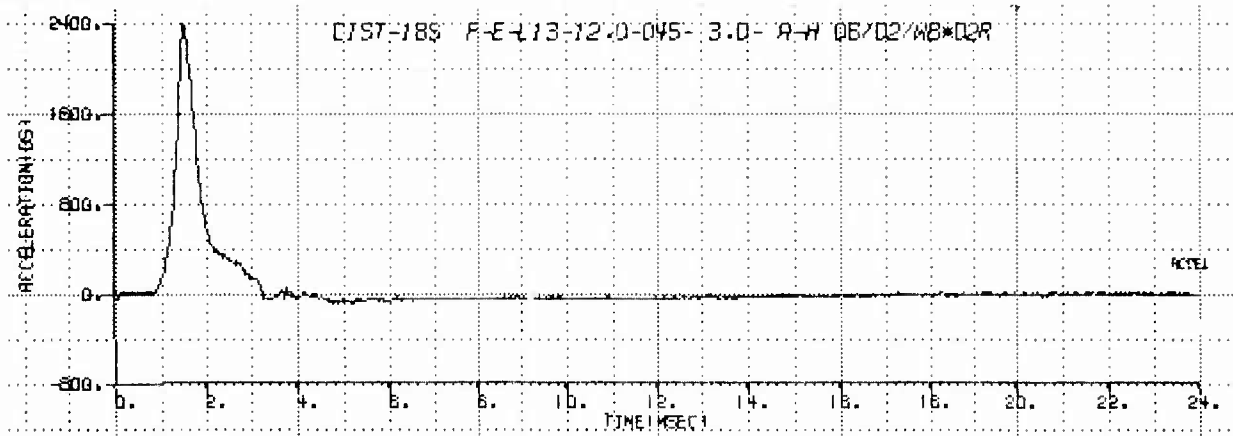
CIST-18S F-E-L13-12.0-045- 3.0- A-H 06/02/WB*02R
ACCELERATION(GS)
TIME(MSEC)
ACCEL

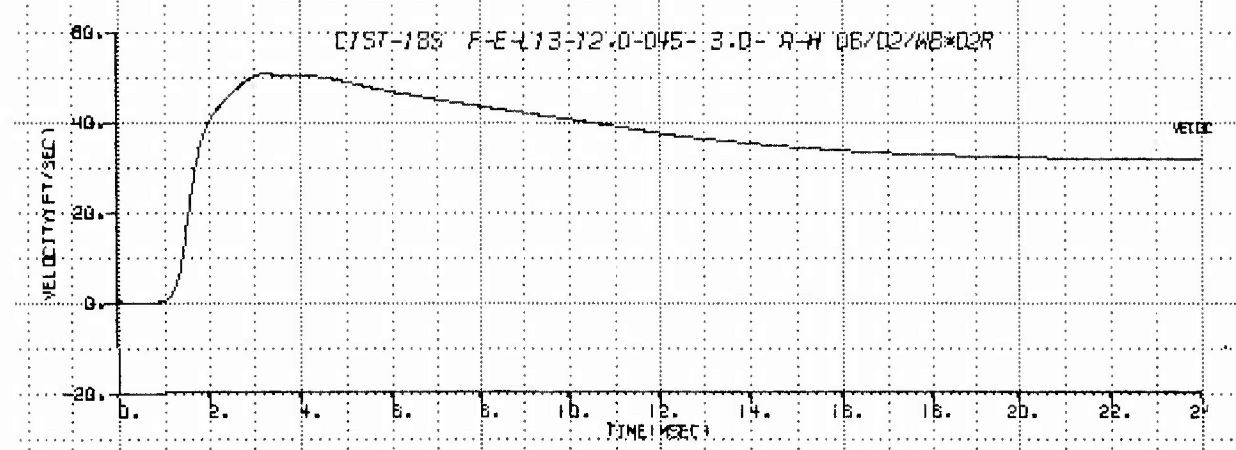
CIST-18S F-E-L13-12.0-045- 3.0- A-H 06/02/WB*02R
VELOCITY(FT/SEC)
TIME(MSEC)
VELOC

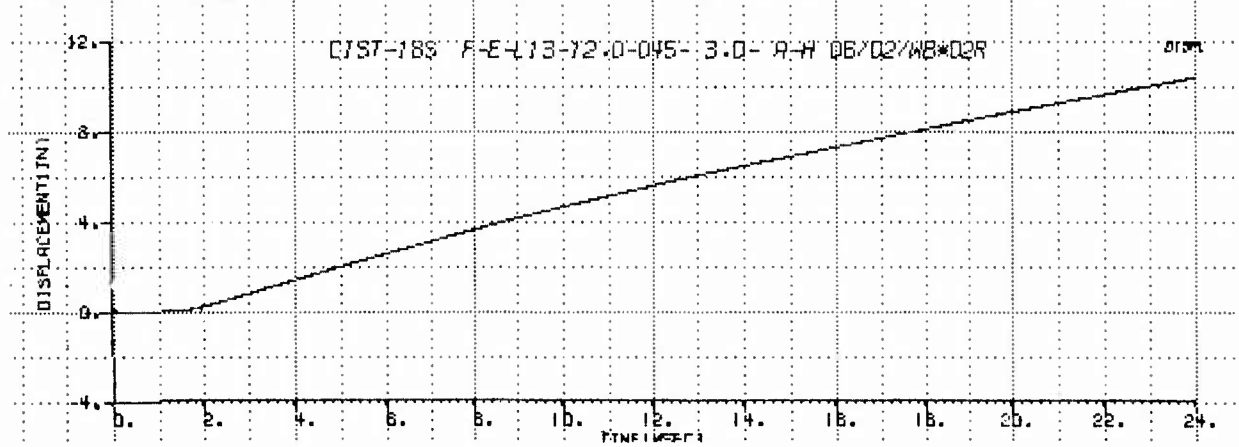
CIST-18S F-E-L13-12.0-045- 3.0- A-H 06/02/WB*02R
DISPLACEMENT(IN)

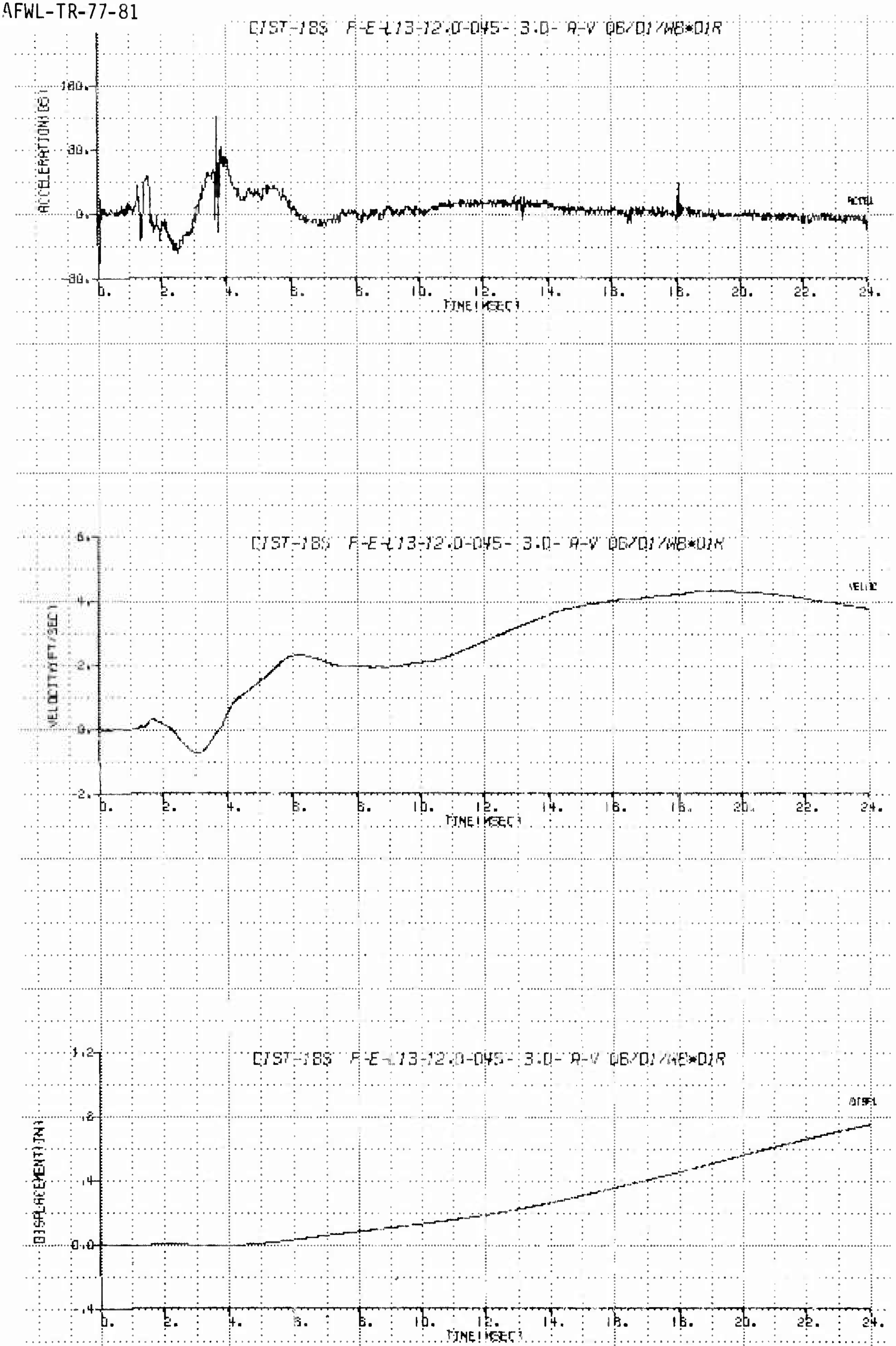
ACCELERATION(G'S)
TIME(MSEC)
VELOCITY(FT/SEC)
TIME(MSEC)
DISPLACEMENT(IN)
TIME(MSEC)

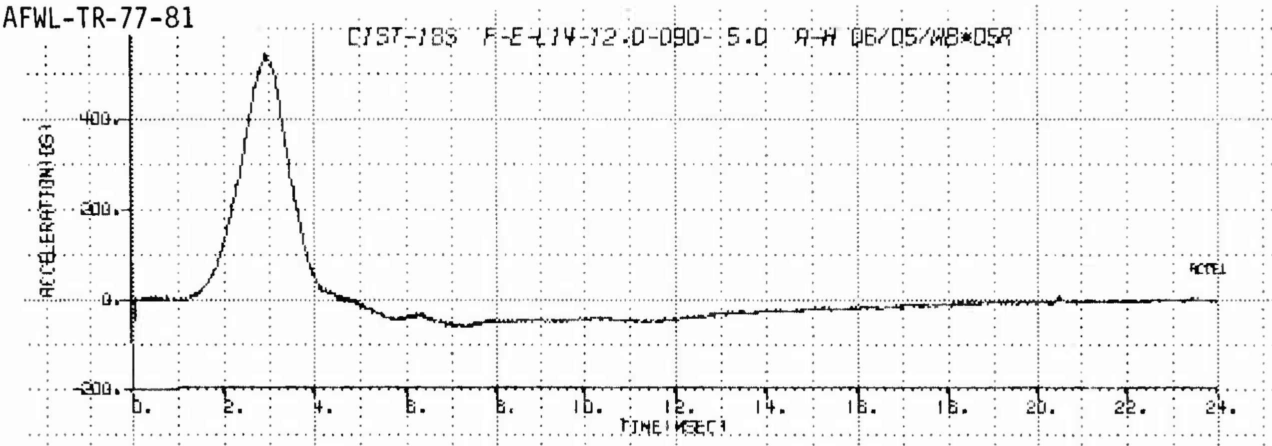
DIST-18S P-E-L14-12.0-090- 5.0 A-H 06/05/WB*05R
ACCELERATION(G'S)
400.
200.
0.
-200.
ACCEL
0.
2.
4.
6.
8.
10.
12.
14.
16.
18.
20.
22.
24.
TIME(MSEC)

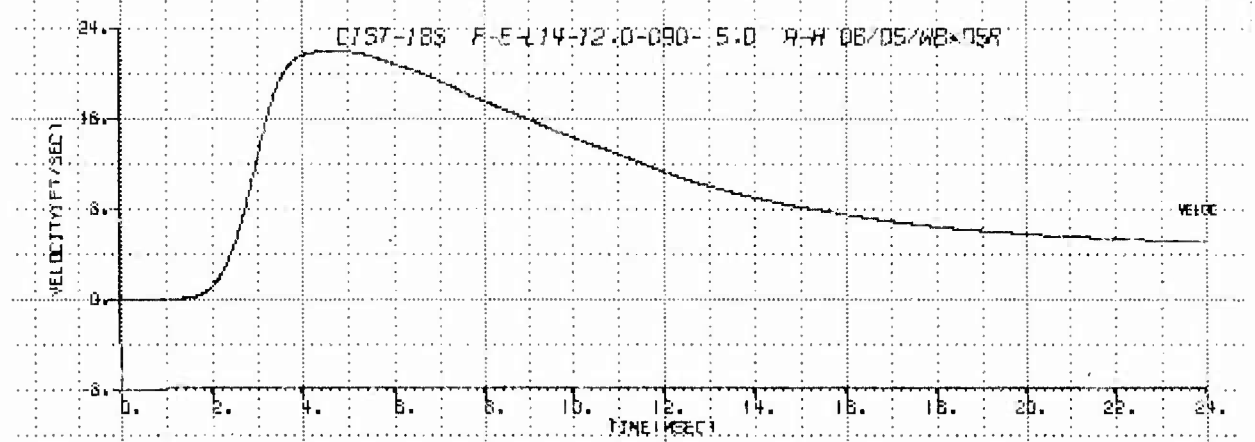
DIST-18S P-E-L14-12.0-090- 5.0 A-H 06/05/WB*05R
VELOCITY(FT/SEC)
24.
16.
8.
0.
-8.
VELOC
0.
2.
4.
6.
8.
10.
12.
14.
16.
18.
20.
22.
24.
TIME(MSEC)

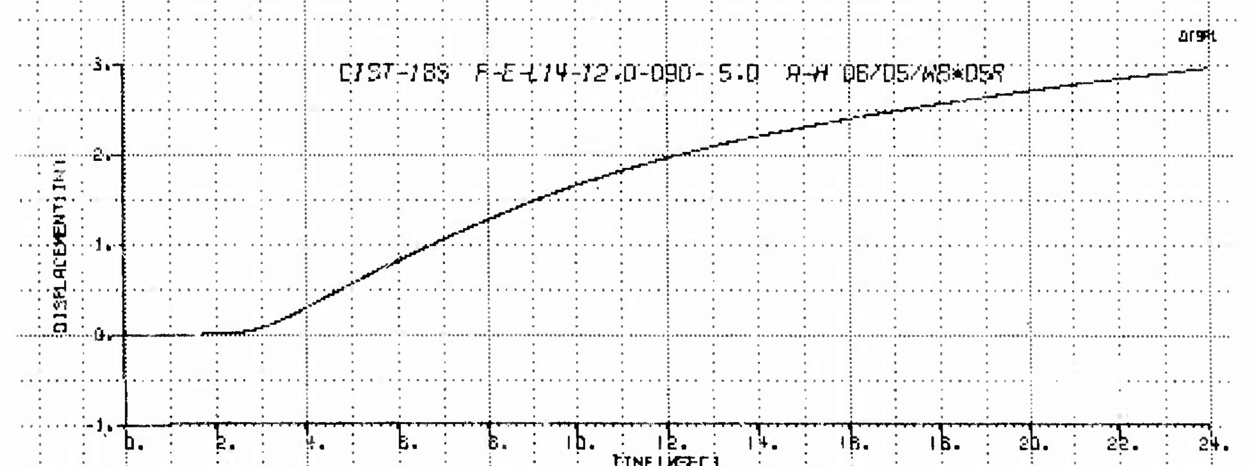
DIST-18S P-E-L14-12.0-090- 5.0 A-H 06/05/WB*05R
DISPLACEMENT(IN)
3.
2.
1.
0.
-1.
DISPL
0.
2.
4.
6.
8.
10.
12.
14.
16.
18.
20.
22.
24.
TIME(MSEC)

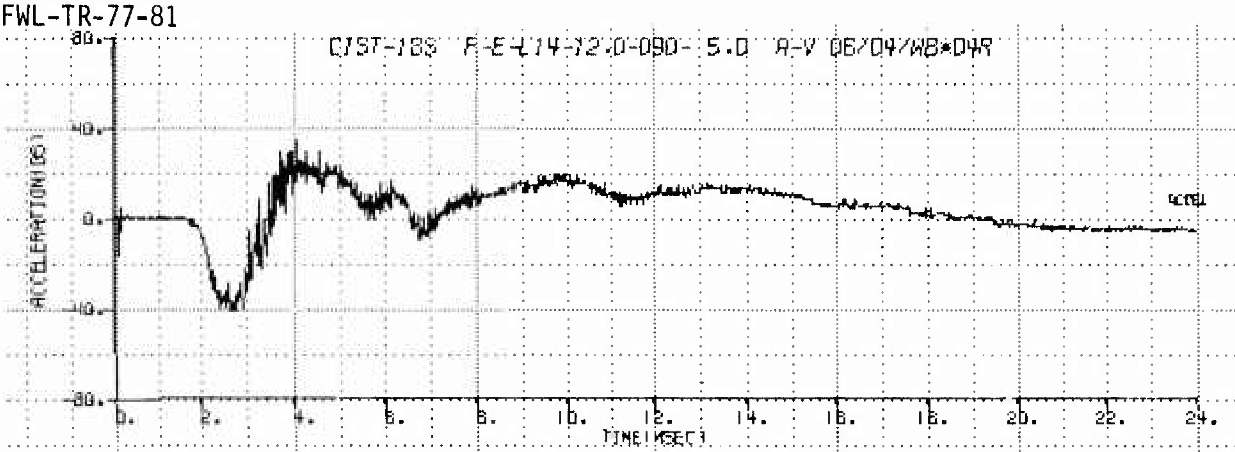
DIST-18S P-E-L14-12.0-090- 5.0 A-V 06/04/WB*04R
ACCELERATION(G)
TIME(MSEC)
ACCEL
80.
40.
0.
-40.
-80.
0.
2.
4.
6.
8.
10.
12.
14.
16.
18.
20.
22.
24.

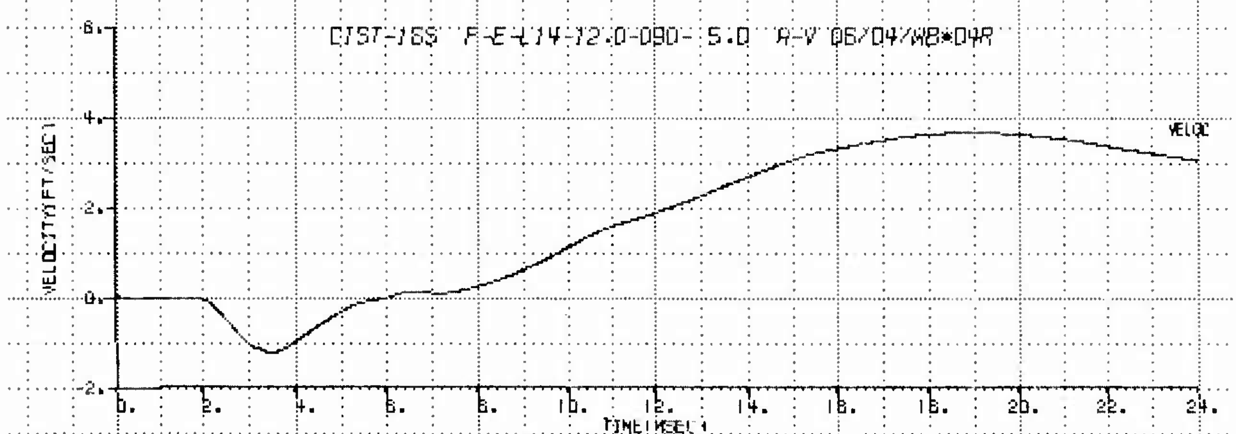
DIST-18S P-E-L14-12.0-090- 5.0 A-V 06/04/WB*04R
VELOCITY(FT/SEC)
TIME(MSEC)
VELOC
6.
4.
2.
0.
-2.
0.
2.
4.
6.
8.
10.
12.
14.
16.
18.
20.
22.
24.

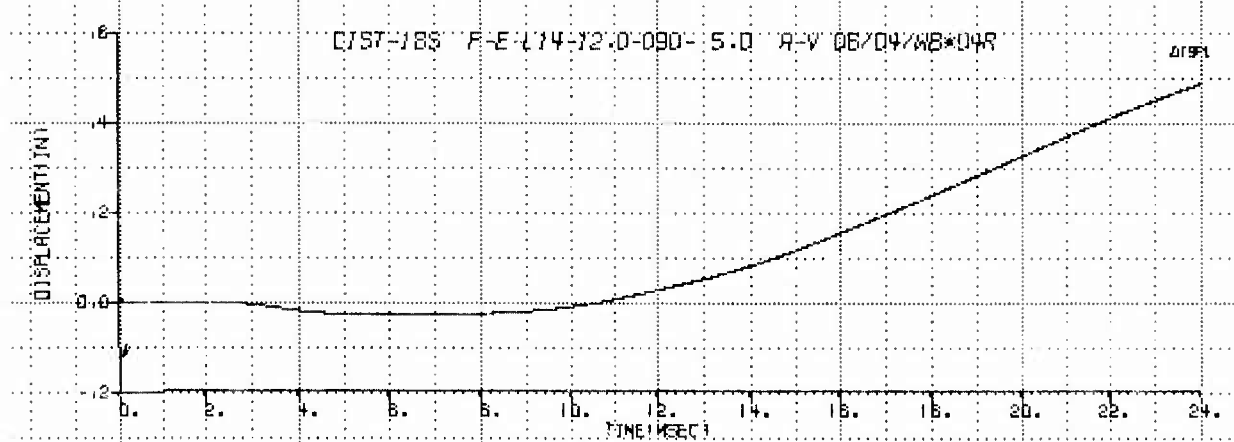
DIST-18S P-E-L14-12.0-090- 5.0 A-V 06/04/WB*04R
DISPLACEMENT(IN)
TIME(MSEC)
DISPL
.6
.4
.2
0.0
-.2
0.
2.
4.
6.
8.
10.
12.
14.
16.
18.
20.
22.
24.

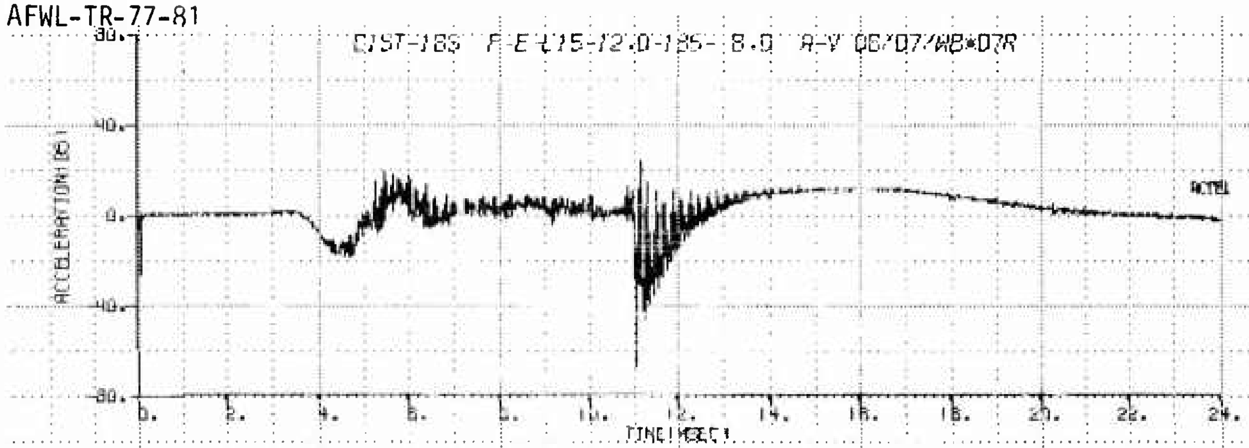
ACCELERATION(G)
TIME(MSEC)
ACCEL
80.
40.
0.
-40.
-80.
0. 2. 4. 6. 8. 10. 12. 14. 16. 18. 20. 22. 24.

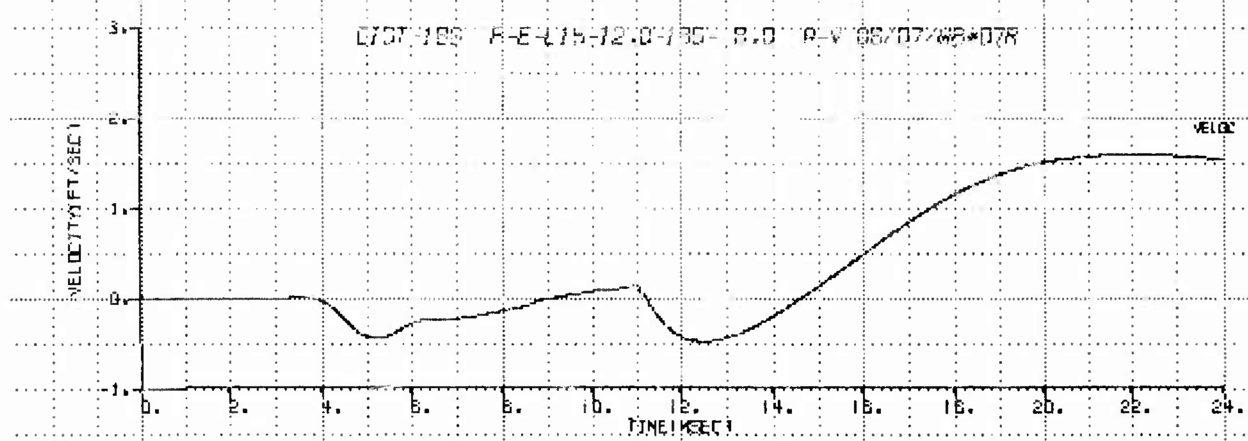
VELOCITY(FT/SEC)
TIME(MSEC)
VELOC
3.
2.
1.
0.
-1.
0. 2. 4. 6. 8. 10. 12. 14. 16. 18. 20. 22. 24.

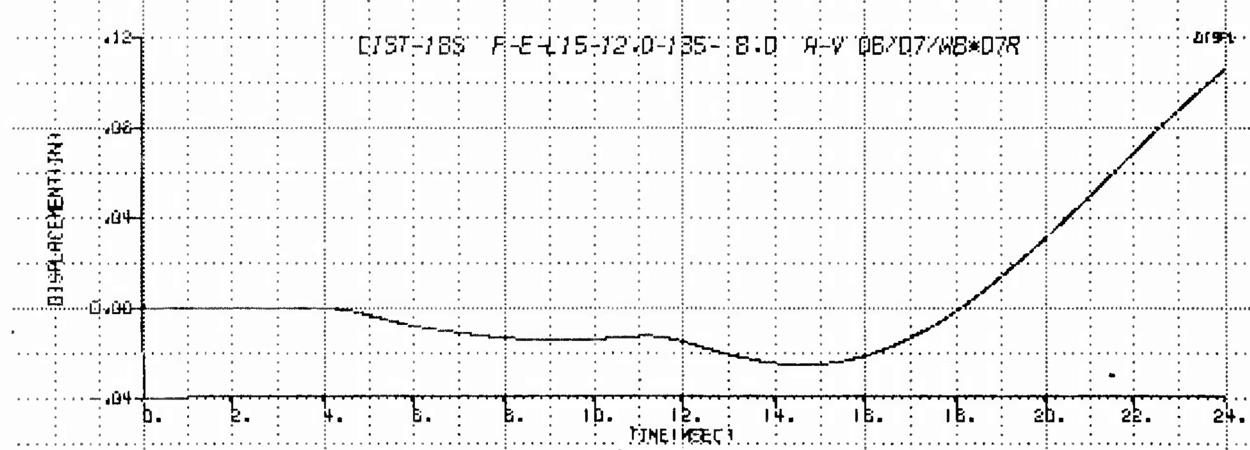
DISPLACEMENT(IN)
TIME(MSEC)
DISPL
.12
.08
.04
0.00
-.04
0. 2. 4. 6. 8. 10. 12. 14. 16. 18. 20. 22. 24.

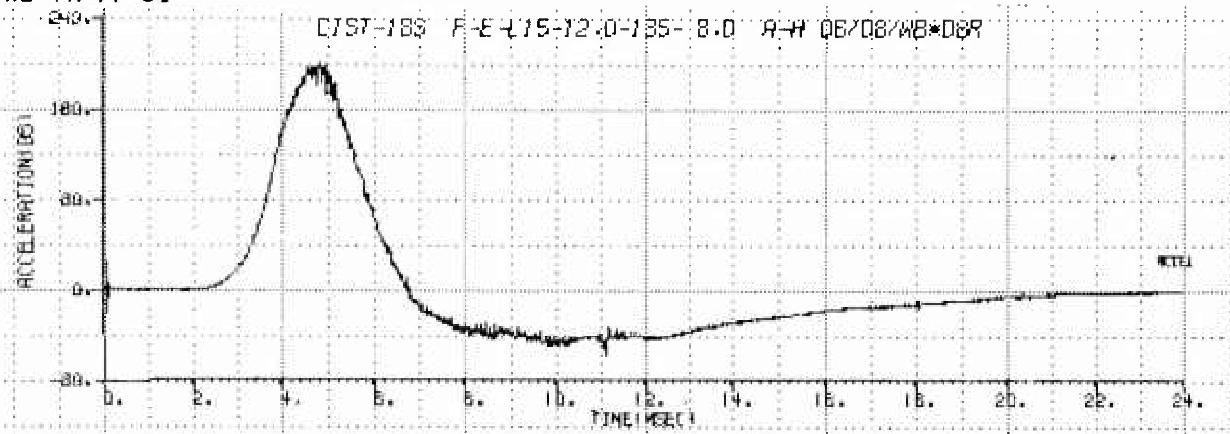
DIST-18S P-E-L15-12.0-135- 8.0 A-H 06/08/WB*D8R
ACCELERATION(GS)
240.
160.
80.
0.
-80.
ACCEL
0. 2. 4. 6. 8. 10. 12. 14. 16. 18. 20. 22. 24.
TIME(MSEC)

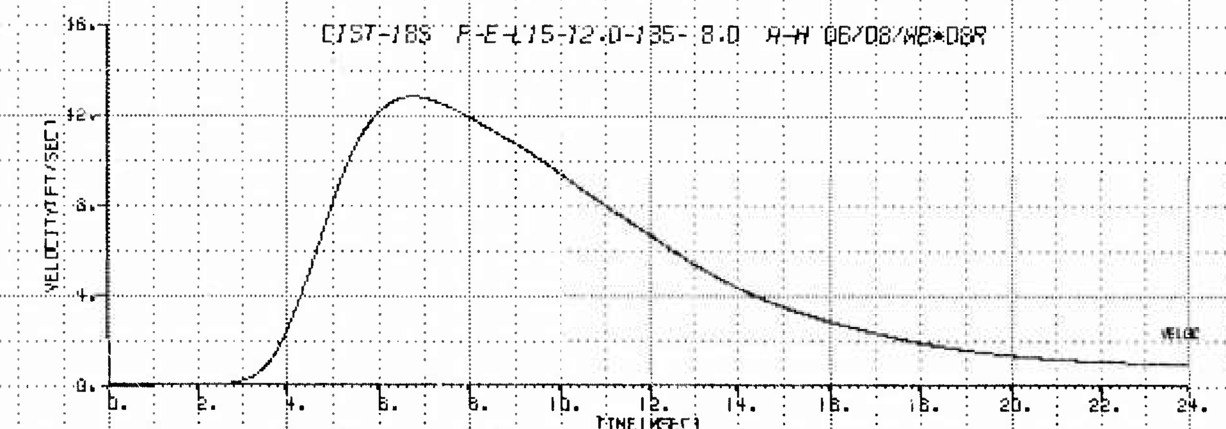
DIST-18S P-E-L15-12.0-135- 8.0 A-H 06/08/WB*D8R
VELOCITY(FT/SEC)
16.
12.
8.
4.
0.
VELOC
0. 2. 4. 6. 8. 10. 12. 14. 16. 18. 20. 22. 24.
TIME(MSEC)

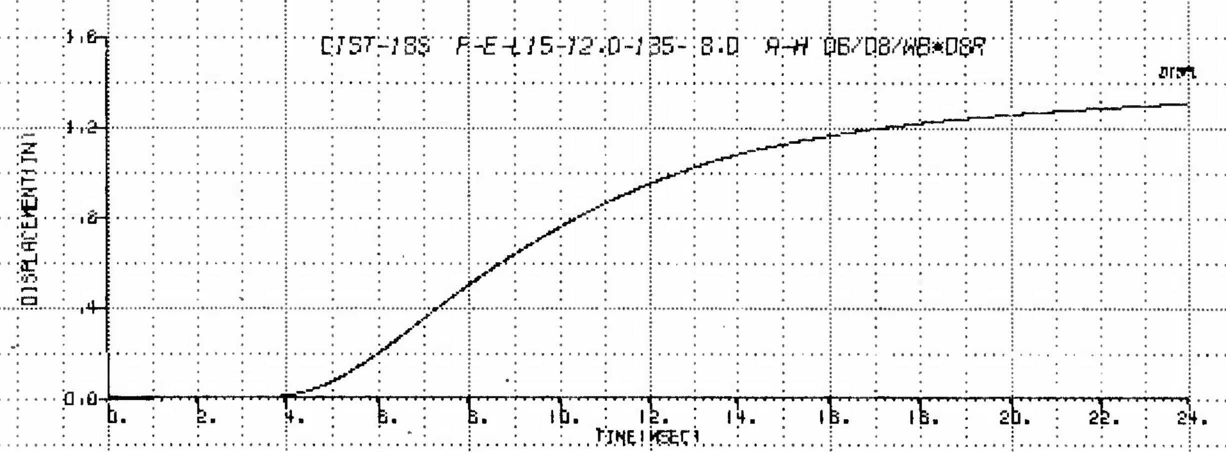
DIST-18S P-E-L15-12.0-135- 8.0 A-H 06/08/WB*D8R
DISPLACEMENT(IN)
1.6
1.2
.8
.4
0.0
DISPL
0. 2. 4. 6. 8. 10. 12. 14. 16. 18. 20. 22. 24.
TIME(MSEC)

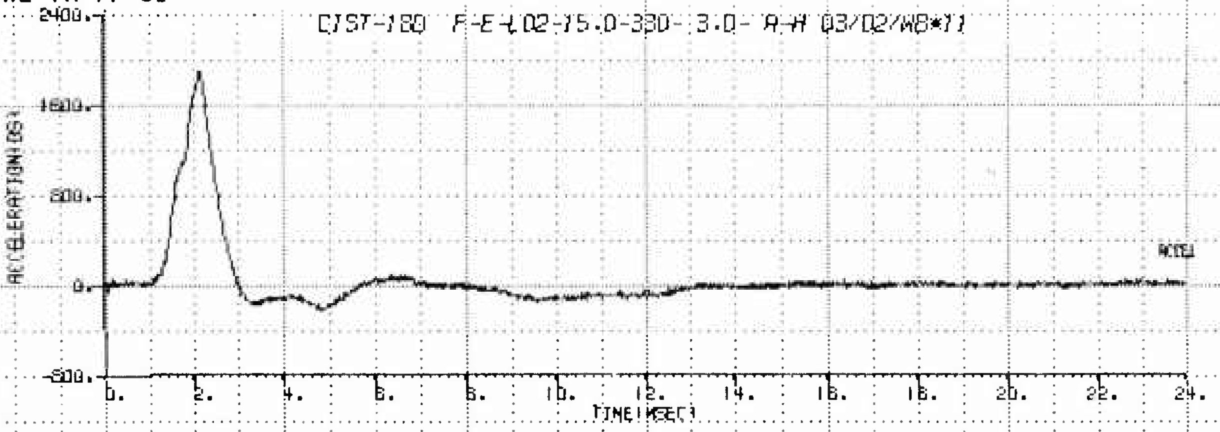
ACCELERATION(GS)
TIME(MSEC)
ACCEL
2400.
1600.
800.
0.
-800.
0. 2. 4. 6. 8. 10. 12. 14. 16. 18. 20. 22. 24.

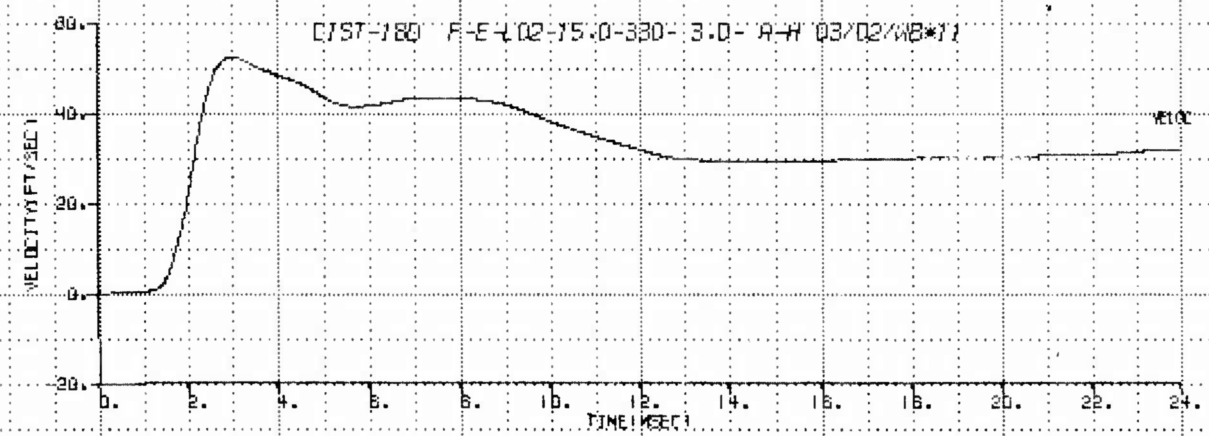
VELOCITY(FT/SEC)
TIME(MSEC)
VELOC
60.
40.
20.
0.
-20.
0. 2. 4. 6. 8. 10. 12. 14. 16. 18. 20. 22. 24.

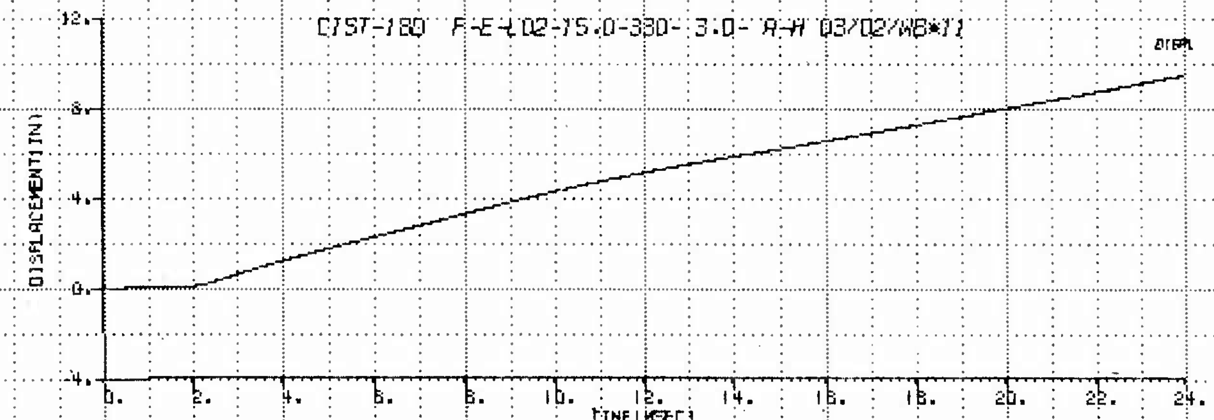
DISPLACEMENT(IN)
TIME(MSEC)
DISPL
12.
8.
4.
0.
-4.
0. 2. 4. 6. 8. 10. 12. 14. 16. 18. 20. 22. 24.

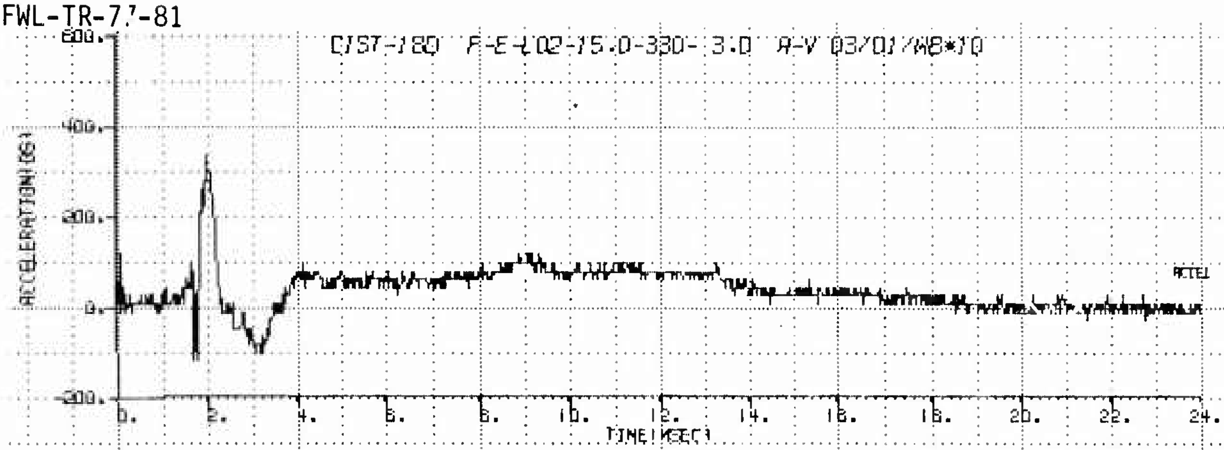
ACCELERATION(G'S)
TIME(MSEC)
ACCEL

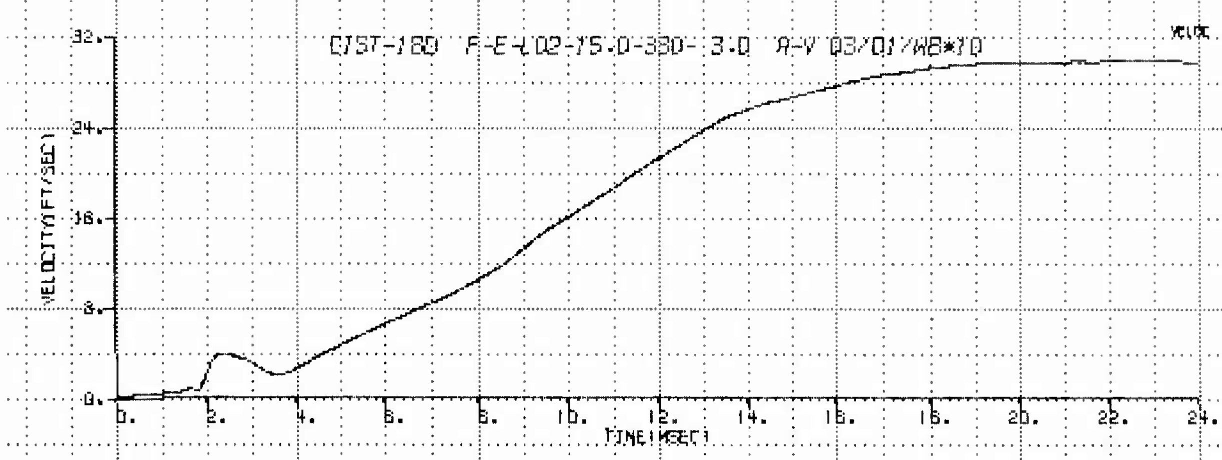
VELOCITY(FT/SEC)
TIME(MSEC)
VELOC

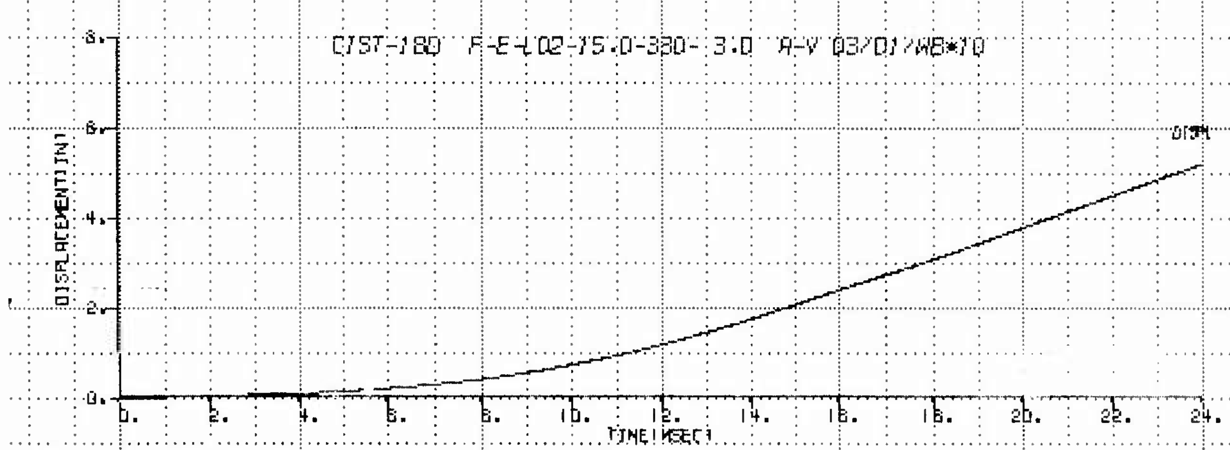
DISPLACEMENT(IN)
TIME(MSEC)
DISPL

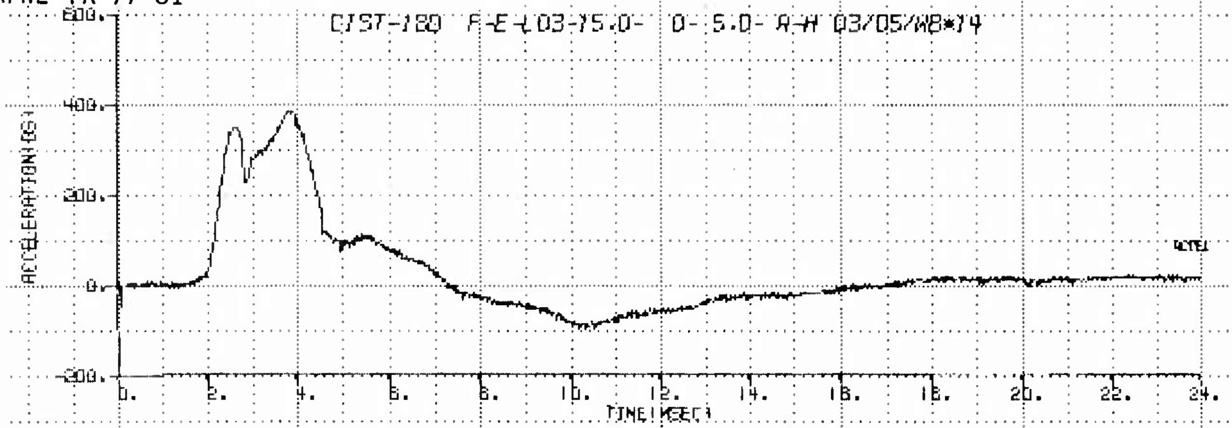
DIST-180 F-E-L03-75.0- 0-5.0- A-H 03/05/WB*74
ACCELERATION(GS)
ACCEL
600.
400.
200.
0.
-200.
0.
2.
4.
6.
8.
10.
12.
14.
16.
18.
20.
22.
24.
TIME(MSEC)

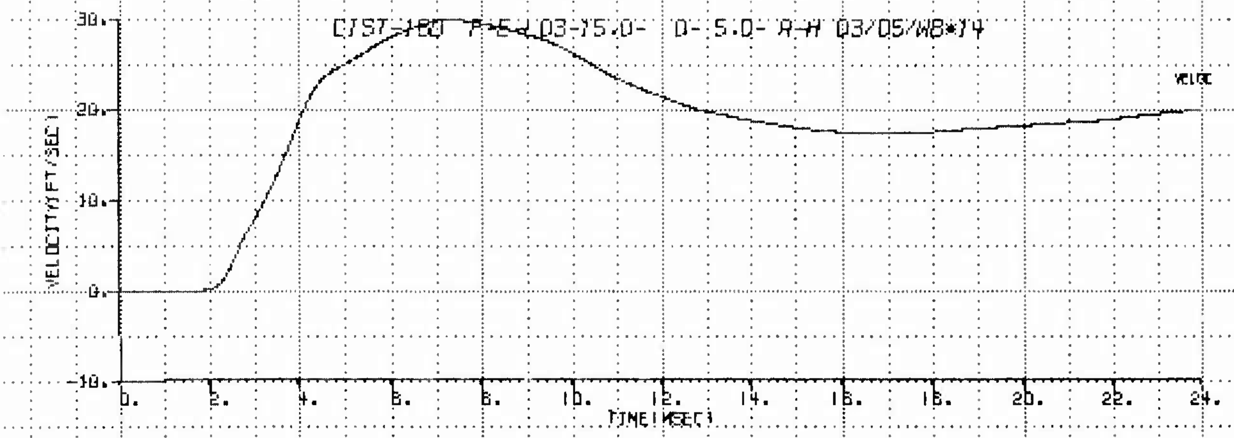
DIST-180 F-E-L03-75.0- 0-5.0- A-H 03/05/WB*74
VELOCITY(FT/SEC)
VELOC
30.
20.
10.
0.
-10.
0.
2.
4.
6.
8.
10.
12.
14.
16.
18.
20.
22.
24.
TIME(MSEC)

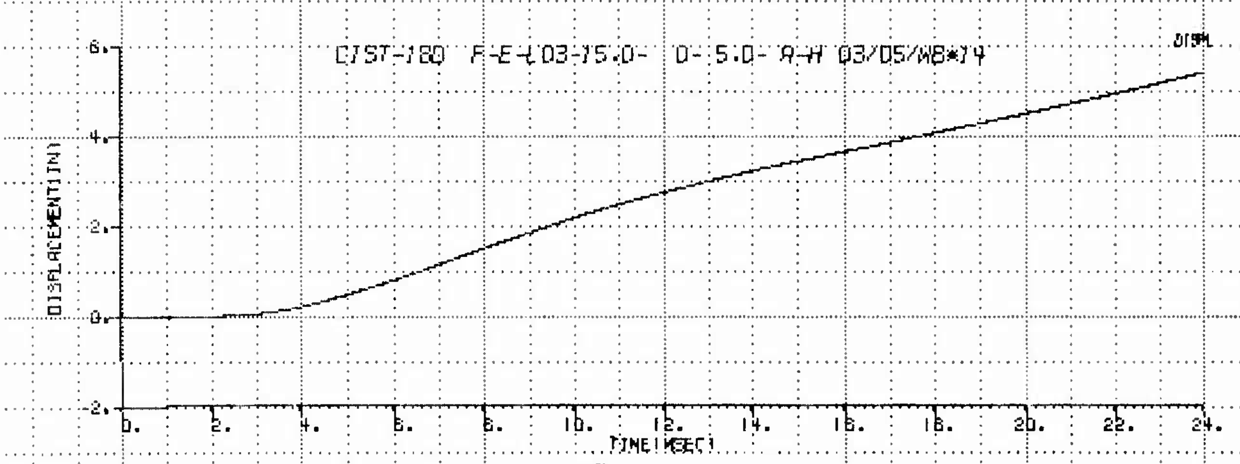
DIST-180 F-E-L03-75.0- 0-5.0- A-H 03/05/WB*74
DISPLACEMENT(IN)
DISPL
6.
4.
2.
0.
-2.
0.
2.
4.
6.
8.
10.
12.
14.
16.
18.
20.
22.
24.
TIME(MSEC)

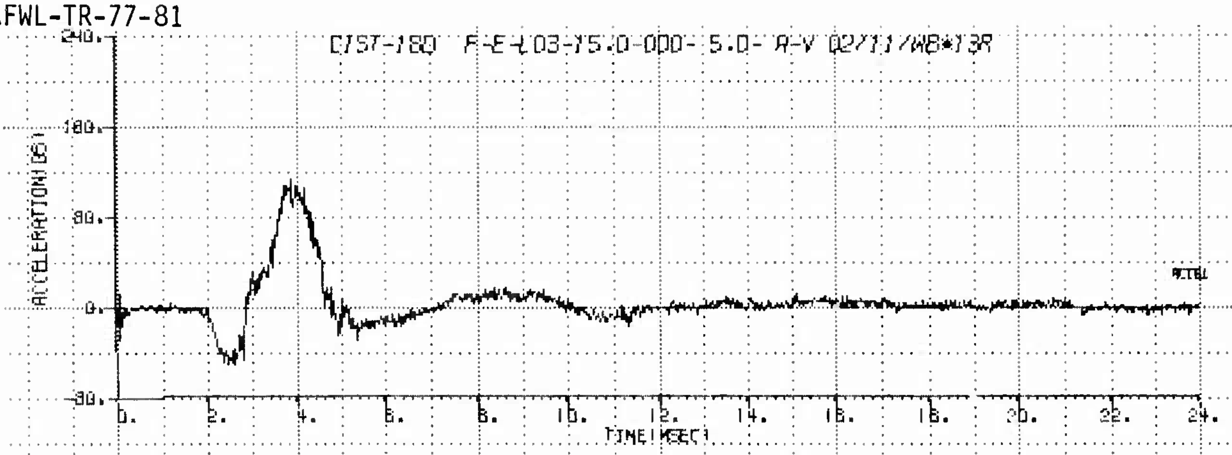
DIST-180 A-E-L03-T5.0-000- 5.0- A-V 02/11/WB*13R
ACCELERATION(GS)
ACCEL
TIME(MSEC)

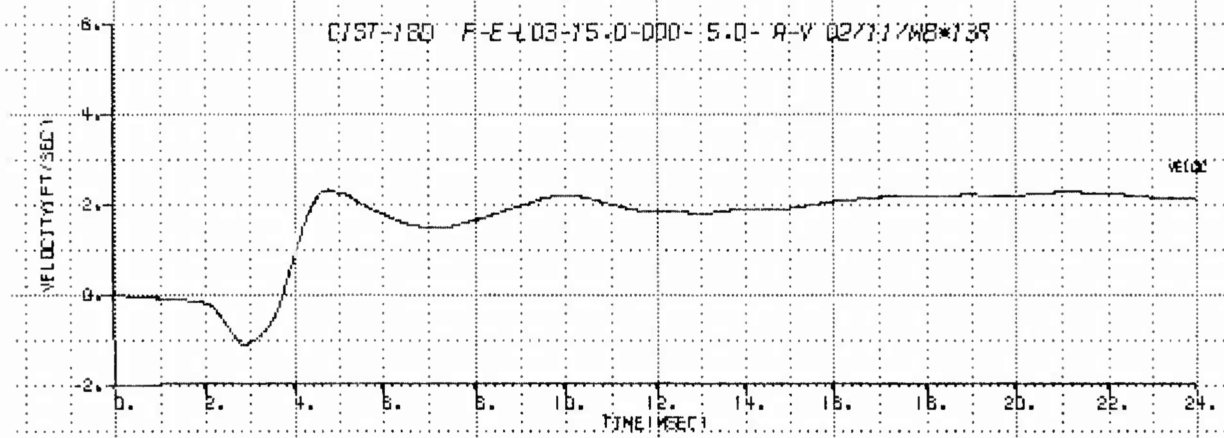
DIST-180 A-E-L03-T5.0-000- 5.0- A-V 02/11/WB*13R
VELOCITY(FT/SEC)
VEL
TIME(MSEC)

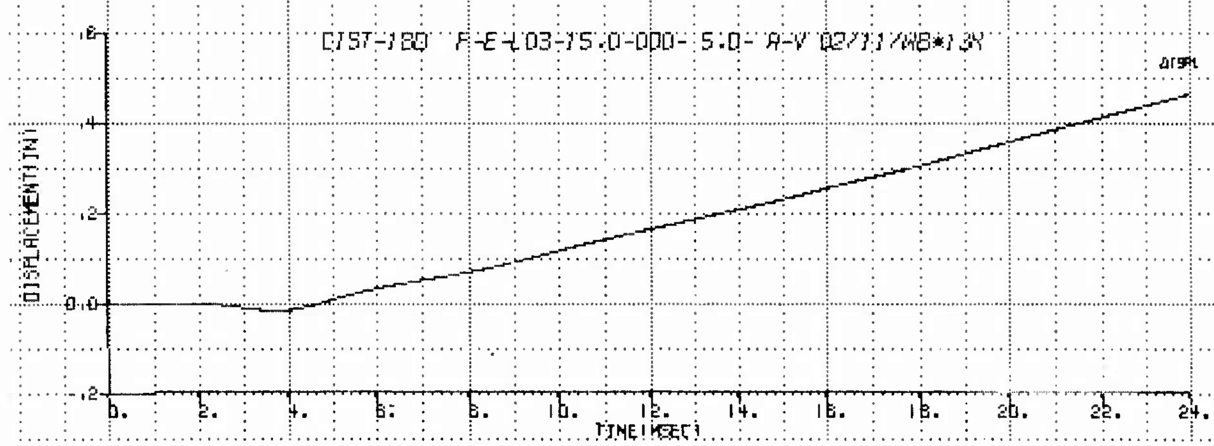
DIST-180 A-E-L03-T5.0-000- 5.0- A-V 02/11/WB*13R
DISPLACEMENT(IN)
DISPL
TIME(MSEC)

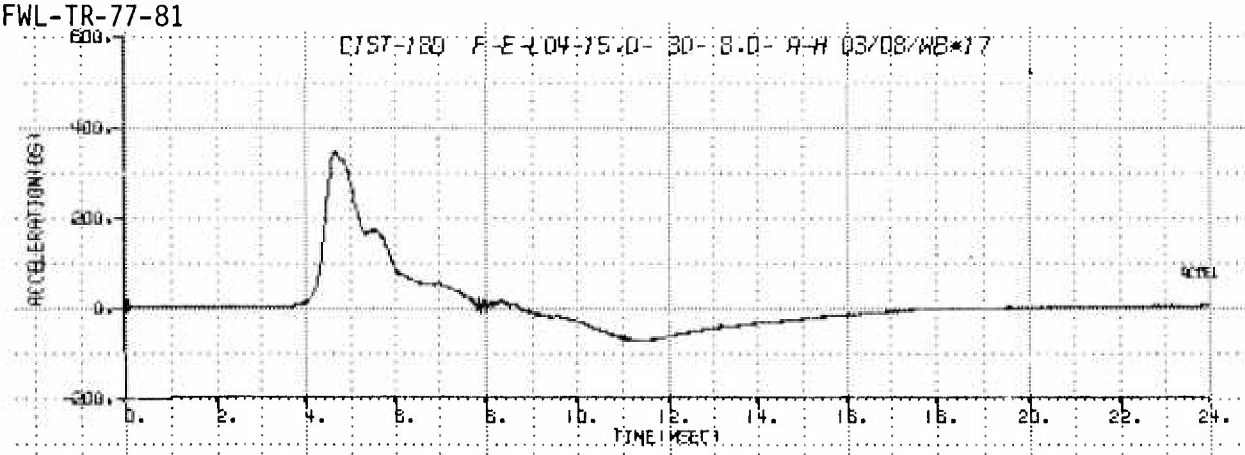
CIST-180 F-E-L04-15.0- 30- 8.0- A-H 03/08/WB*17
ACCELERATION(GS)
TIME(MSEC)
ACCEL

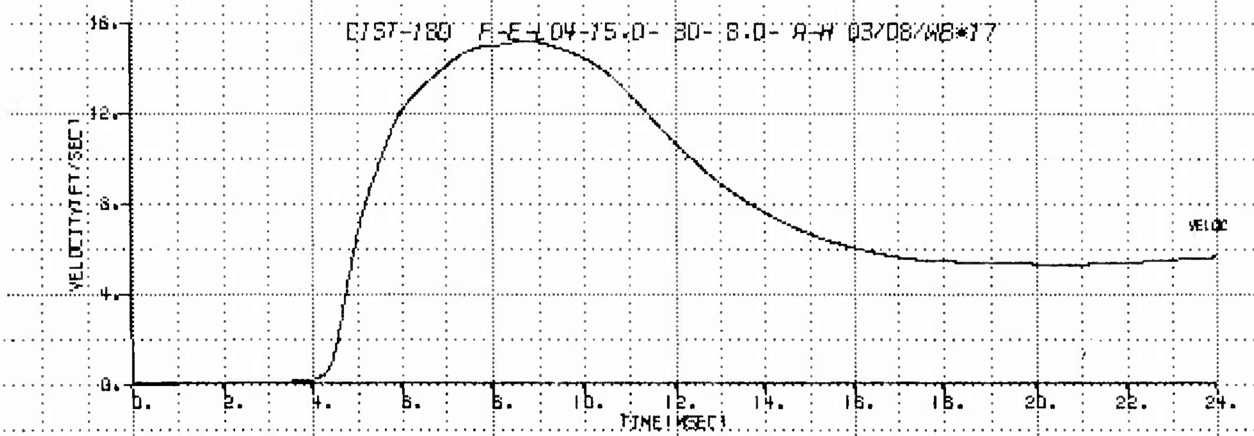
CIST-180 F-E-L04-15.0- 30- 8.0- A-H 03/08/WB*17
VELOCITY(FT/SEC)
TIME(MSEC)
VELOC

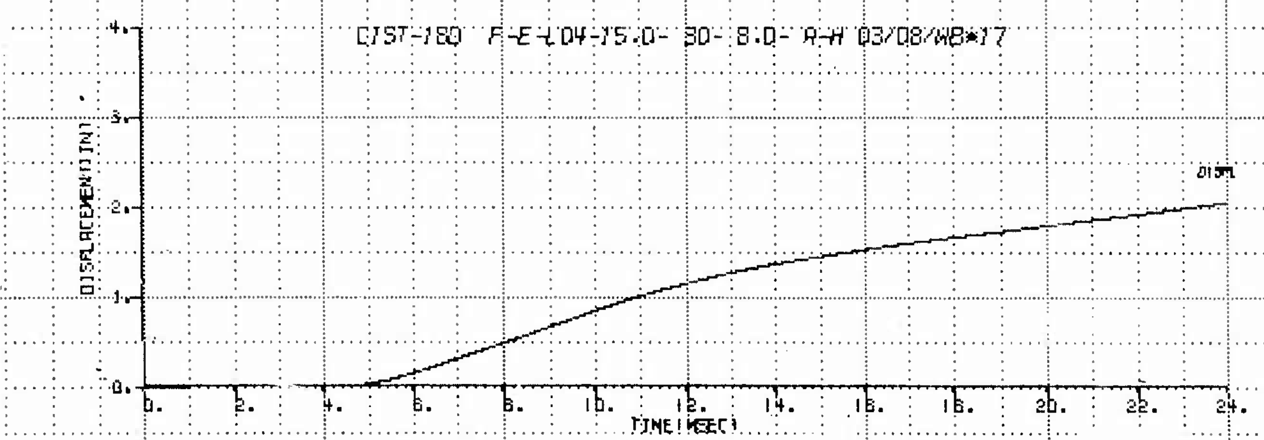
CIST-180 F-E-L04-15.0- 30- 8.0- A-H 03/08/WB*17
DISPLACEMENT(IN)
TIME(MSEC)
DISPL

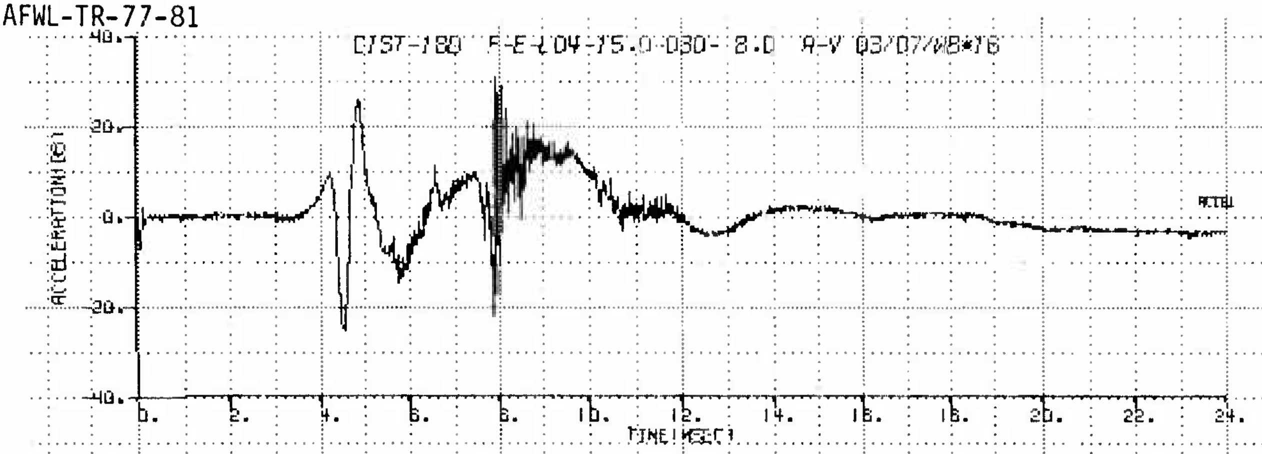
ACCELERATION(G)
TIME(MSEC)
40.
20.
0.
-20.
-40.
0. 2. 4. 6. 8. 10. 12. 14. 16. 18. 20. 22. 24.

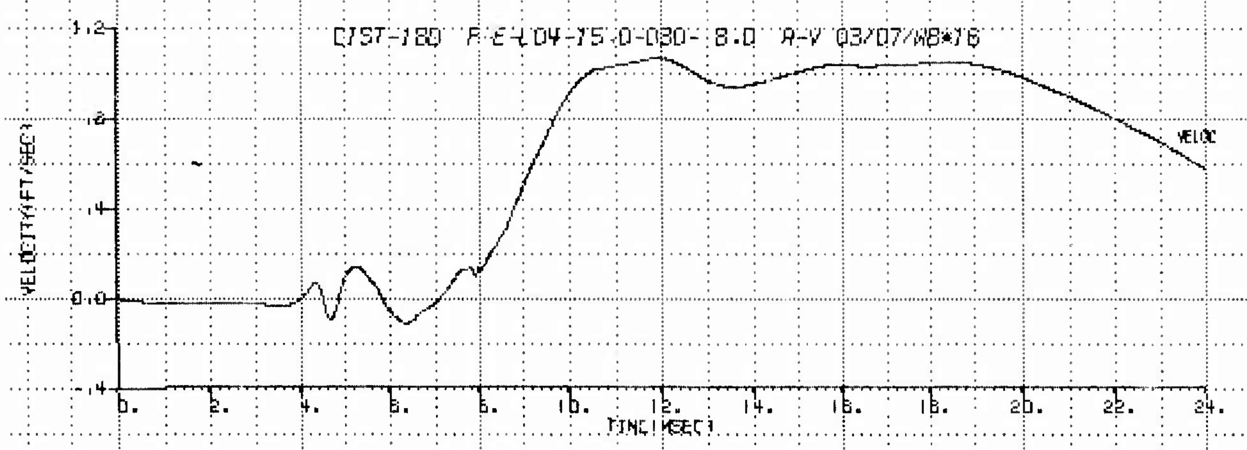
VELOCITY(FT/SEC)
TIME(MSEC)
1.2
.8
.4
0.0
-.4
0. 2. 4. 6. 8. 10. 12. 14. 16. 18. 20. 22. 24.

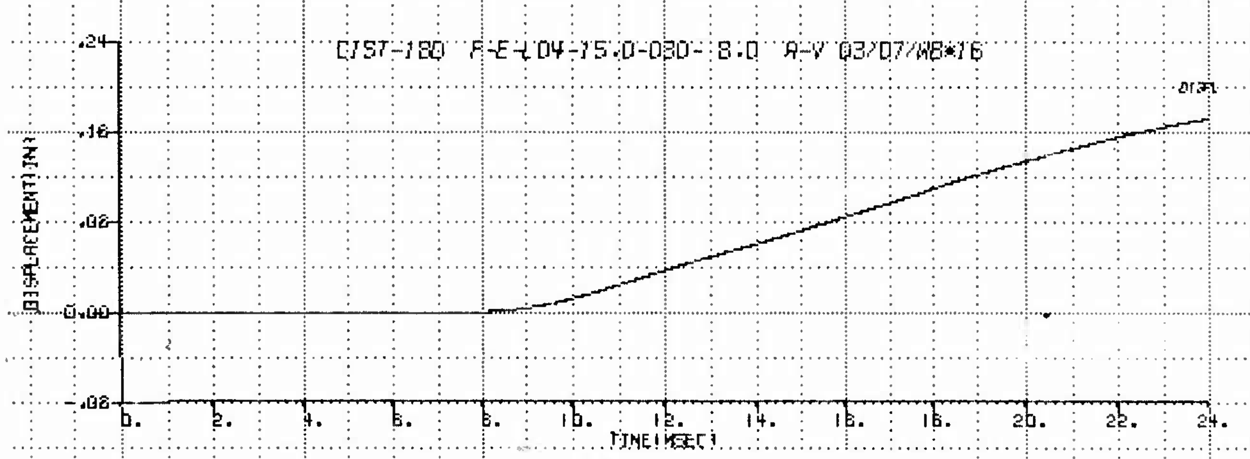
DISPLACEMENT(IN)
TIME(MSEC)
.24
.16
.08
0.00
-.08
0. 2. 4. 6. 8. 10. 12. 14. 16. 18. 20. 22. 24.

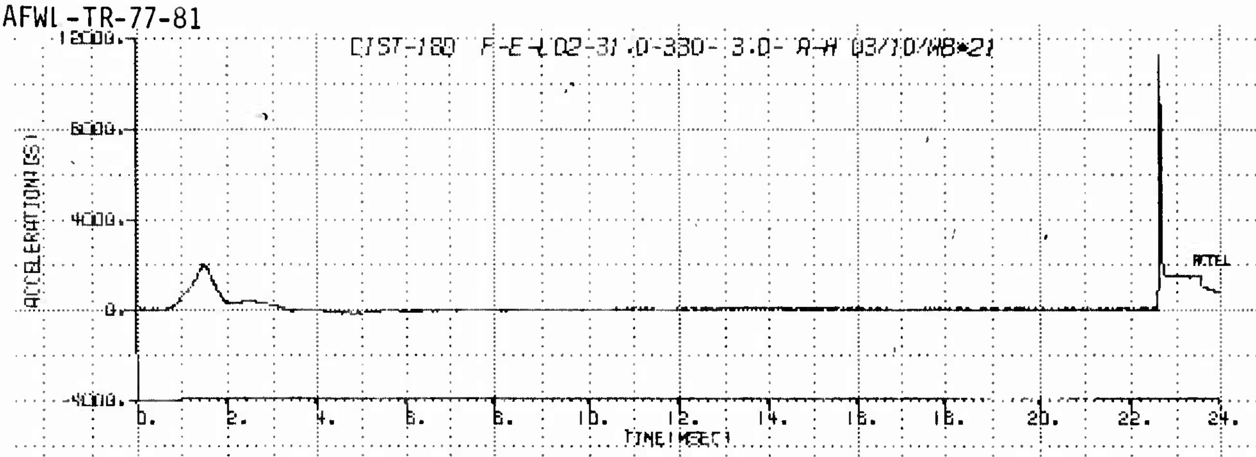
DIST-180 F-E-L 02-31.0-330- 3.0- A-H 03/10/WB*21
ACCELERATION(G)
TIME(MSEC)
ACCEL

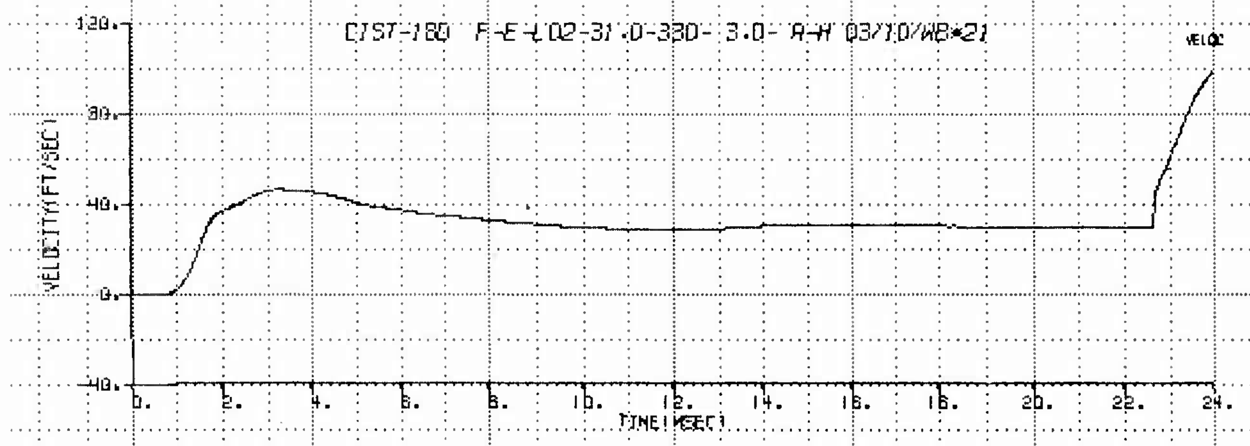
DIST-180 F-E-L 02-31.0-330- 3.0- A-H 03/10/WB*21
VELOCITY(FT/SEC)
TIME(MSEC)
VELOC

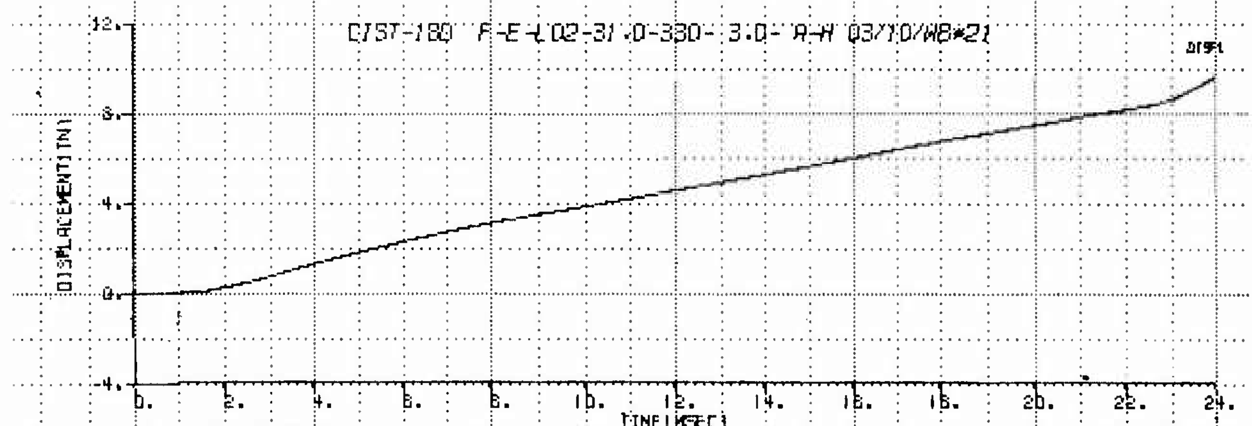
DIST-180 F-E-L 02-31.0-330- 3.0- A-H 03/10/WB*21
DISPLACEMENT(IN)
TIME(MSEC)
DISPL

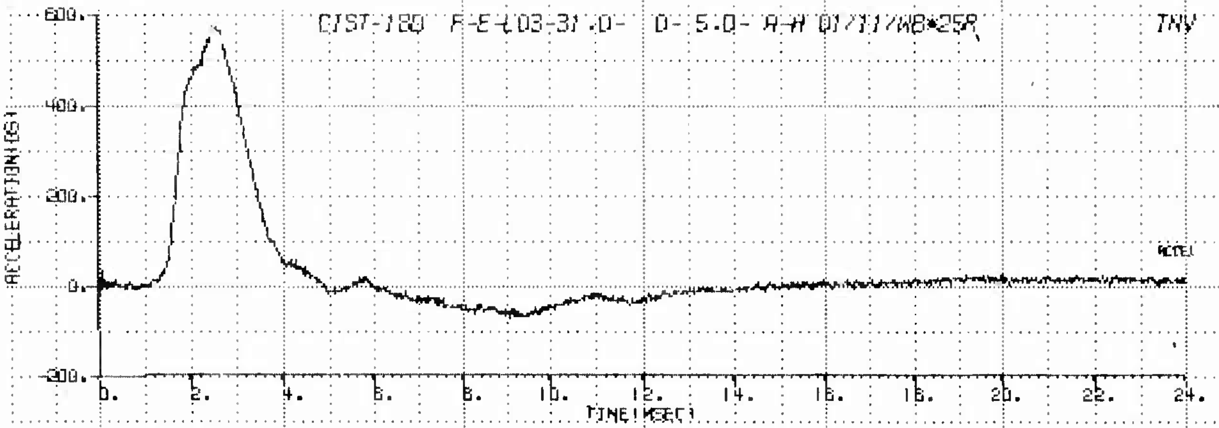
TNV
ACCELERATION(G'S)
600.
400.
200.
0.
-200.
ACCEL
0.
2.
4.
6.
8.
10.
12.
14.
16.
18.
20.
22.
24.
TIME(MSEC)

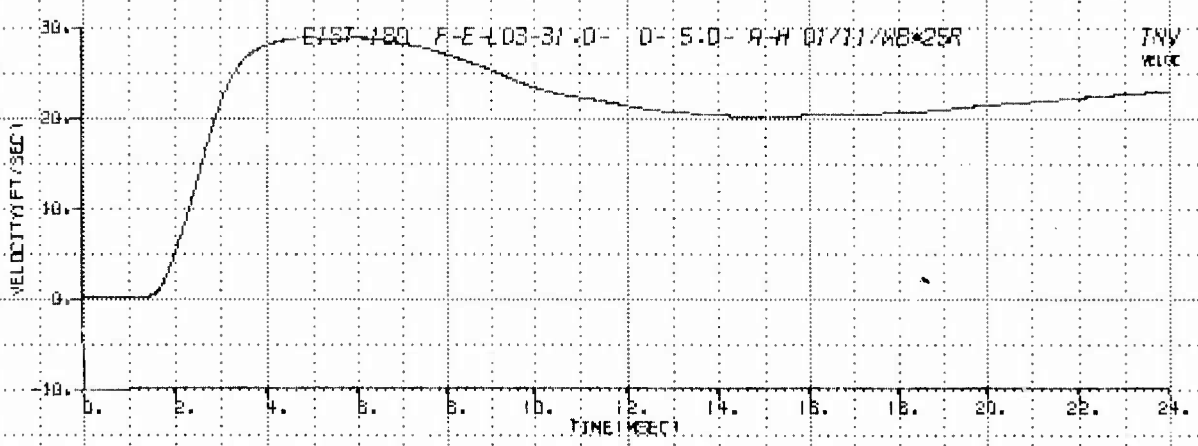
TNV
VELOC
VELOCITY(FT/SEC)
30.
20.
10.
0.
-10.
0.
2.
4.
6.
8.
10.
12.
14.
16.
18.
20.
22.
24.
TIME(MSEC)

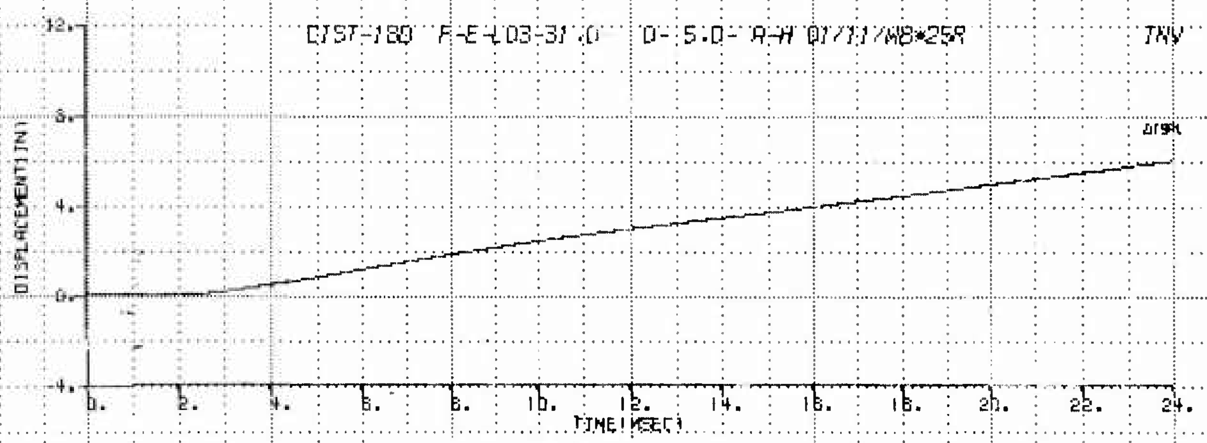
TNV
DISPL
DISPLACEMENT(IN)
12.
8.
4.
0.
-4.
0.
2.
4.
6.
8.
10.
12.
14.
16.
18.
20.
22.
24.
TIME(MSEC)

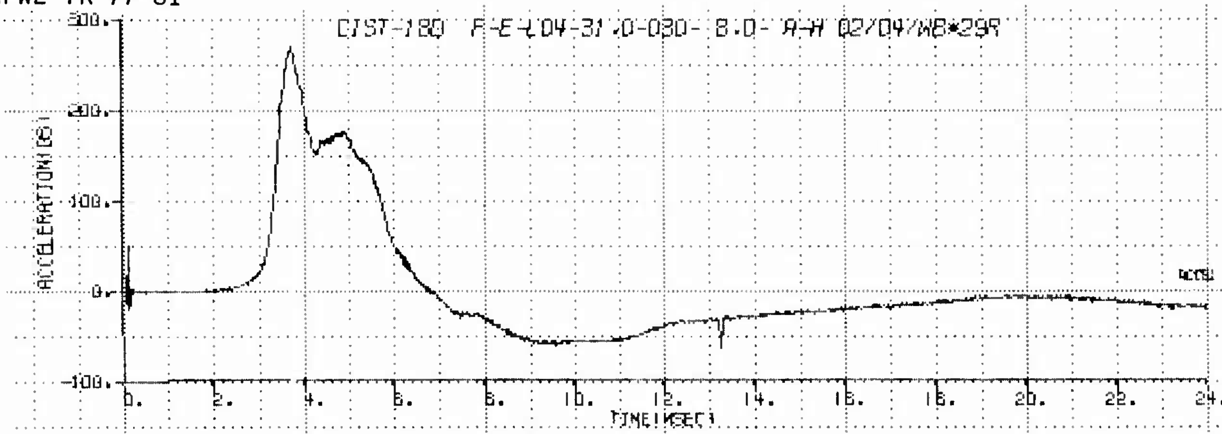
CIST-180 F-E-L04-31-0-030- 8.0- A-H 02/04/WB*29R
ACCELERATION(GS)
300.
200.
100.
0.
-100.
0. 2. 4. 6. 8. 10. 12. 14. 16. 18. 20. 22. 24.
TIME(MSEC)

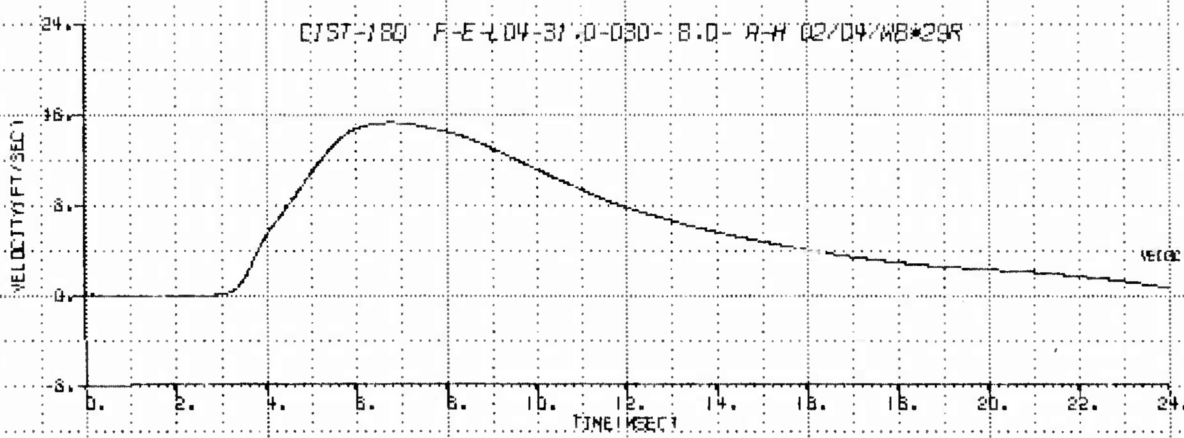
CIST-180 F-E-L04-31-0-030- 8.0- A-H 02/04/WB*29R
VELOCITY(FT/SEC)
24.
16.
8.
0.
-8.
0. 2. 4. 6. 8. 10. 12. 14. 16. 18. 20. 22. 24.
TIME(MSEC)

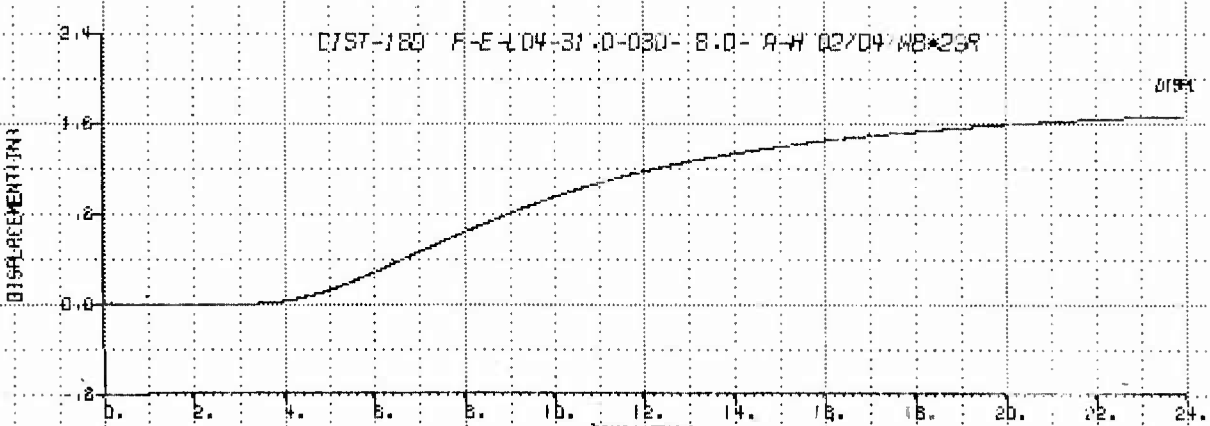
CIST-180 F-E-L04-31-0-030- 8.0- A-H 02/04/WB*29R
DISPLACEMENT(IN)
0.0
0. 2. 4. 6. 8. 10. 12. 14. 16. 18. 20. 22. 24.
TIME(MSEC)

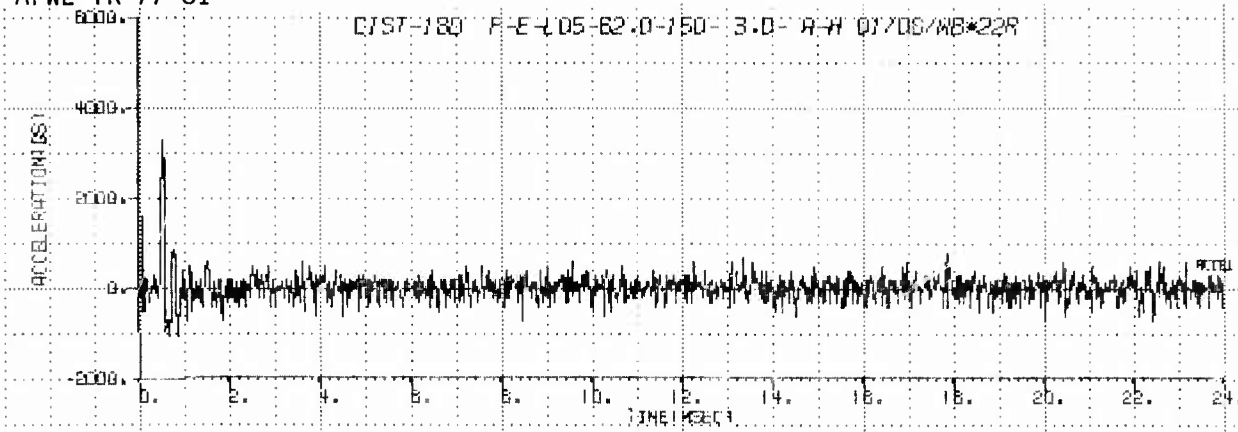

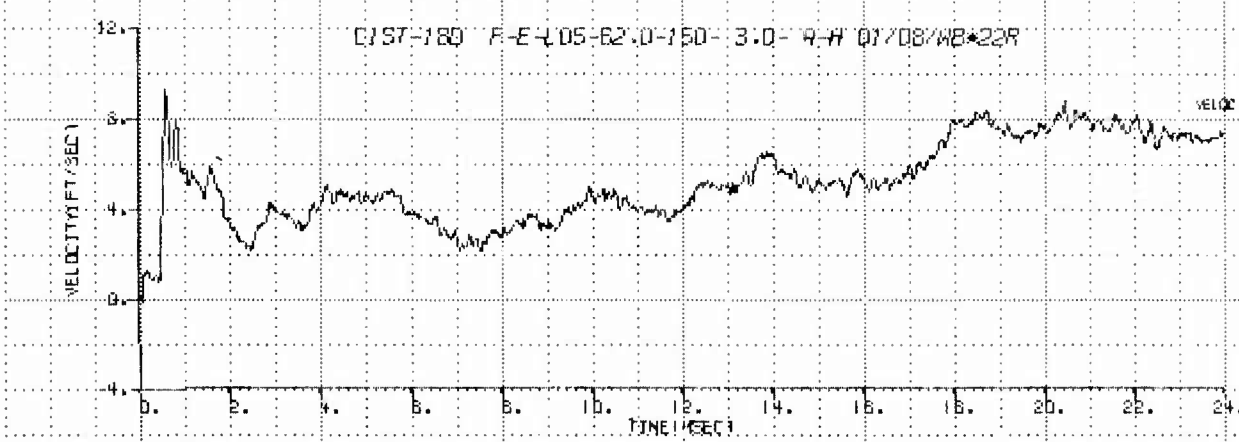

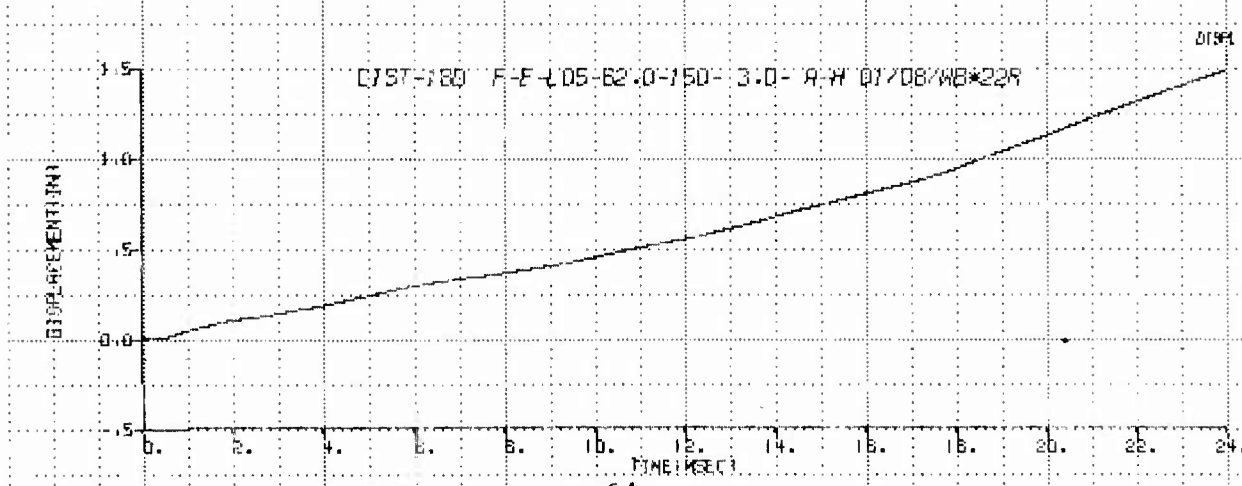

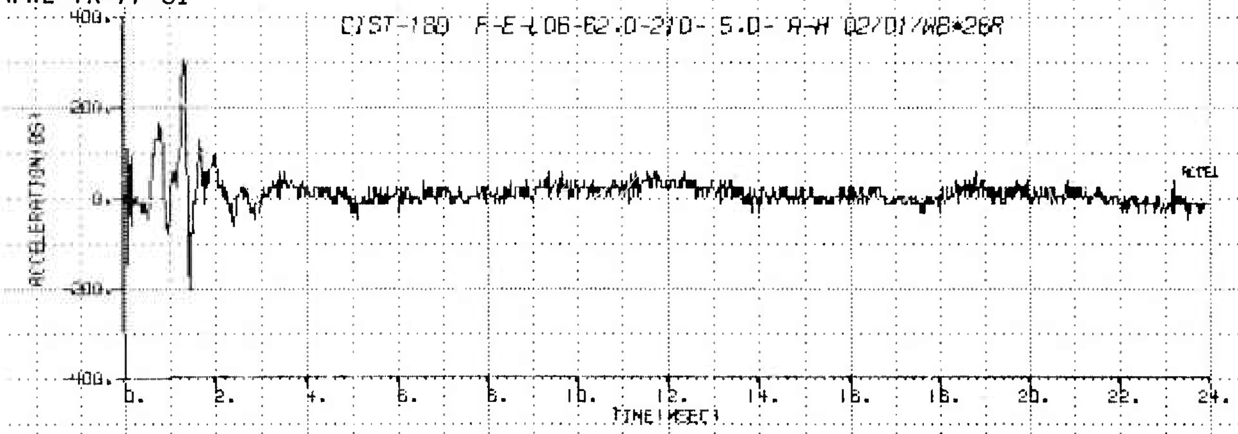
CIST-180 F-E-L06-62.0-270-5.0-A-H 02/01/WB*26R
ACCEL
ACCELERATION(GS)
TIME(MSEC)

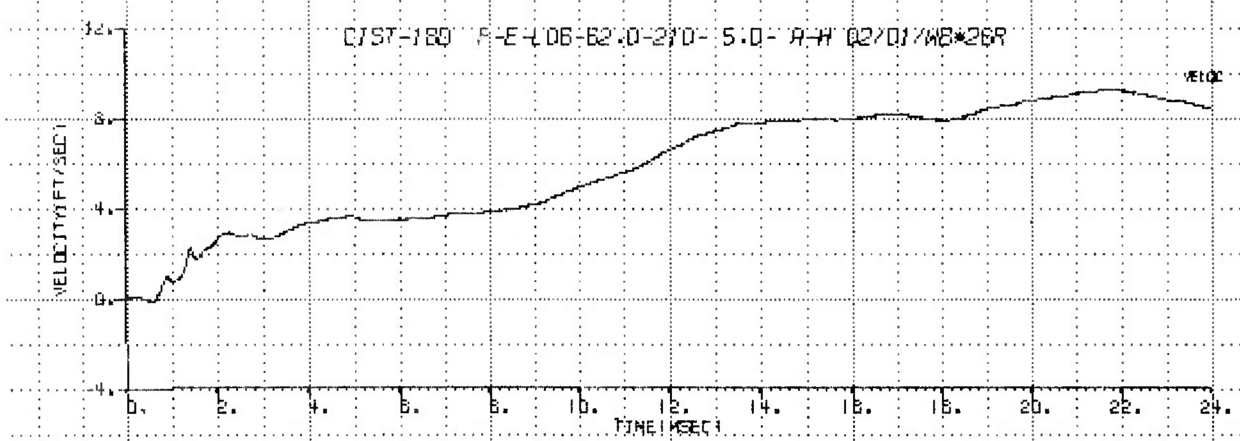
CIST-180 F-E-L06-62.0-270-5.0-A-H 02/01/WB*26R
VELOC
VELOCITY(FT/SEC)
TIME(MSEC)

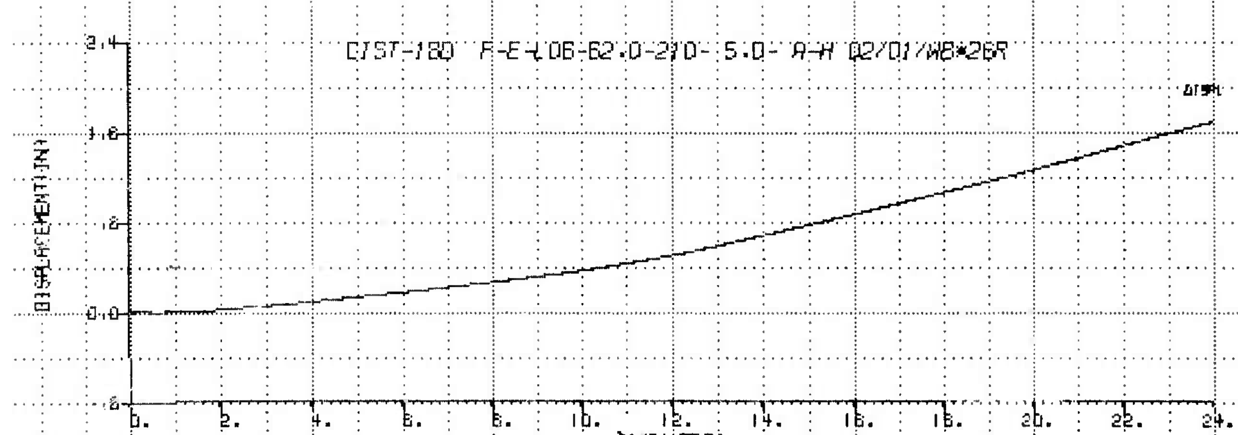
CIST-180 F-E-L06-62.0-270-5.0-A-H 02/01/WB*26R
DISPL
DISPLACEMENT(IN)
TIME(MSEC)

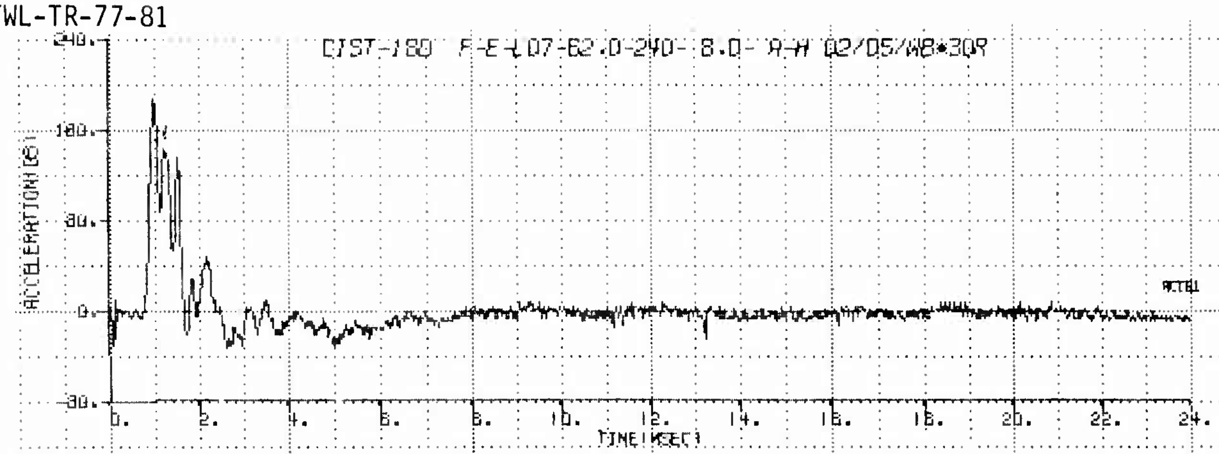
DIST-180 A-E-L07-62.0-240- 8.0- A-H 02/05/WB*30R
ACCELERATION(G)
TIME(MSEC)
ACCEL

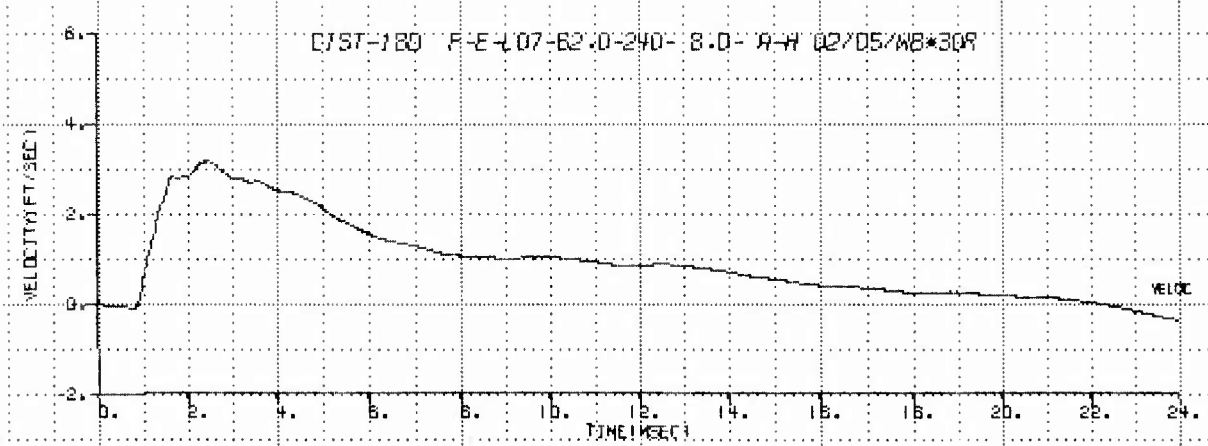
DIST-180 A-E-L07-62.0-240- 8.0- A-H 02/05/WB*30R
VELOCITY(FT/SEC)
TIME(MSEC)
VELOC

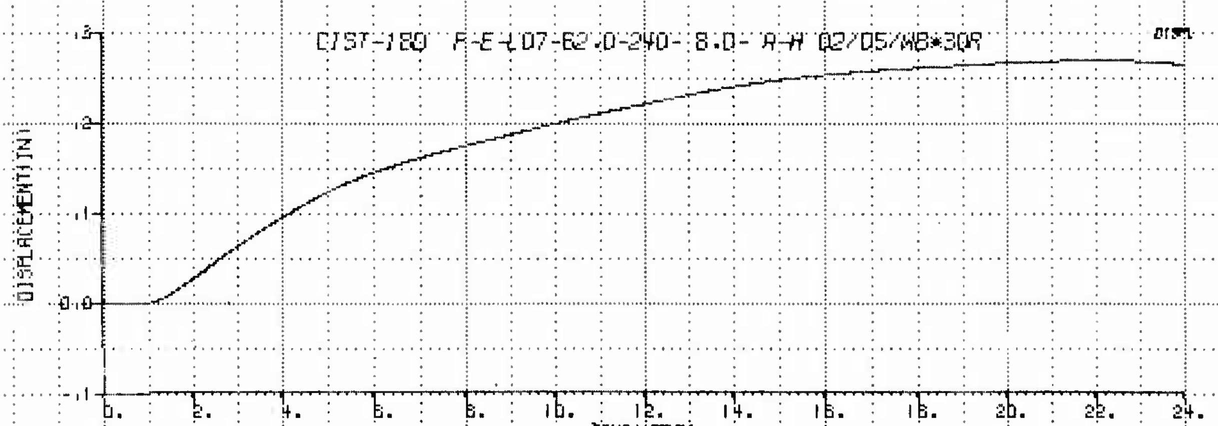
DIST-180 A-E-L07-62.0-240- 8.0- A-H 02/05/WB*30R
DISPLACEMENT(IN)
TIME(MSEC)

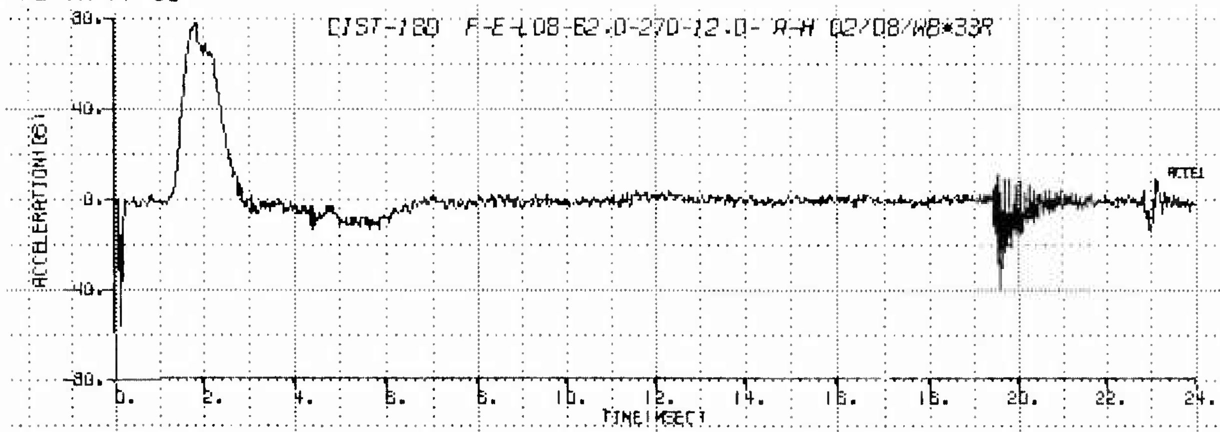
DIST-180 F-E-L08-62.0-270-12.0- A-H 02/08/WB*33R
ACCELERATION(G)
80.
40.
0.
-40.
-80.
ACCEL
0.
2.
4.
6.
8.
10.
12.
14.
16.
18.
20.
22.
24.
TIME(MSEC)

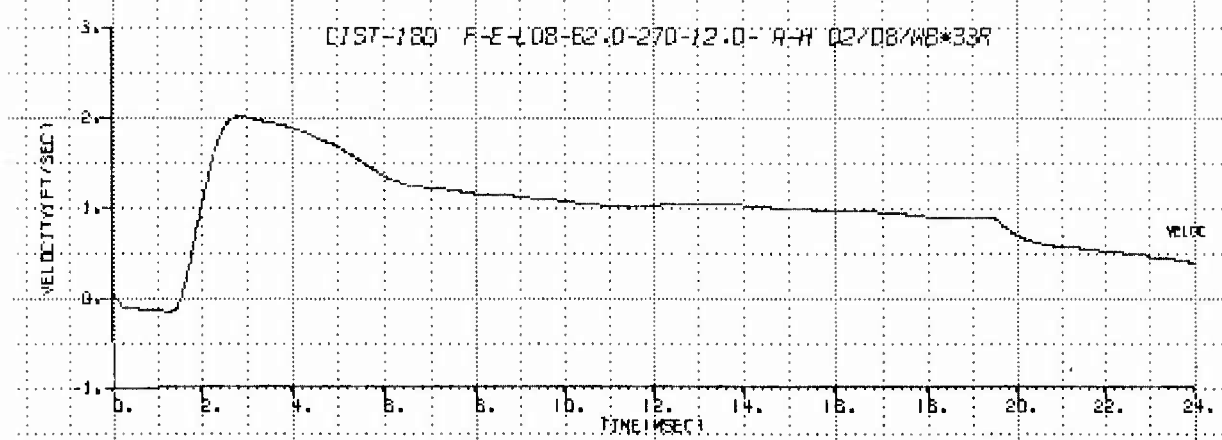
DIST-180 F-E-L08-62.0-270-12.0- A-H 02/08/WB*33R
VELOCITY(FT/SEC)
3.
2.
1.
0.
-1.
VELOC
0.
2.
4.
6.
8.
10.
12.
14.
16.
18.
20.
22.
24.
TIME(MSEC)

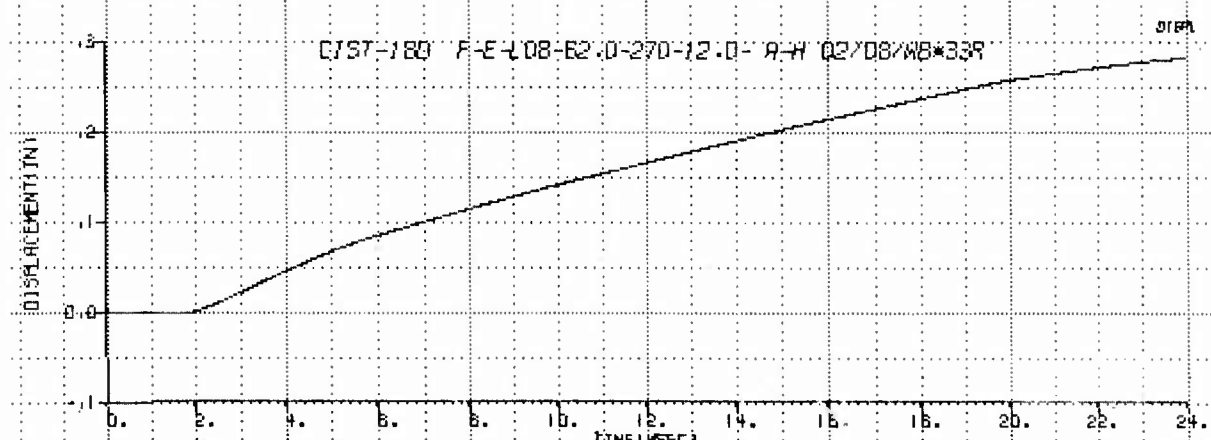
DIST-180 F-E-L08-62.0-270-12.0- A-H 02/08/WB*33R
DISPLACEMENT(IN)
.3
.2
.1
0.0
-.1
DISPL
0.
2.
4.
6.
8.
10.
12.
14.
16.
18.
20.
22.
24.
TIME(MSEC)

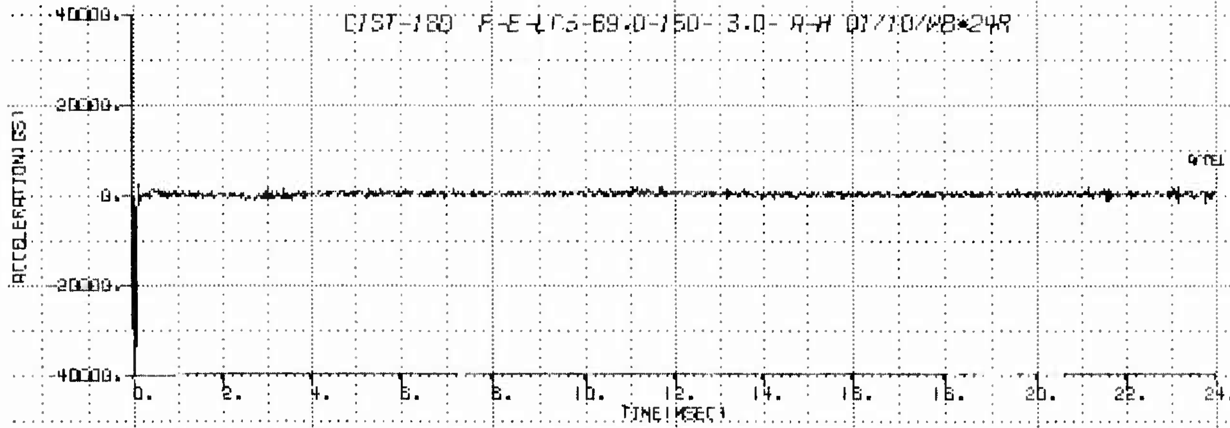
DIST-180 F-E-L05-69.0-150- 3.0- A-H 01710/WB*24R
ACCELERATION(GS)
40000.
20000.
0.
-20000.
-40000.
ACCEL
0.
2.
4.
6.
8.
10.
12.
14.
16.
18.
20.
22.
24.
TIME(MSEC)

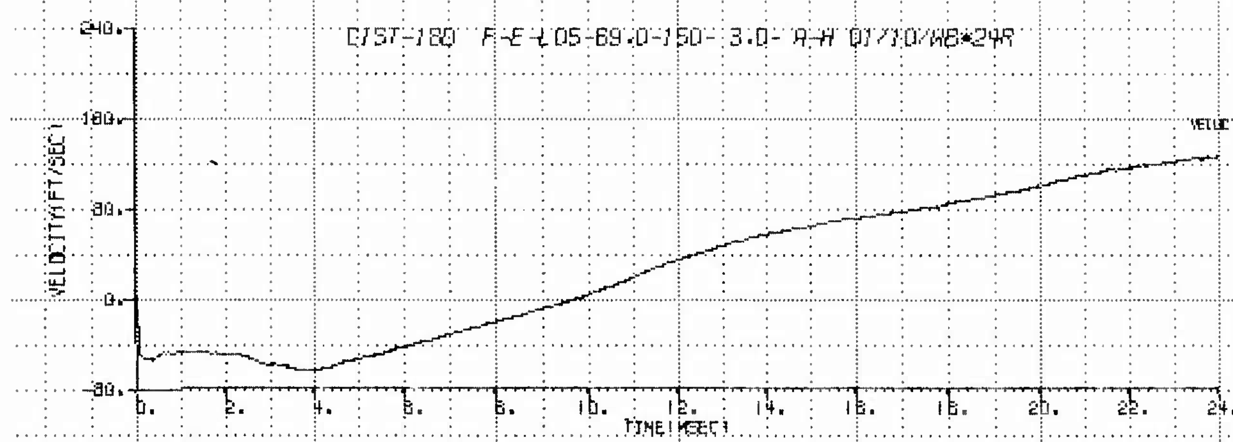
DIST-180 F-E-L05-69.0-150- 3.0- A-H 01710/WB*24R
VELOCITY(FT/SEC)
240.
160.
80.
0.
-80.
VELOC
0.
2.
4.
6.
8.
10.
12.
14.
16.
18.
20.
22.
24.
TIME(MSEC)

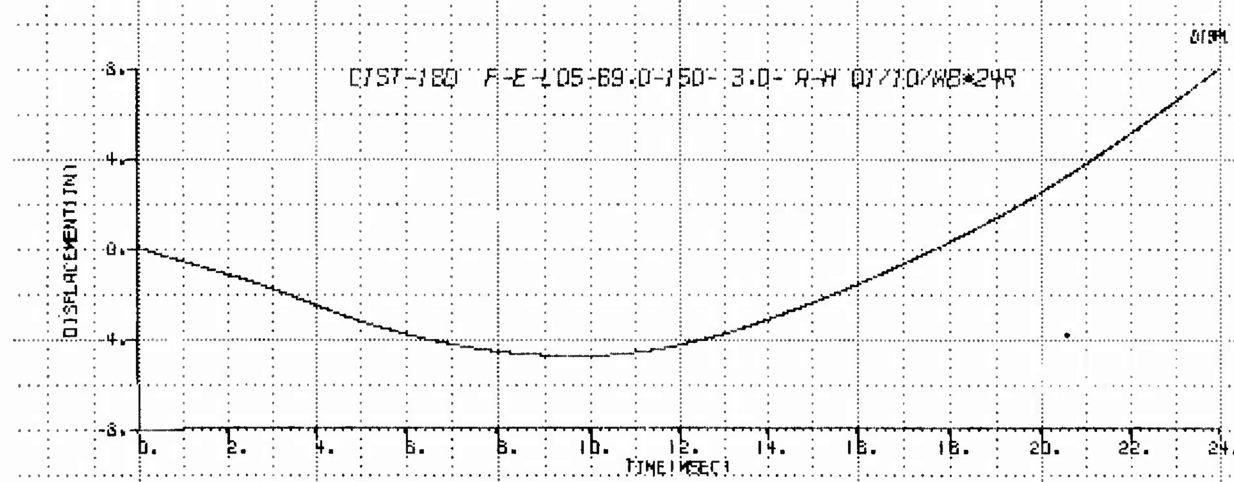
DIST-180 F-E-L05-69.0-150- 3.0- A-H 01710/WB*24R
DISPLACEMENT(IN)
8.
4.
0.
-4.
-8.
DISPL
0.
2.
4.
6.
8.
10.
12.
14.
16.
18.
20.
22.
24.
TIME(MSEC)

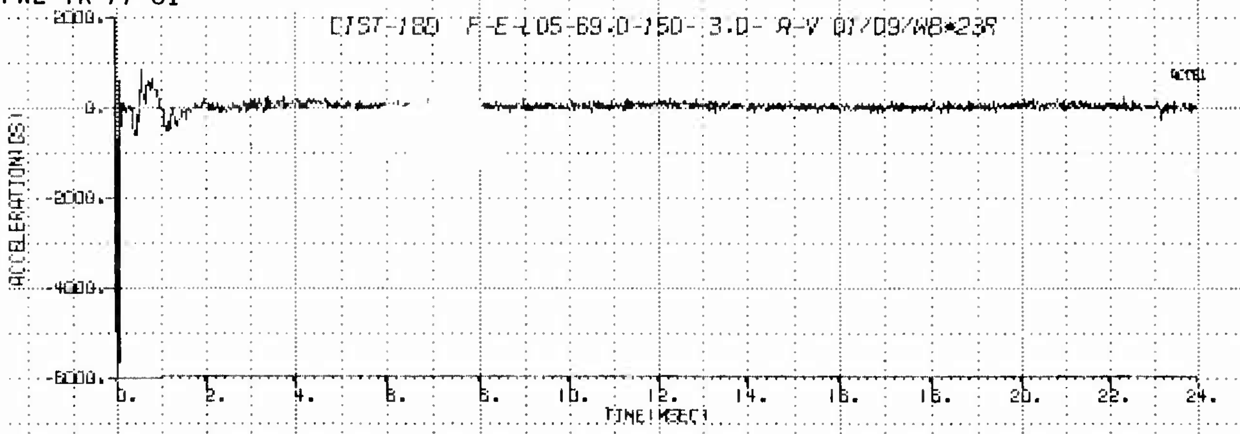
DIST-180 F-E-L05-69.0-150- 3.0- A-V 01/09/WB*23R
ACCEL
ACCELERATION(GS)
2000.
0.
-2000.
-4000.
-6000.
0. 2. 4. 6. 8. 10. 12. 14. 16. 18. 20. 22. 24.
TIME(MSEC)

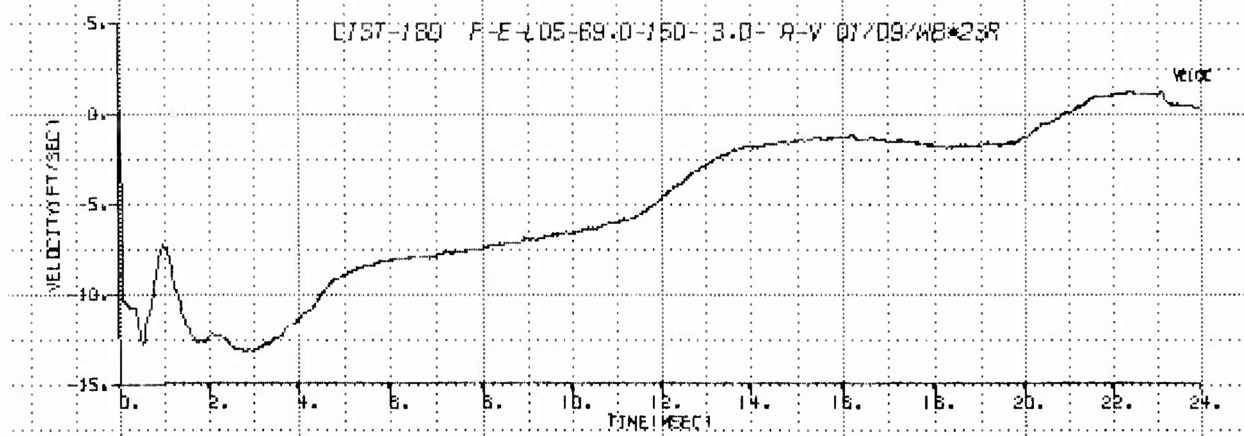
DIST-180 F-E-L05-69.0-150- 3.0- A-V 01/09/WB*23R
VELOC
VELOCITY(FT/SEC)
5.
0.
-5.
-10.
-15.
0. 2. 4. 6. 8. 10. 12. 14. 16. 18. 20. 22. 24.
TIME(MSEC)

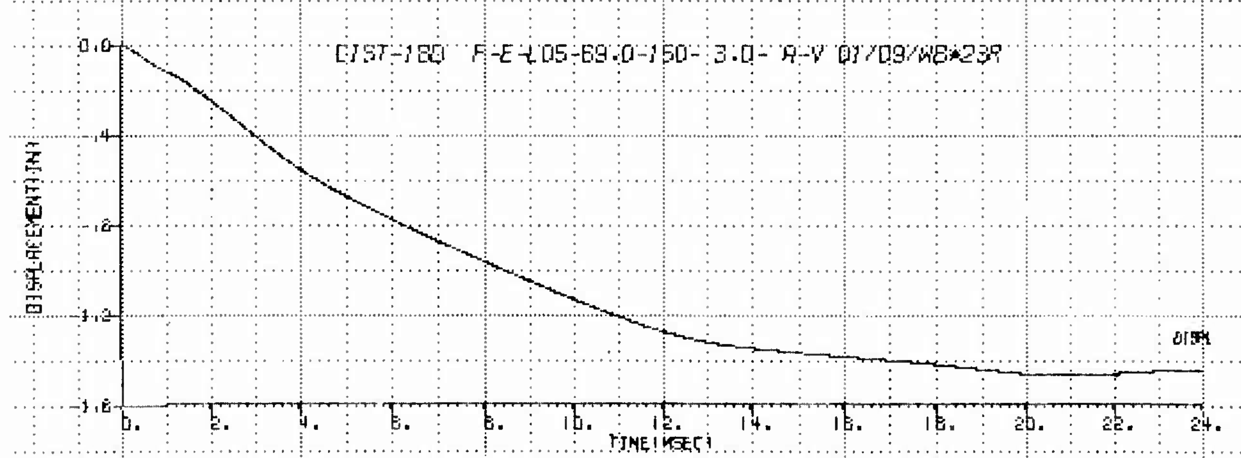
DIST-180 F-E-L05-69.0-150- 3.0- A-V 01/09/WB*23R
DISPL
DISPLACEMENT(IN)
0.0
-.4
-.8
-1.2
-1.6
0. 2. 4. 6. 8. 10. 12. 14. 16. 18. 20. 22. 24.
TIME(MSEC)

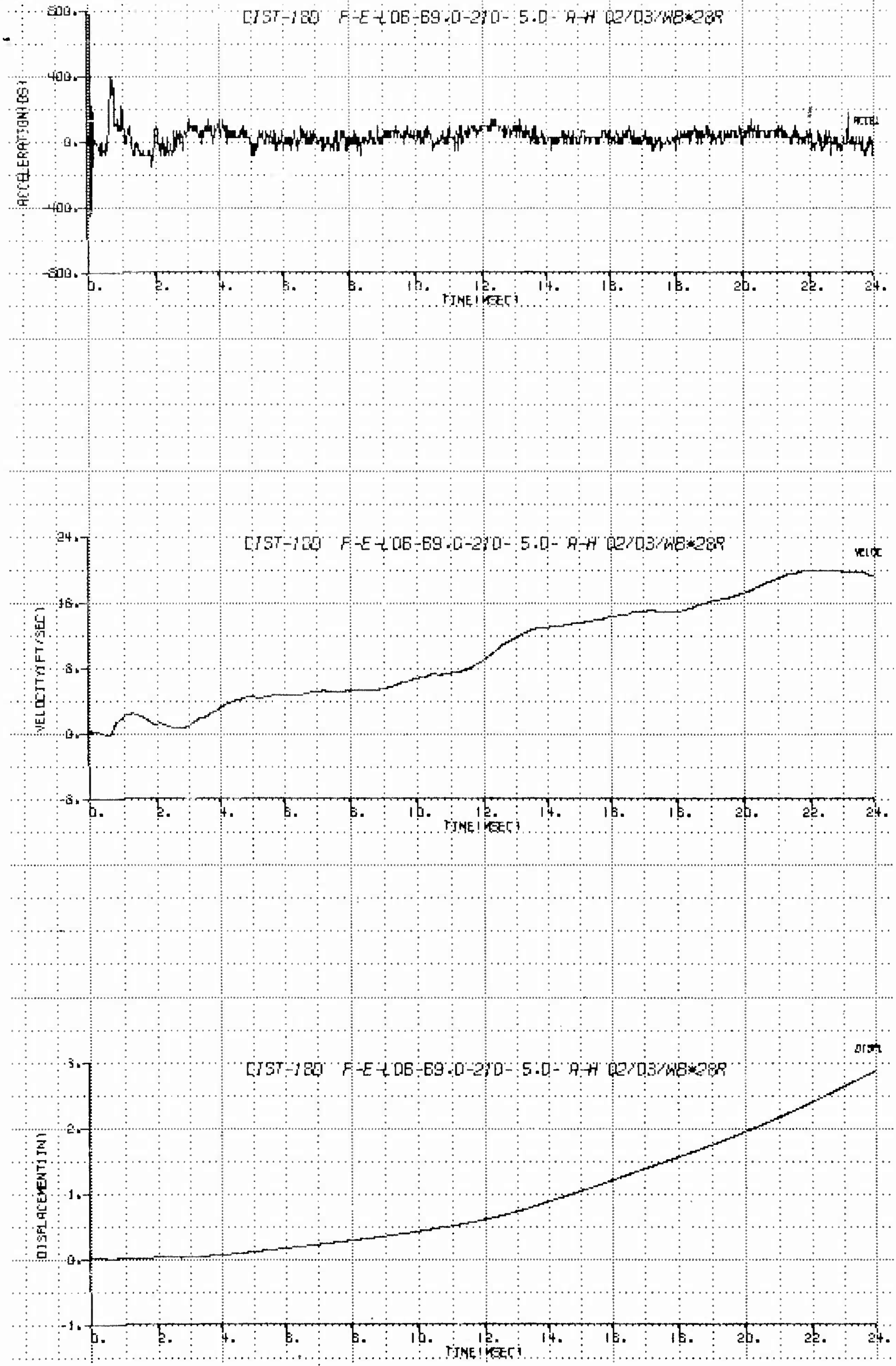
DIST-180 A-E-LOB-B9-0-270-5.0-A-H 02/03/WB*28R
ACCELERATION(GS)
800.
400.
0.
-400.
-800.
ACCEL
0. 2. 4. 6. 8. 10. 12. 14. 16. 18. 20. 22. 24.
TIME(MSEC)
DIST-180 A-E-LOB-B9-0-270-5.0-A-H 02/03/WB*28R
VELOCITY(FT/SEC)
24.
16.
8.
0.
-8.
VELOC
0. 2. 4. 6. 8. 10. 12. 14. 16. 18. 20. 22. 24.
TIME(MSEC)
DIST-180 A-E-LOB-B9-0-270-5.0-A-H 02/03/WB*28R
DISPLACEMENT(IN)
3.
2.
1.
0.
-1.
DISPL
0. 2. 4. 6. 8. 10. 12. 14. 16. 18. 20. 22. 24.
TIME(MSEC)

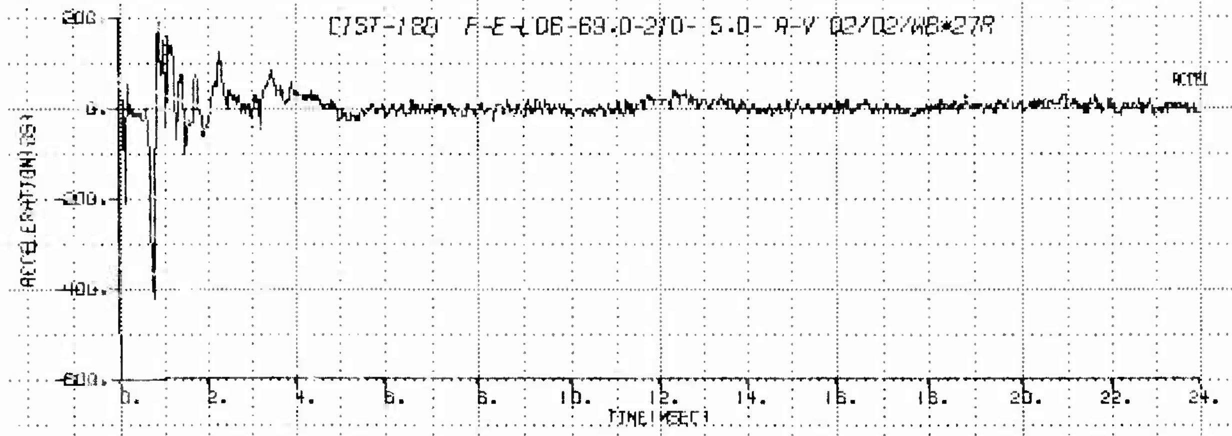
DIST-180 F-E-L DB-69.0-270- 5.0- A-V 02/02/WB*27R
ACCEL
ACCELERATION(G)
200.
0.
-200.
-400.
-600.
0.
2.
4.
6.
8.
10.
12.
14.
16.
18.
20.
22.
24.
TIME(MSEC)

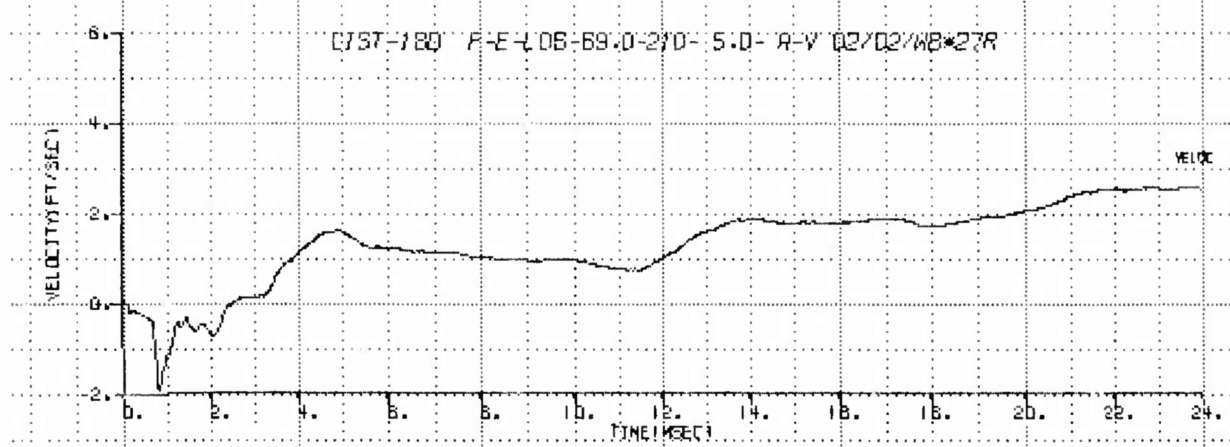
DIST-180 F-E-L DB-69.0-270- 5.0- A-V 02/02/WB*27R
VELOC
VELOCITY(FT/SEC)
6.
4.
2.
0.
-2.
0.
2.
4.
6.
8.
10.
12.
14.
16.
18.
20.
22.
24.
TIME(MSEC)

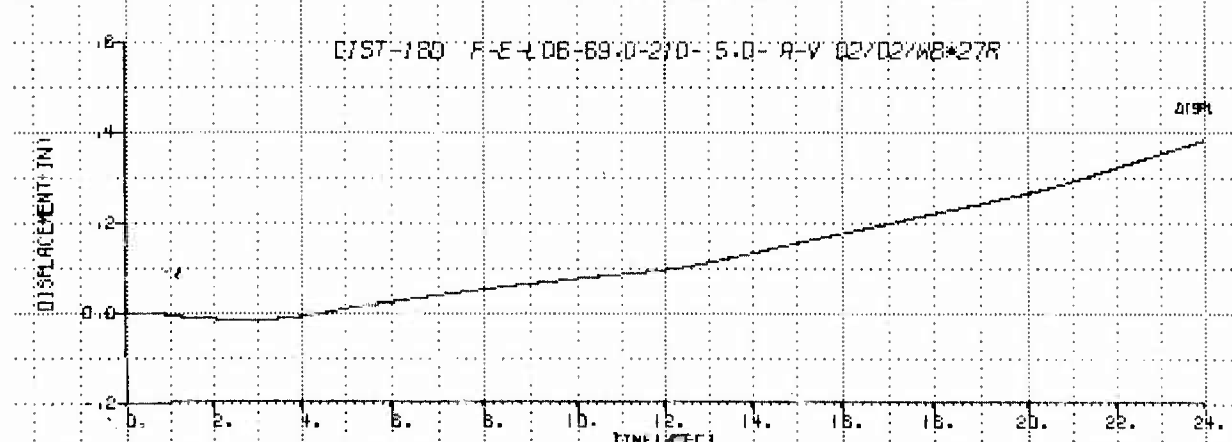
DIST-180 F-E-L DB-69.0-270- 5.0- A-V 02/02/WB*27R
DISPL
DISPLACEMENT(IN)
.6
.4
.2
0.0
-.2
0.
2.
4.
6.
8.
10.
12.
14.
16.
18.
20.
22.
24.
TIME(MSEC)

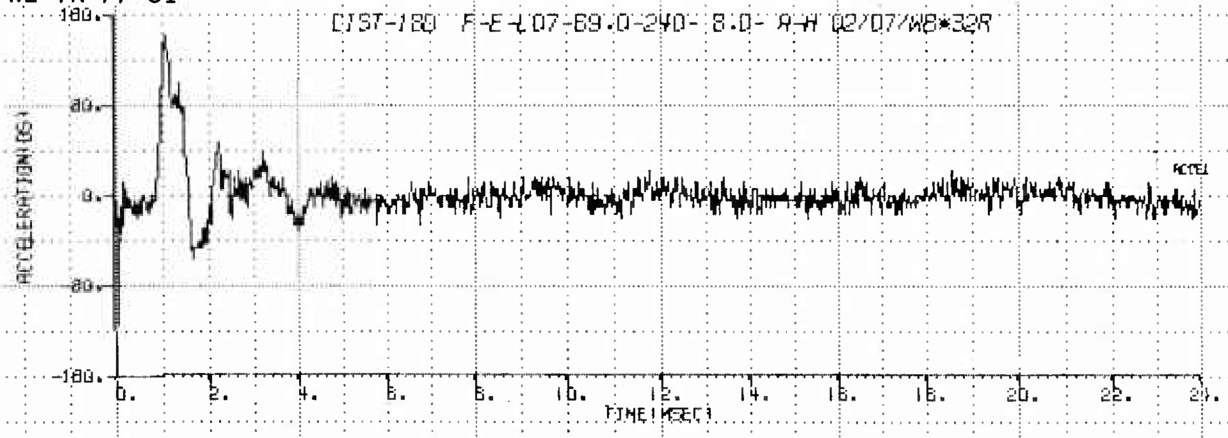
DIST-180 P-E-L07-B9.0-240- 8.0- A-H 02/07/WB*32R
ACCELERATION(GS)
ACCEL
TIME(MSEC)

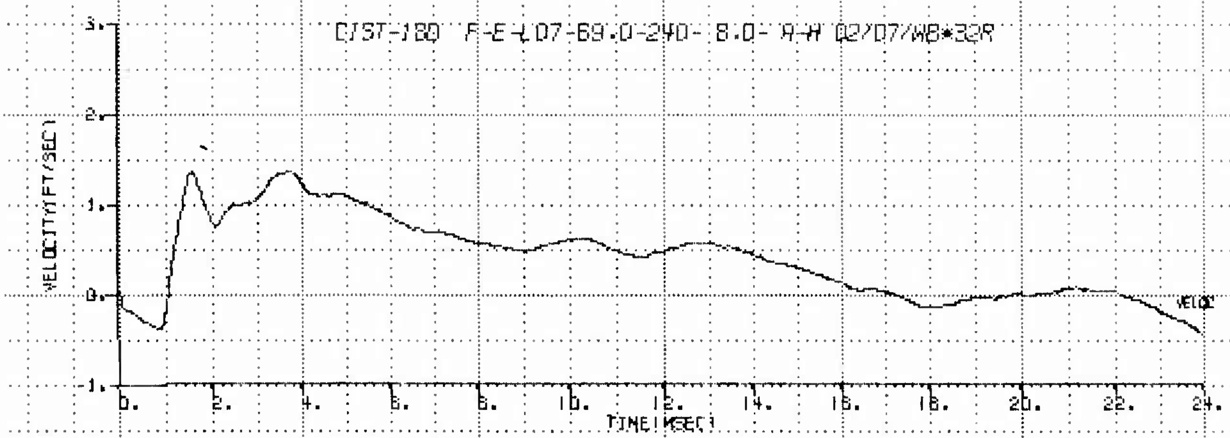
DIST-180 P-E-L07-B9.0-240- 8.0- A-H 02/07/WB*32R
VELOCITY(FT/SEC)
VELOC
TIME(MSEC)

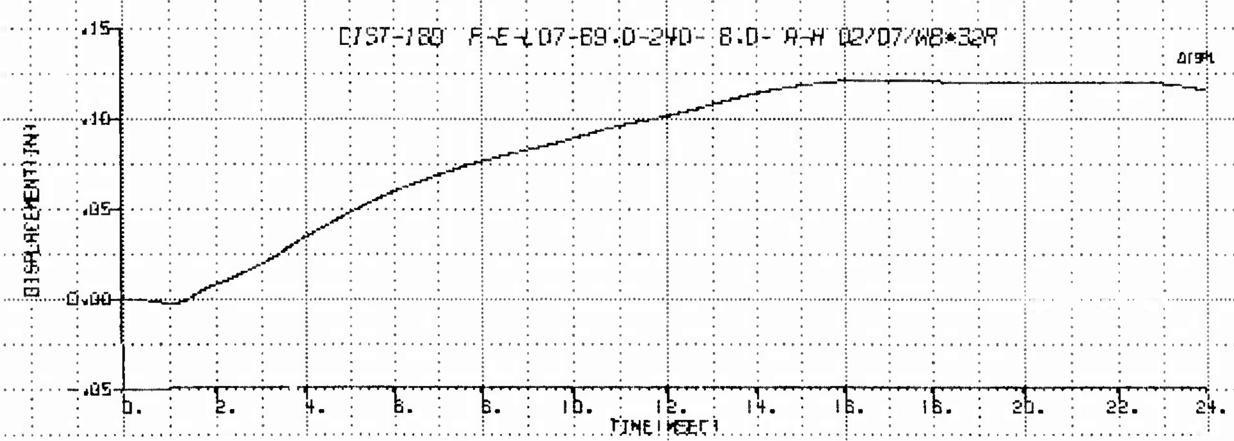
DIST-180 P-E-L07-B9.0-240- 8.0- A-H 02/07/WB*32R
DISPLACEMENT(IN)
DISPL
TIME(MSEC)

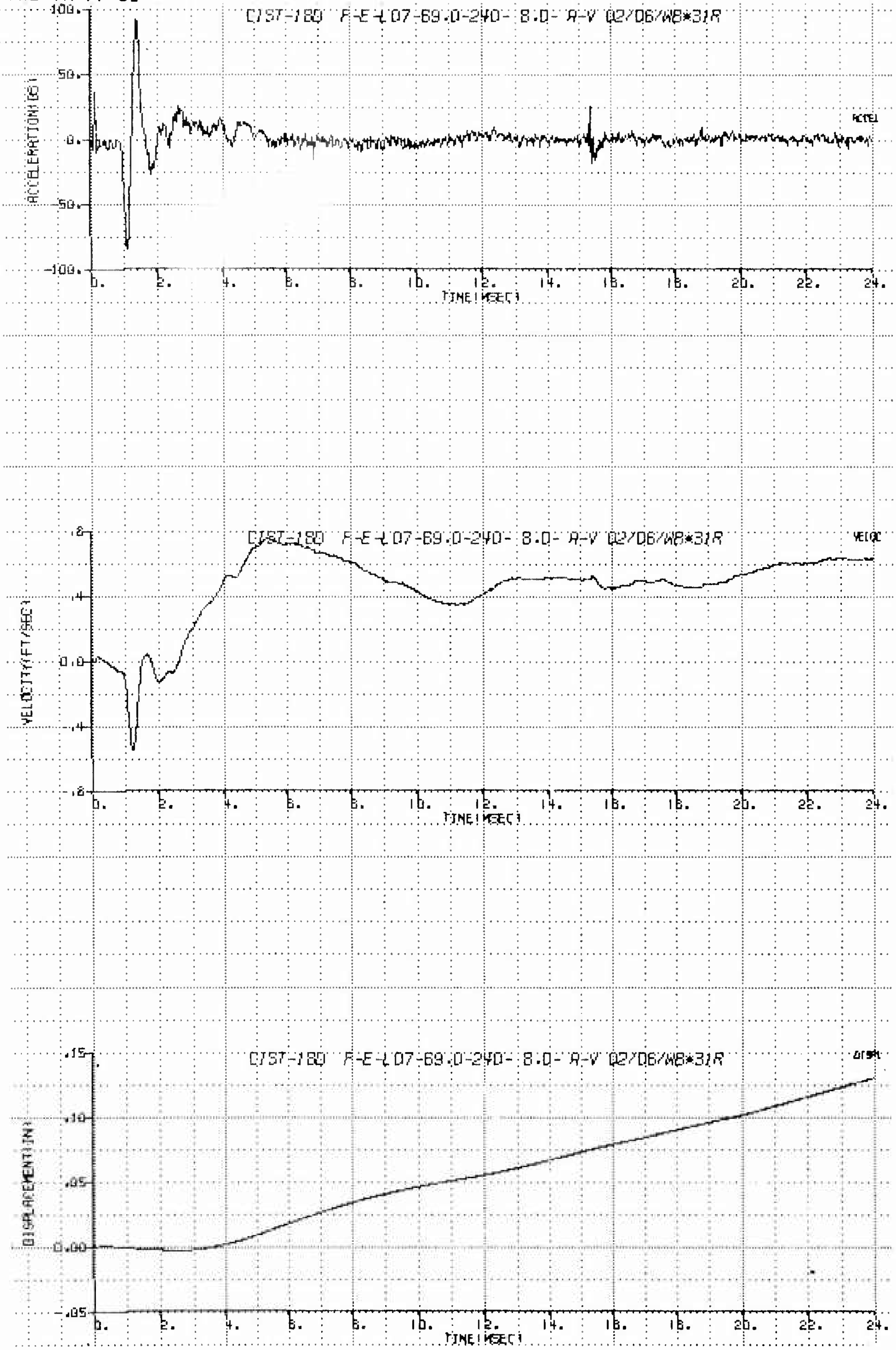
DIST-180 A-E-L07-69.0-240- 8.0- A-V 02/06/WB*31R
ACCELERATION(G)
100.
50.
0.
-50.
-100.
ACCEL
0.
2.
4.
6.
8.
10.
12.
14.
16.
18.
20.
22.
24.
TIME(MSEC)
DIST-180 A-E-L07-69.0-240- 8.0- A-V 02/06/WB*31R
VELOCITY(FT/SEC)
.8
.4
0.0
-.4
-.8
VELOC
TIME(MSEC)
DIST-180 A-E-L07-69.0-240- 8.0- A-V 02/06/WB*31R
DISPLACEMENT(IN)
.15
.10
.05
0.00
-.05
DISPL
TIME(MSEC)

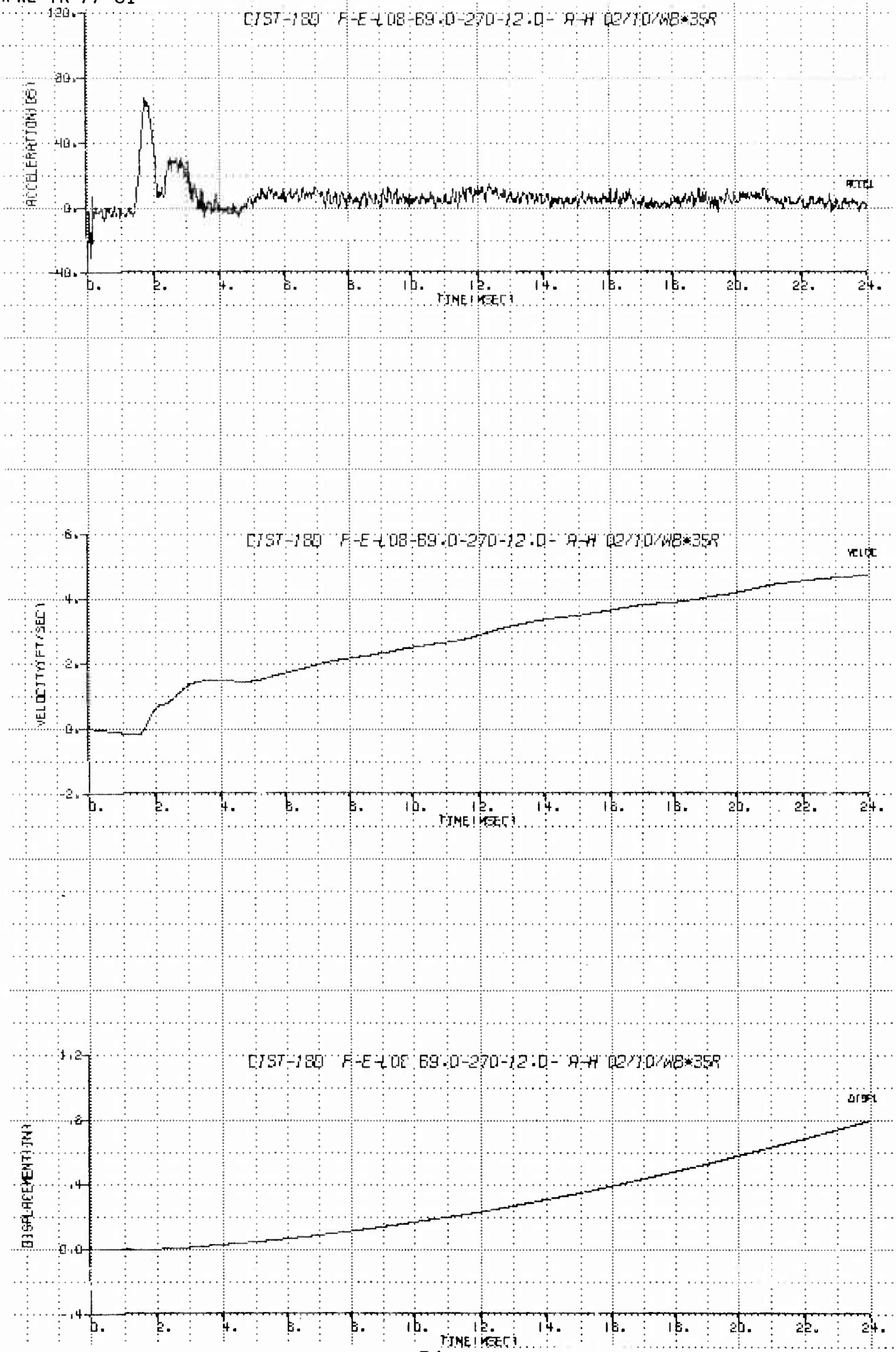
DIST-180 A-E-L08-69.0-270-12.0- A-H 02/10/WB*35R
ACCELERATION(GS)
ACCEL
TIME(MSEC)
VELOCITY(FT/SEC)
VELOC
DISPLACEMENT(IN)
DISPL

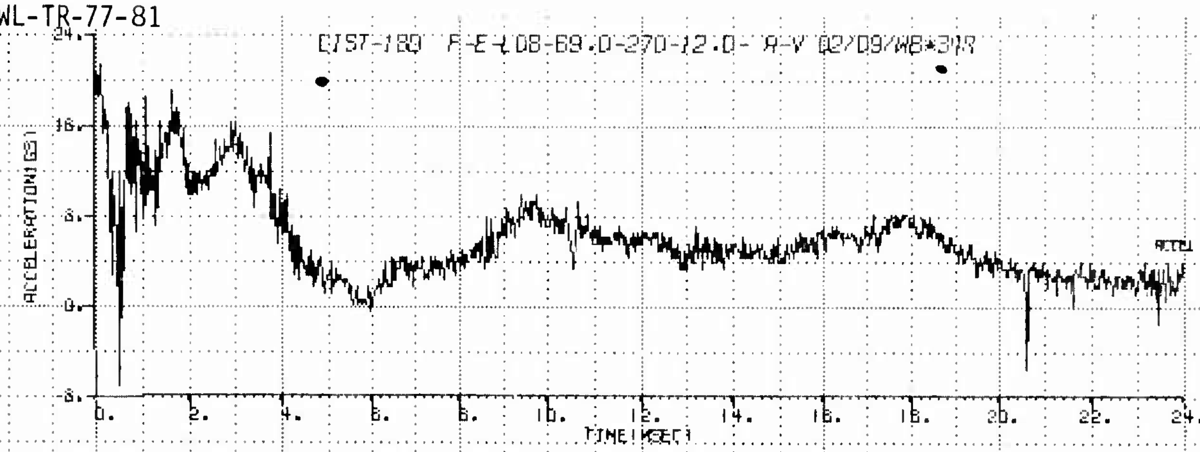
DIST-180 F-E-L 08-69.0-270-12.0- A-V 02/09/WB*34R
ACCELERATION(G)
ACCEL
TIME(MSEC)

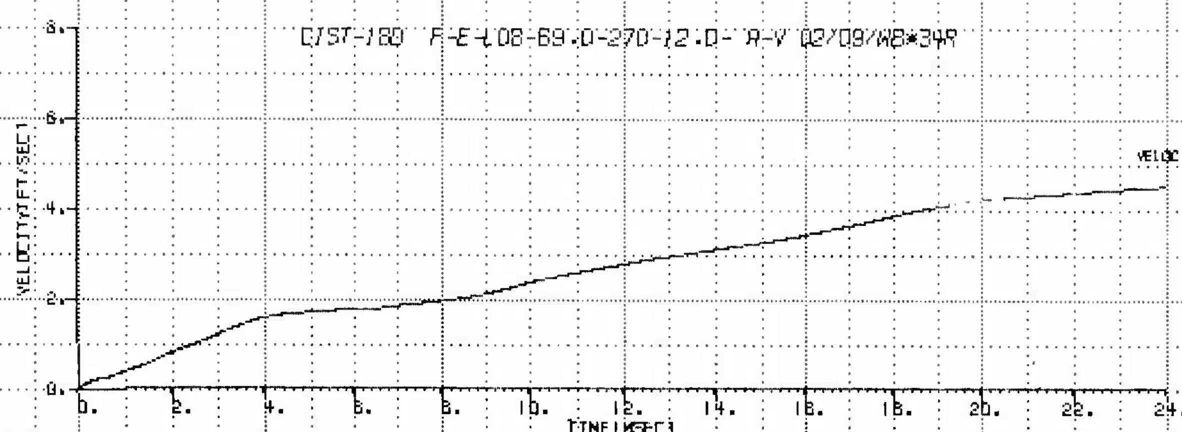
DIST-180 F-E-L 08-69.0-270-12.0- A-V 02/09/WB*34R
VELOCITY(FT/SEC)
VELOC
TIME(MSEC)

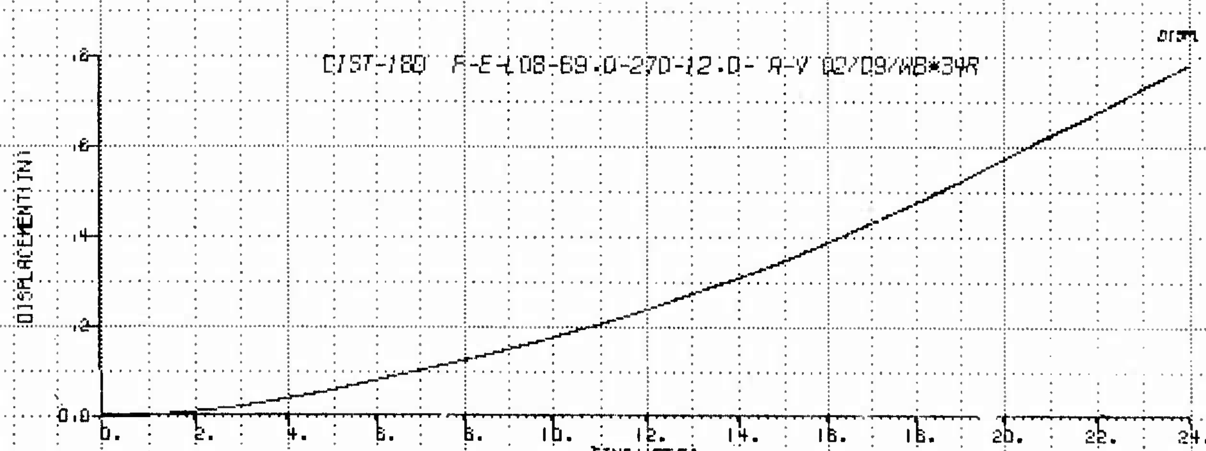
DIST-180 F-E-L 08-69.0-270-12.0- A-V 02/09/WB*34R
DISPLACEMENT(IN)
DISPL
TIME(MSEC)

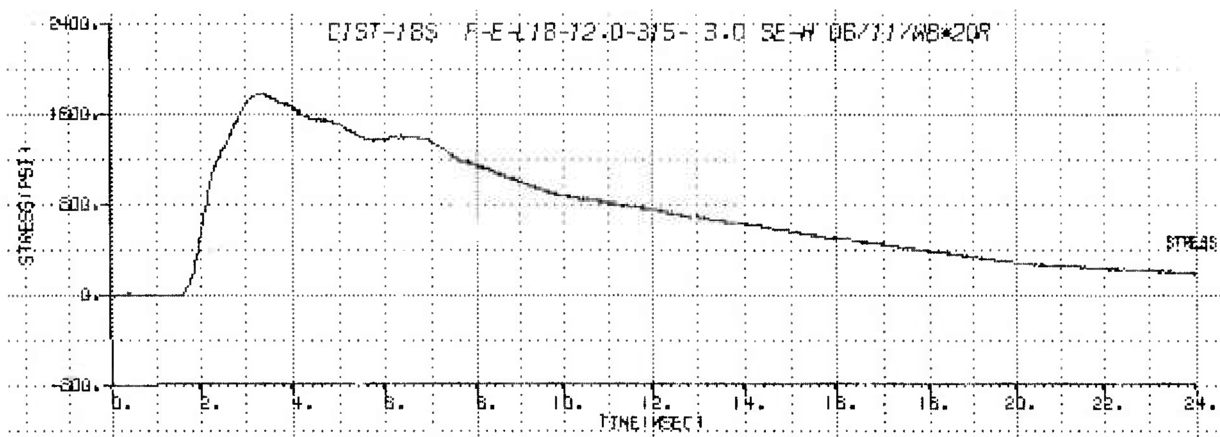
DIST-18S F-E-L18-12.0-3/5- 3.0 SE-H 06/11/WB*20R
STRESS(PSI)
STRESS
TIME(MSEC)

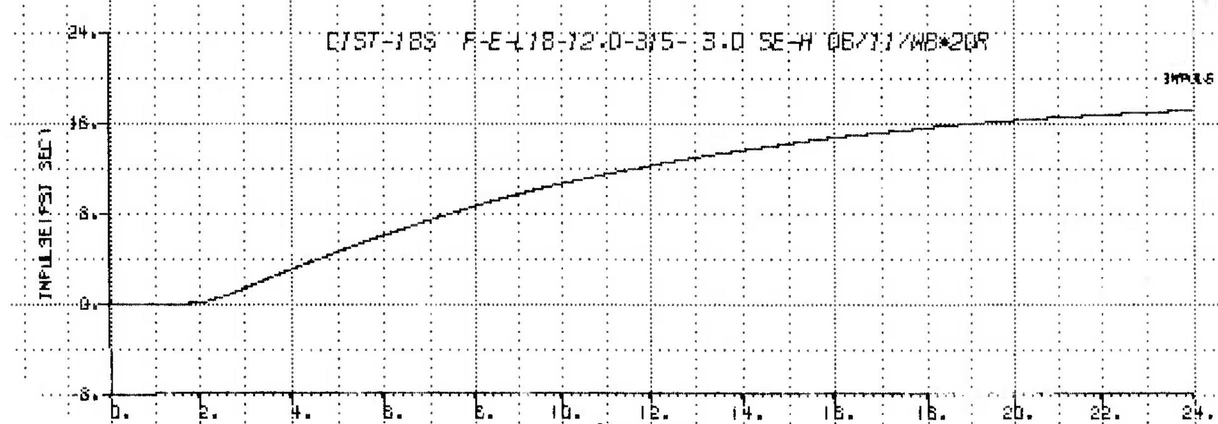
DIST-18S F-E-L18-12.0-3/5- 3.0 SE-H 06/11/WB*20R
IMPULSE(PSI SEC)
IMPULS
TIME(MSEC)

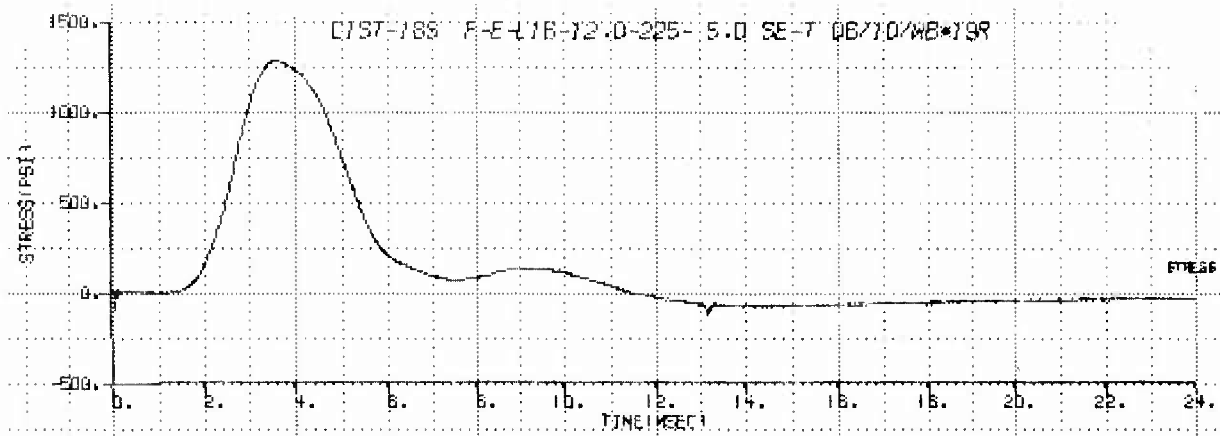
STRESS(PSI)
TIME(MSEC)
STRESS

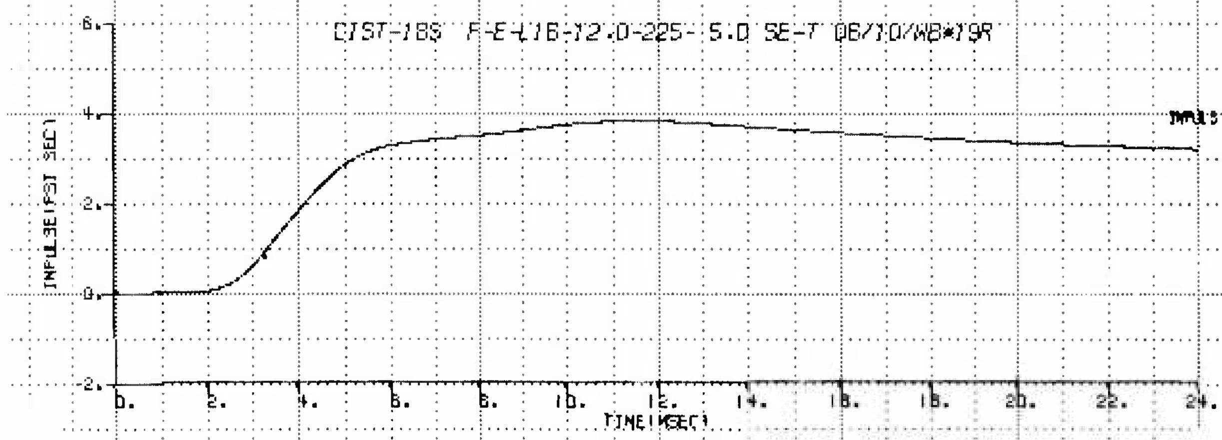
IMPULSE(PSI SEC)
TIME(MSEC)

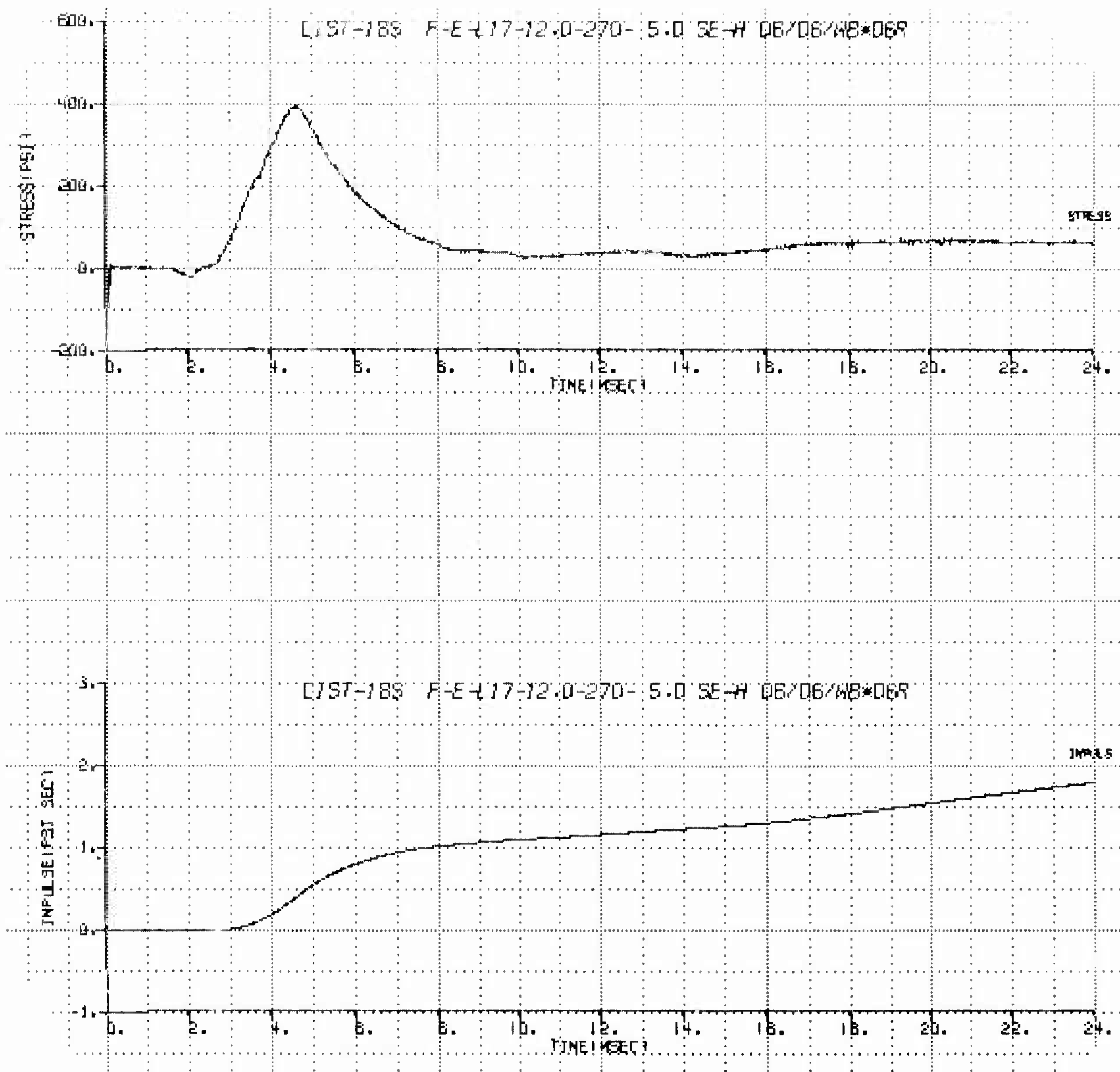

CIST-18S F-E-17-12.0-270- 5.0 SE-H 06/06/48*06R
STRESS(PSI)
STRESS
TIME(MSEC)
IMPULSE(PSI SEC)
IMPULS

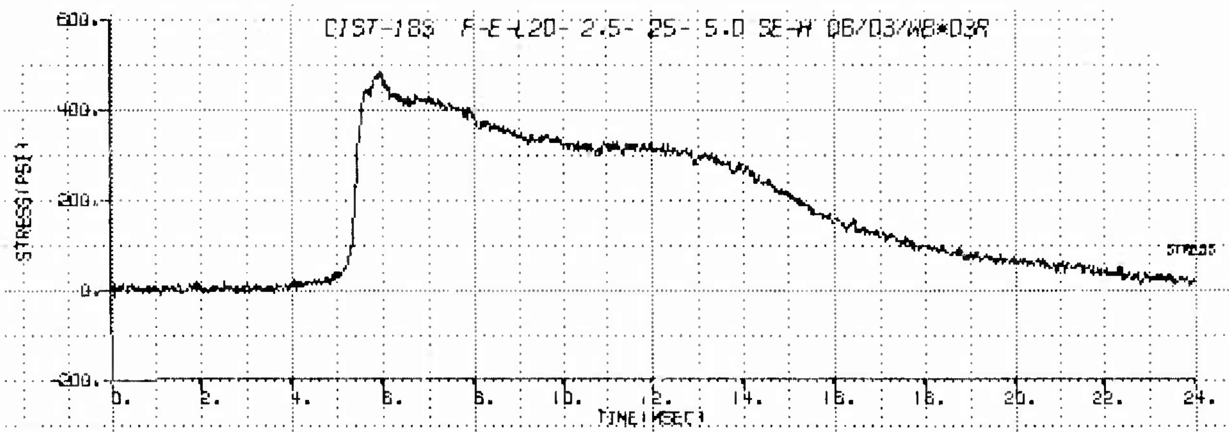
DIST-18S F-E-120- 2.5- 25- 5.0 SE-H 08/03/WB*D3R
STRESS(PSI)
600.
400.
200.
0.
-200.
0.
2.
4.
6.
8.
10.
12.
14.
16.
18.
20.
22.
24.
TIME(MSEC)
STRESS

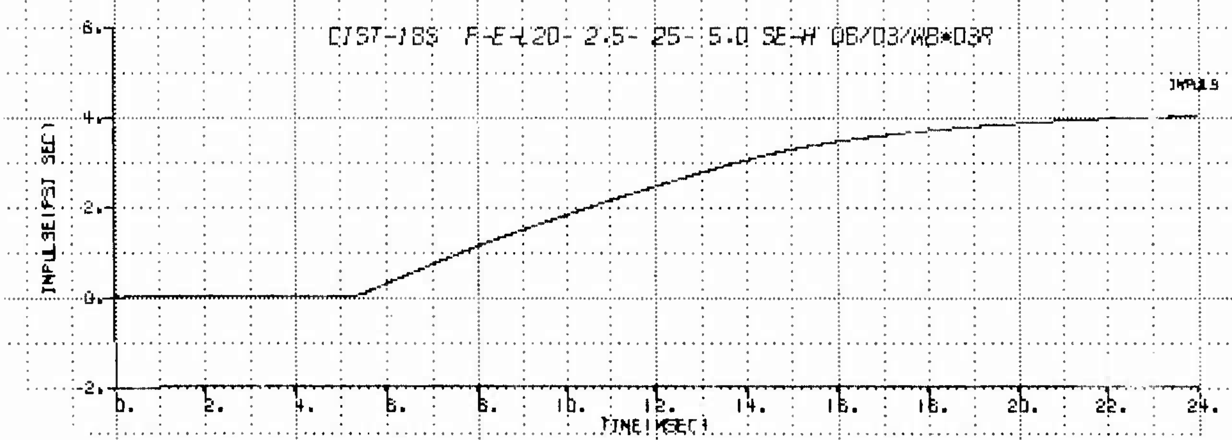
DIST-18S F-E-120- 2.5- 25- 5.0 SE-H 08/03/WB*D3R
IMPULSE(PSI SEC)
6.
4.
2.
0.
-2.
0.
2.
4.
6.
8.
10.
12.
14.
16.
18.
20.
22.
24.
TIME(MSEC)
IMPULS

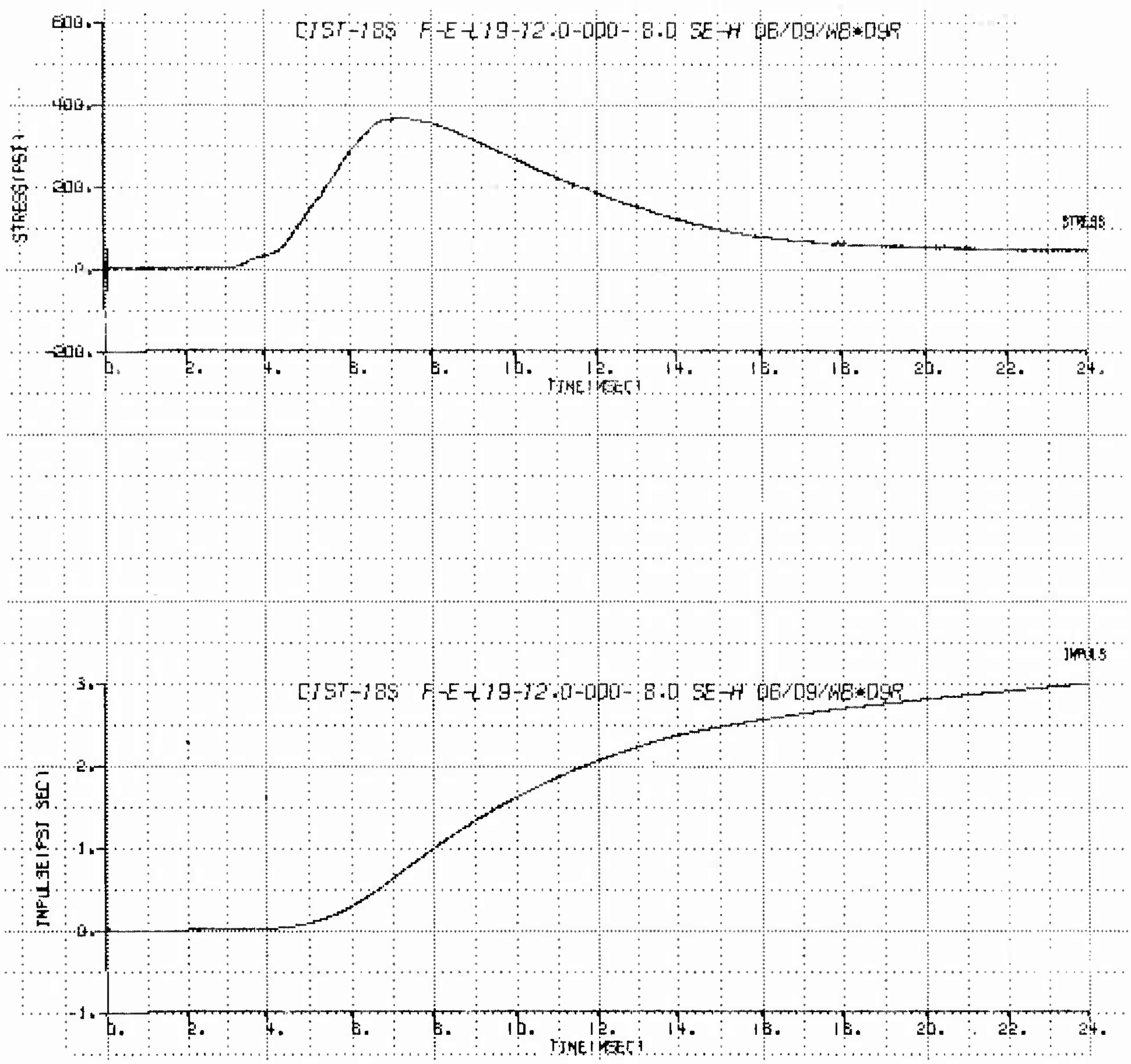
CIST-18S F-E-L19-72.0-000- 8.0 SE-H 06/09/48*09R
STRESS(PSI)
600.
400.
200.
0.
-200.
STRESS
TIME(MSEC)
0. 2. 4. 6. 8. 10. 12. 14. 16. 18. 20. 22. 24.
CIST-18S F-E-L19-72.0-000- 8.0 SE-H 06/09/48*09R
IMPULSE(PSI SEC)
3.
2.
1.
0.
-1.
IMPULS
TIME(MSEC)
0. 2. 4. 6. 8. 10. 12. 14. 16. 18. 20. 22. 24.

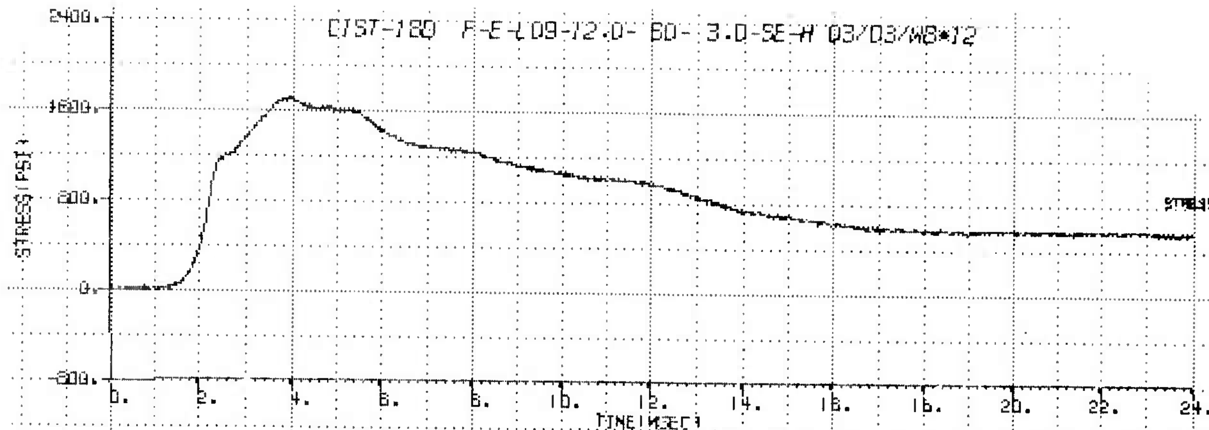
STRESS(PSI)
TIME(MSEC)
STRESS

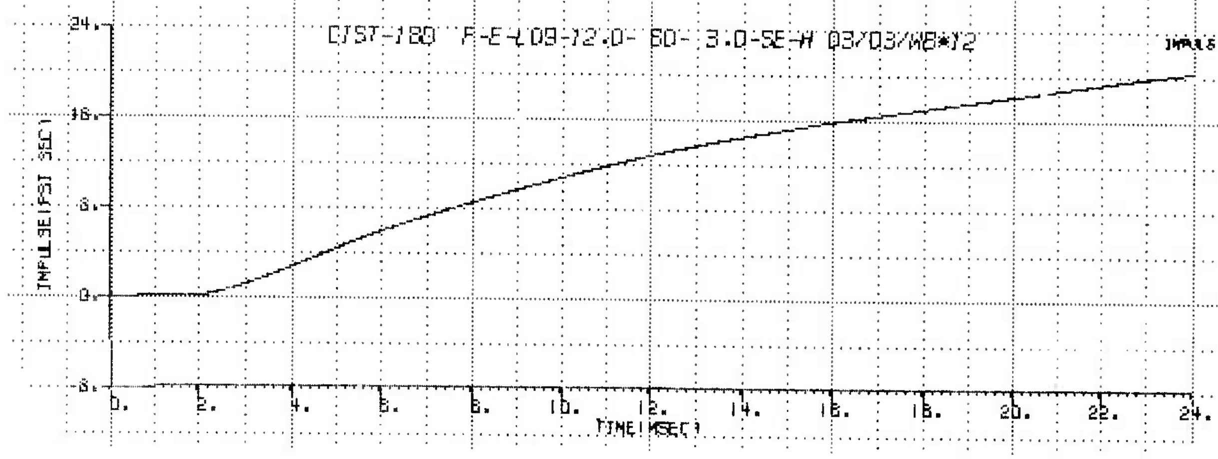
TIME(MSEC)
IMPULS

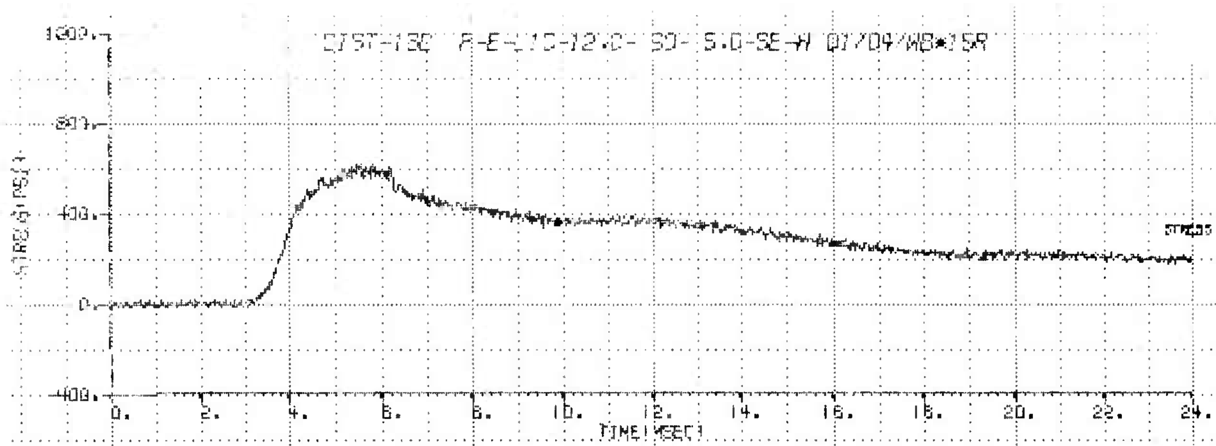
DIST-180 R-E-L10-12.0-30-5.0-SE-H 01/04/WB*15R
STRESS(PSI)
TIME(MSEC)
0. 2. 4. 6. 8. 10. 12. 14. 16. 18. 20. 22. 24.
1200.
800.
400.
0.
-400.

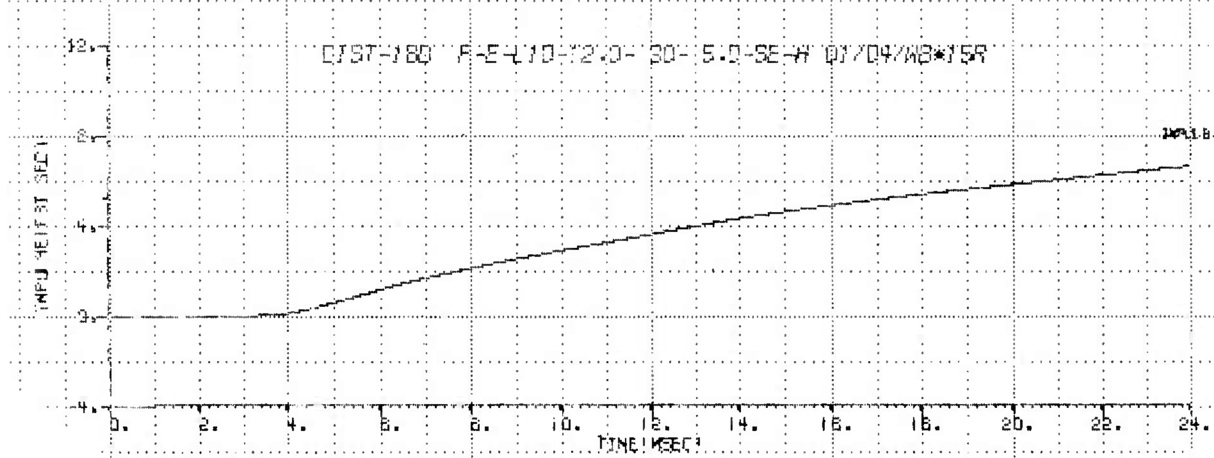
DIST-180 R-E-L10-12.0-30-5.0-SE-H 01/04/WB*15R
TIME(MSEC)
0. 2. 4. 6. 8. 10. 12. 14. 16. 18. 20. 22. 24.
12.
8.
4.
0.
-4.

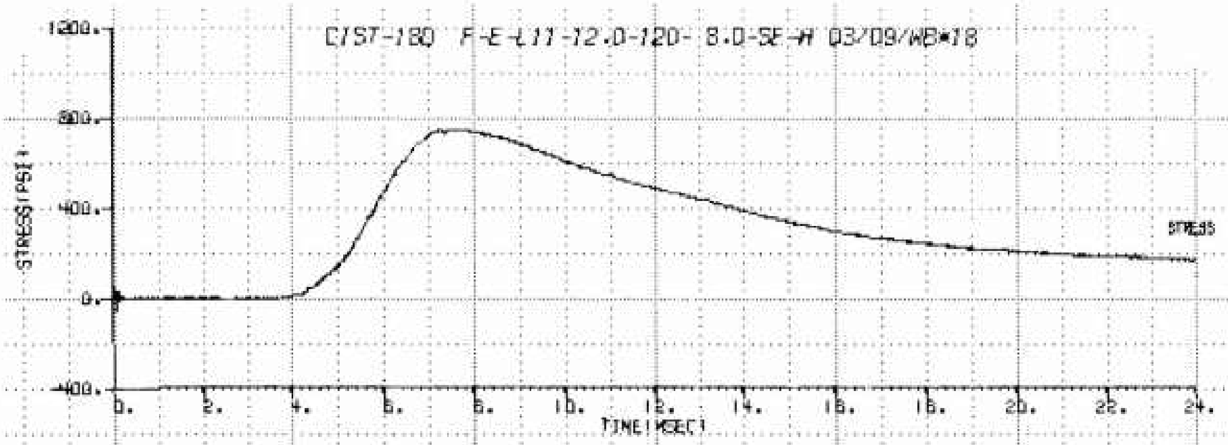
CIST-180 F-E-L11-12.0-120- 8.0-SE-H 03/09/WB*18
STRESS(PSI)
STRESS
TIME(MSEC)
1200.
800.
400.
0.
-400.
0.
2.
4.
6.
8.
10.
12.
14.
16.
18.
20.
22.
24.

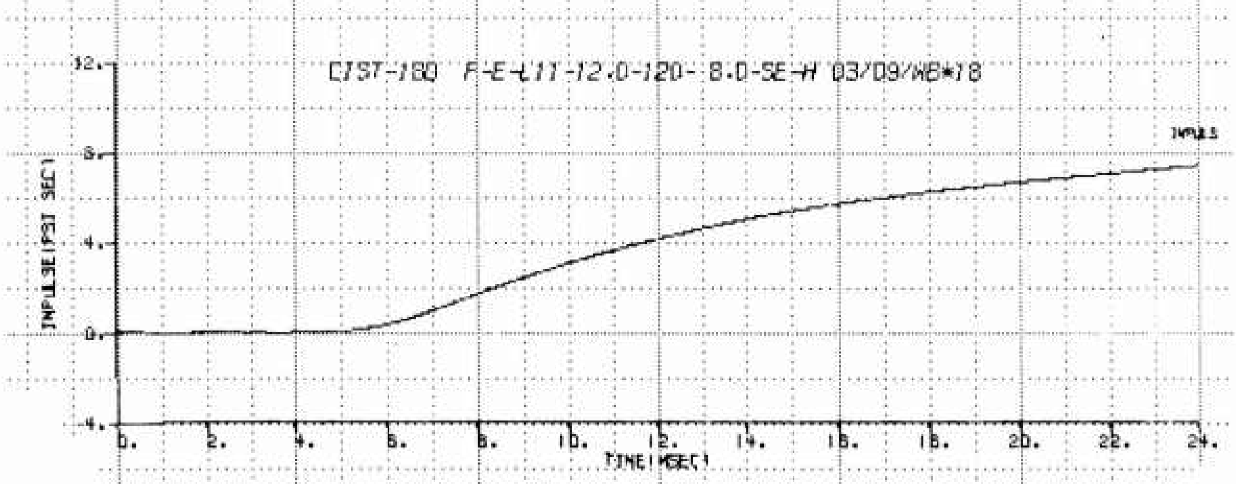
CIST-180 F-E-L11-12.0-120- 8.0-SE-H 03/09/WB*18
IMPULSE(PSI SEC)
IMPULS
TIME(MSEC)
12.
8.
4.
0.
-4.
0.
2.
4.
6.
8.
10.
12.
14.
16.
18.
20.
22.
24.

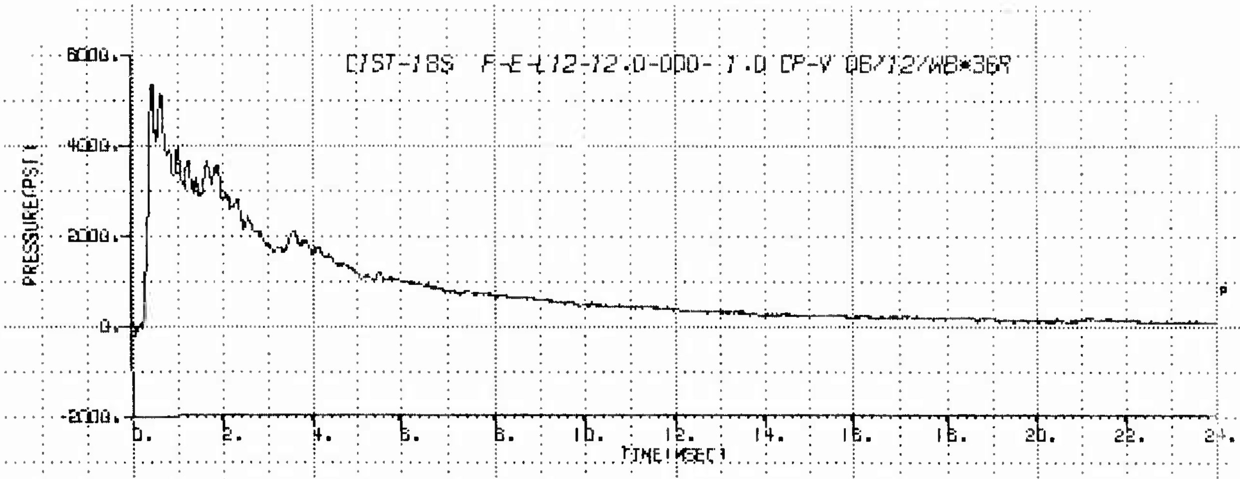
CIST-18S F-E-L12-12.0-000- 1.0 CP-V 06/12/W8*36R
PRESSURE(PSI)
TIME(MSEC)

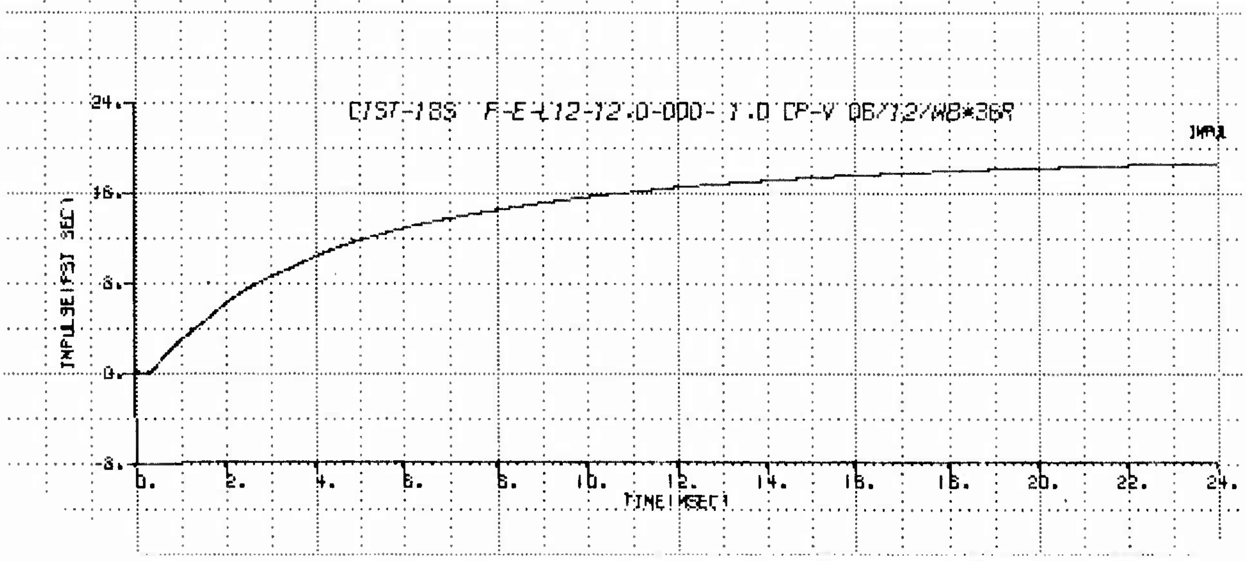
CIST-18S F-E-L12-12.0-000- 1.0 CP-V 06/12/W8*36R
IMPULSE(PSI SEC)
TIME(MSEC)

APPENDIX B

MATERIAL MODEL COMPARISONS

C - Calculated Horizontal Velocity

V - Calculated Vertical Velocity

E - Experimental Horizontal Velocity (Uncorrected)

O - Experimental Vertical Velocity (Uncorrected)

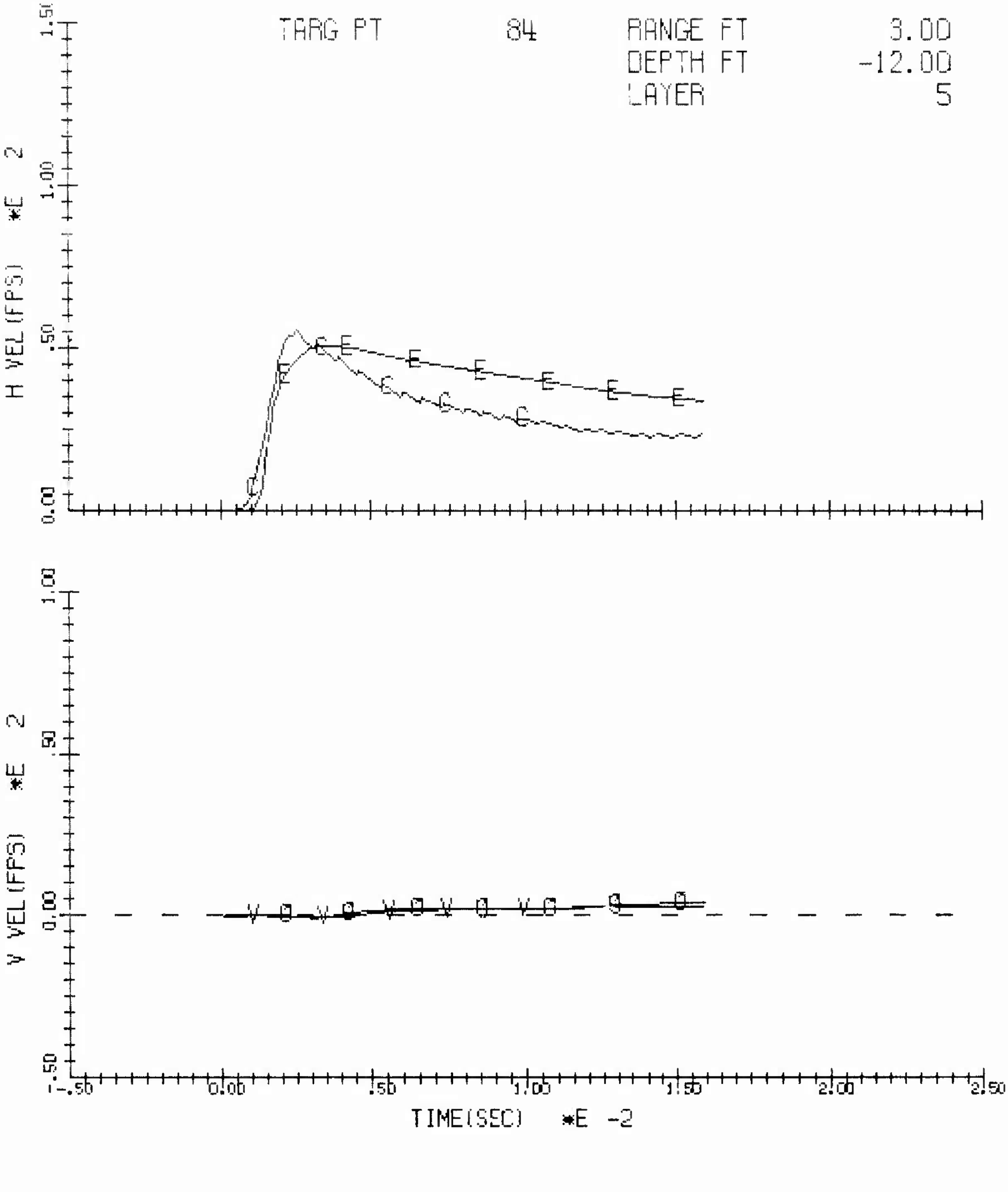

Figure B.1. Comparison of experimental data and AFTON calculation for 3' range and 12' depth in CIST 18S.

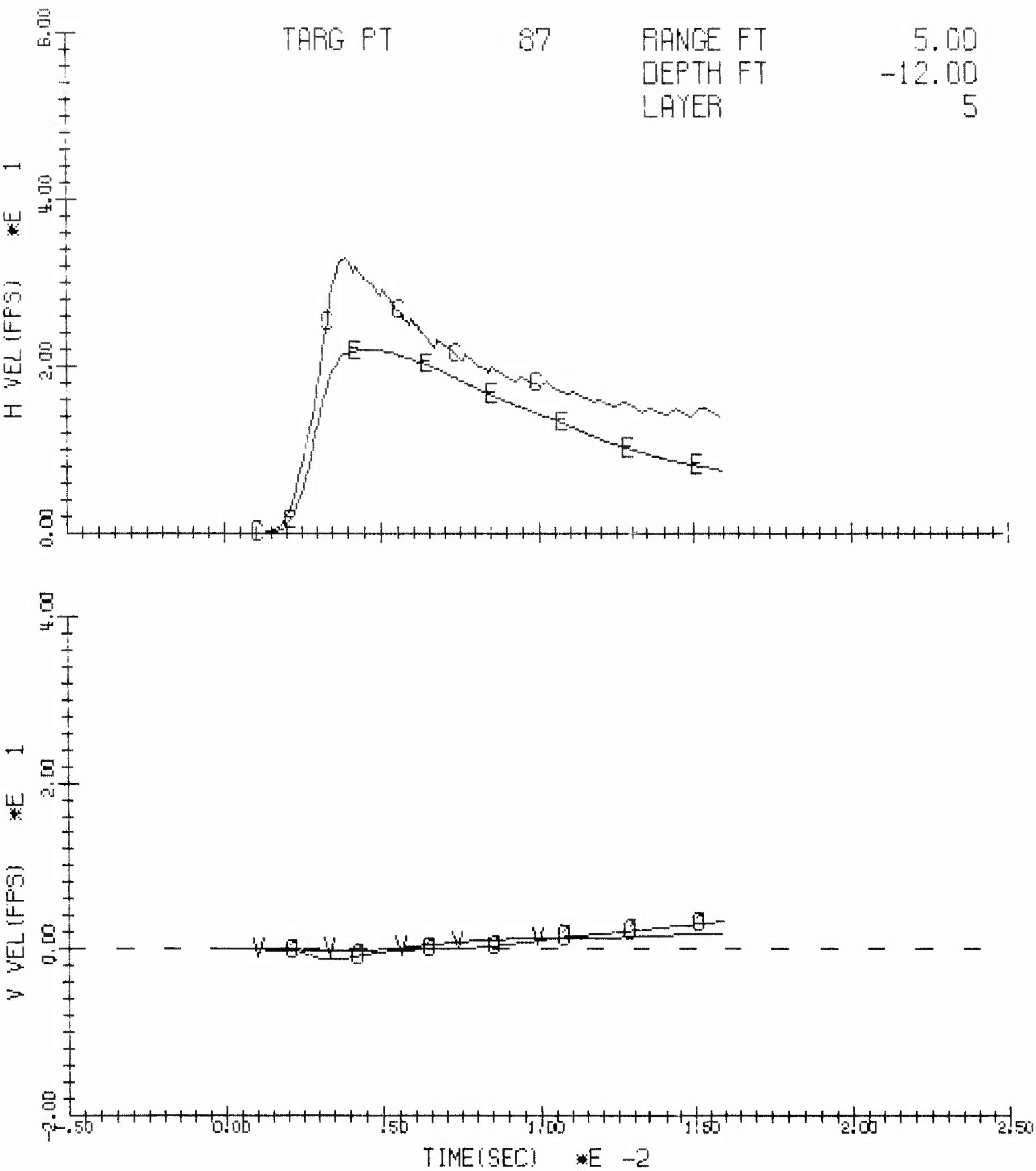

Figure B.2. Comparison of experimental data and AFTON calculation for 5' range and 12' depth for CIST 18S.

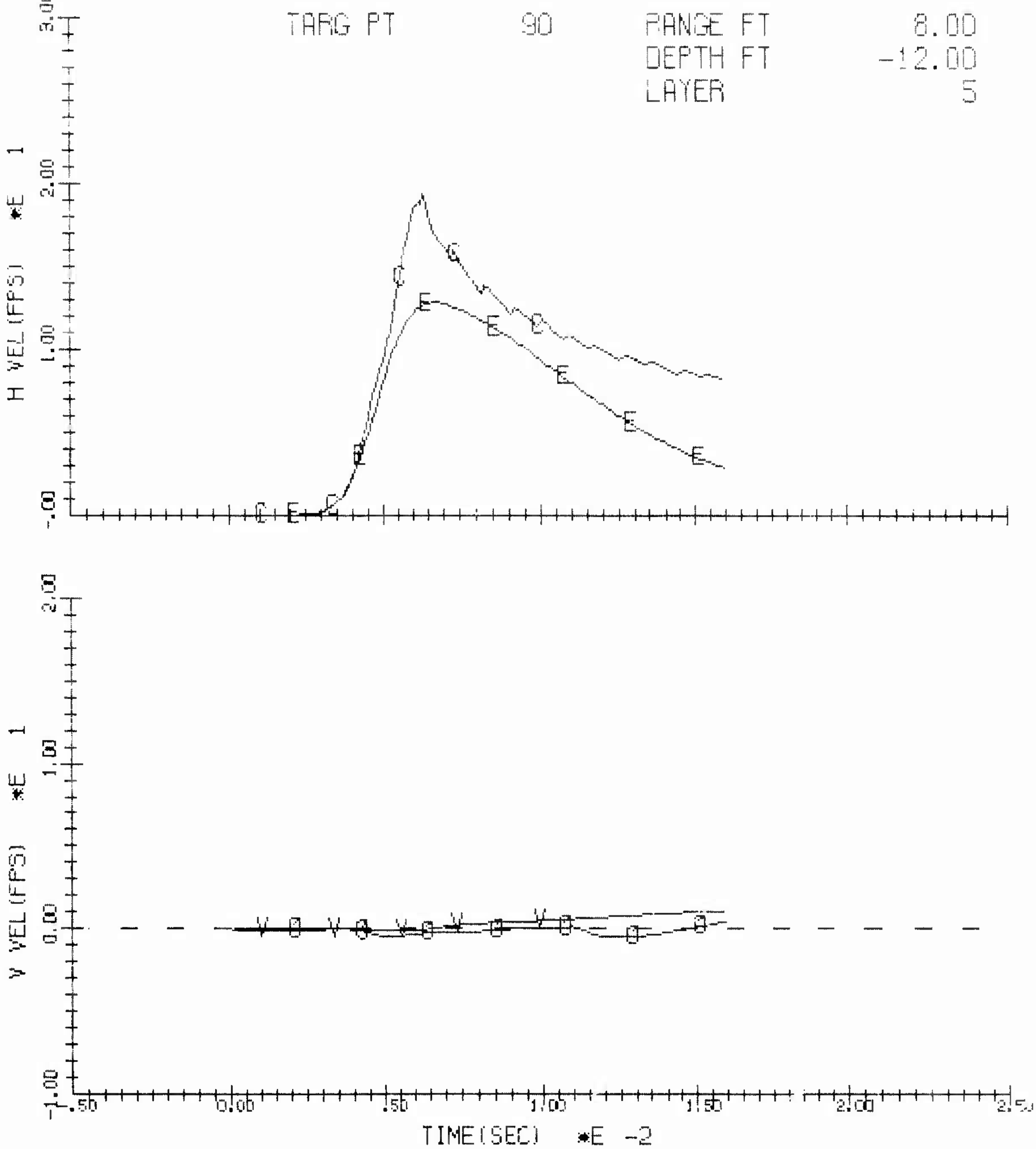

Figure B.3. Comparison of experimental data and AFTON calculation for 8' range and 12' depth for CIST 18S.

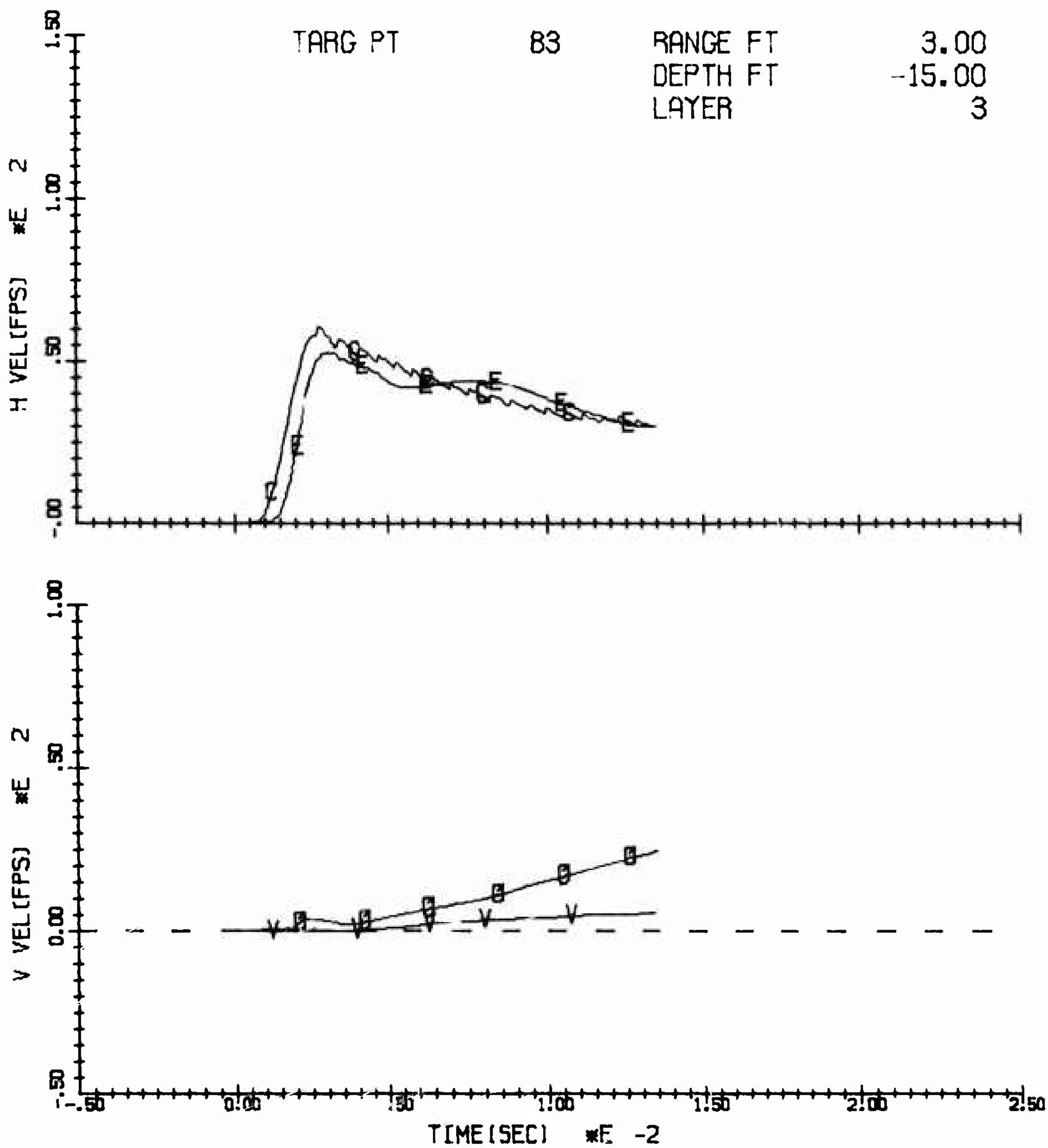

Figure B.4. Comparison of experimental data and AFTON calculation for 3' range and 15' depth in CIST 18D.

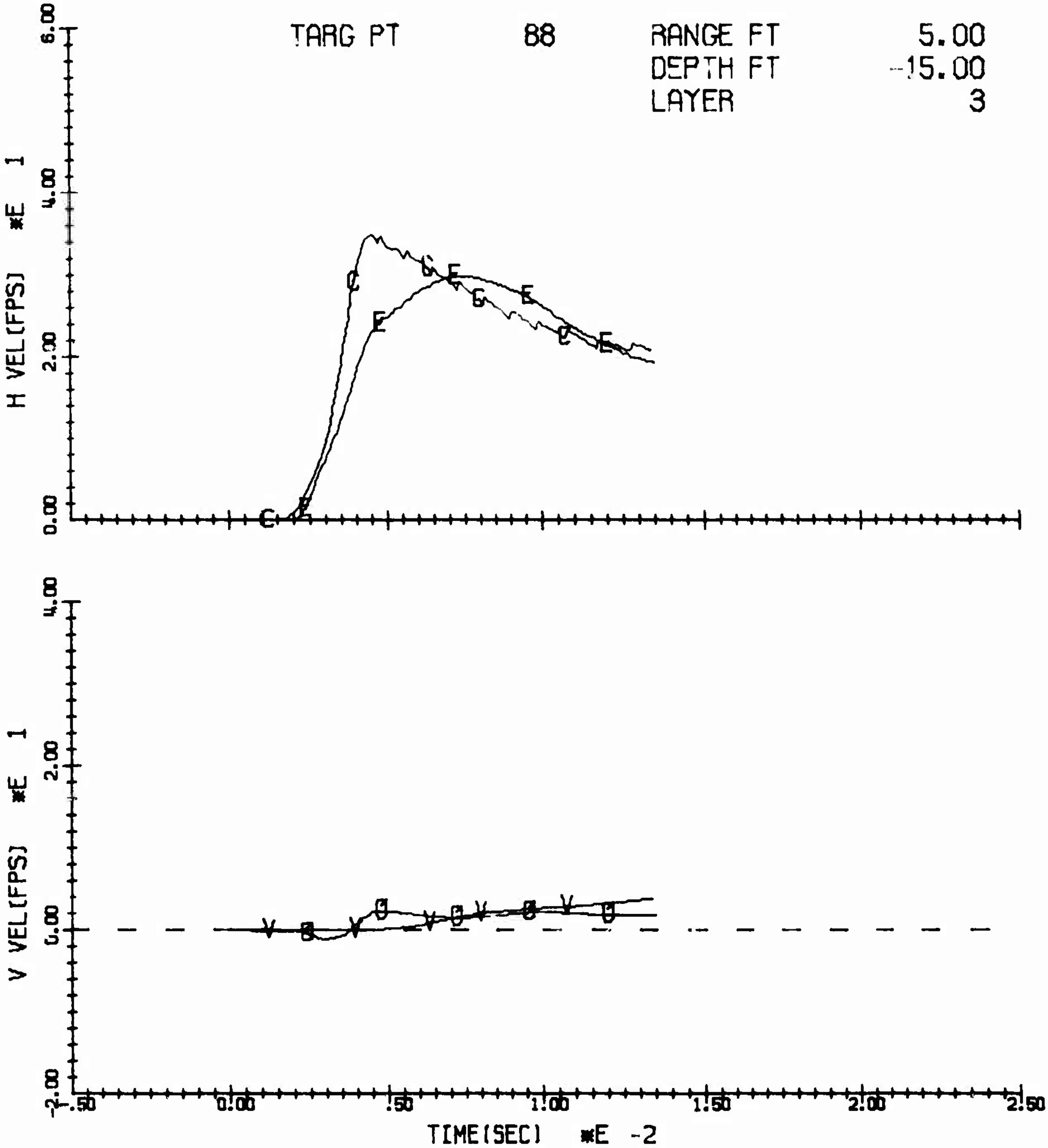

Figure B.5. Comparison of experimental data and AFTON calculation for 5' range and 15' depth for CIST 18D.

THIS REPORT HAS BEEN DELIMITED
AND CLEARED FOR PUBLIC RELEASE
UNDER DOD DIRECTIVE 5200.20 AND
NO RESTRICTIONS ARE IMPOSED UPON
ITS USE AND DISCLOSURE.

DISTRIBUTION STATEMENT A

APPROVED FOR PUBLIC RELEASE;
DISTRIBUTION UNLIMITED.

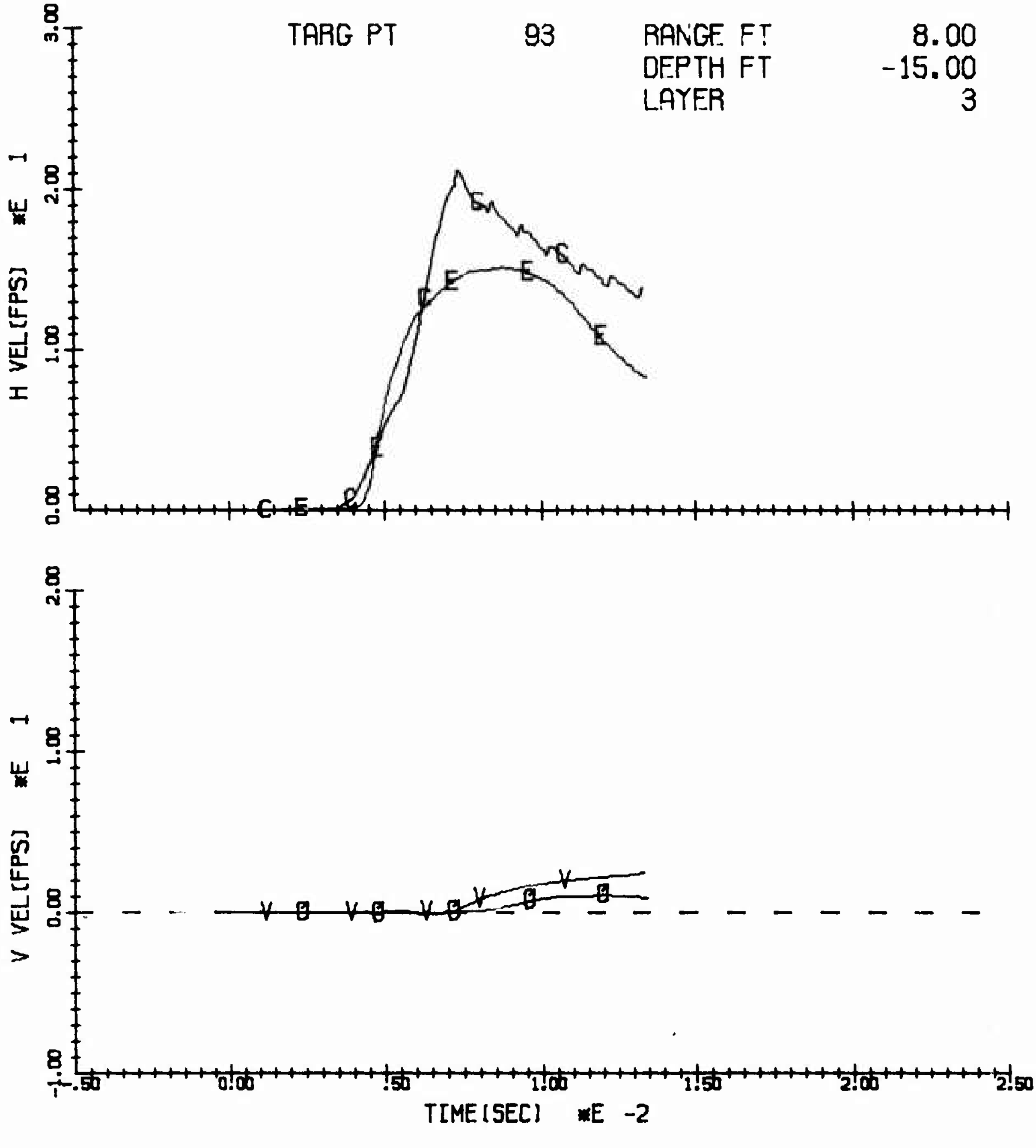

Figure B.6. Comparison of experimental data and AFTON calculation for 8' range and 15' depth for CIST 18D.

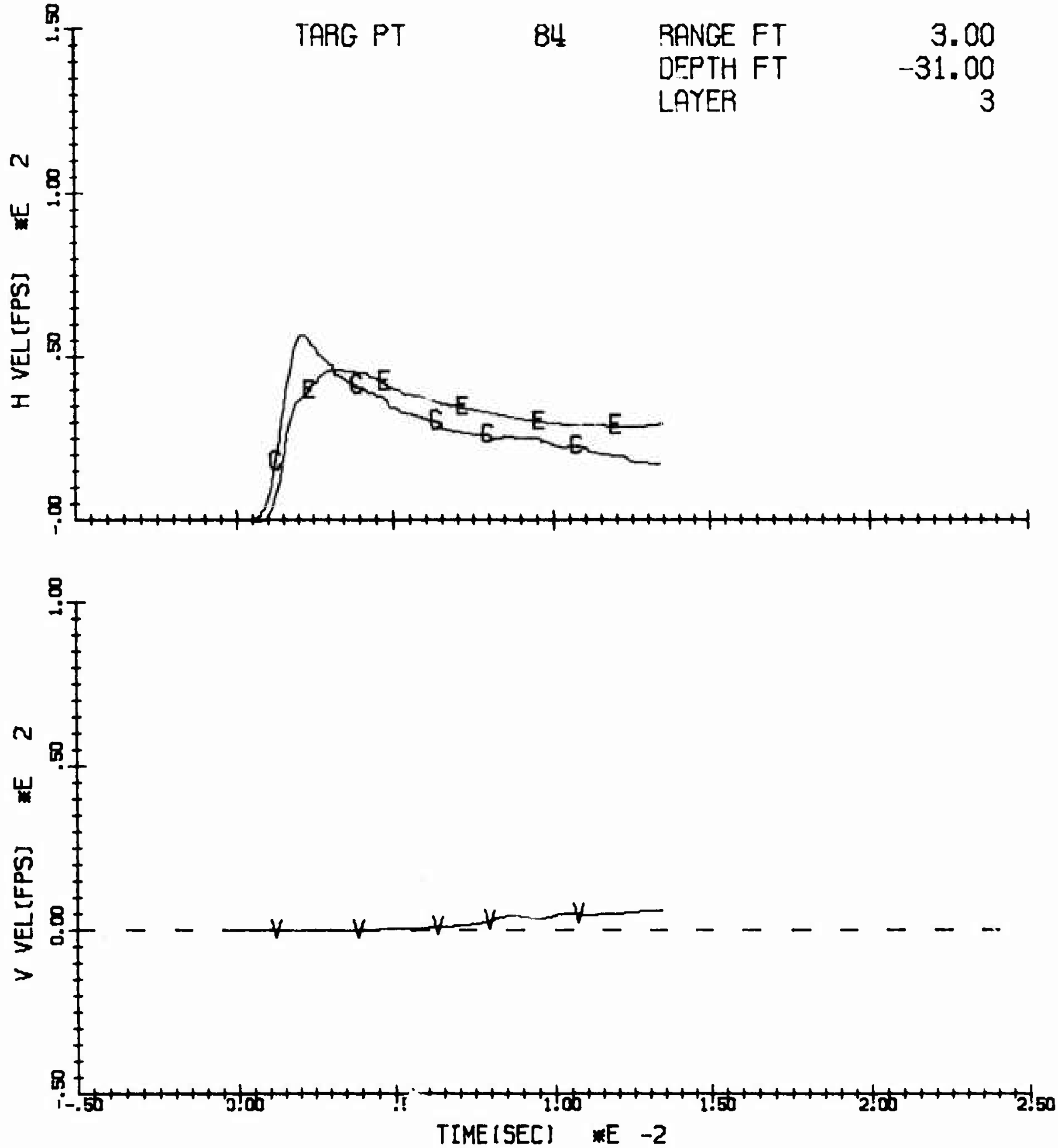

Figure B.7. Comparison of experimental data and AFTON calculation for 3' range and 31' depth for CIST 18D.

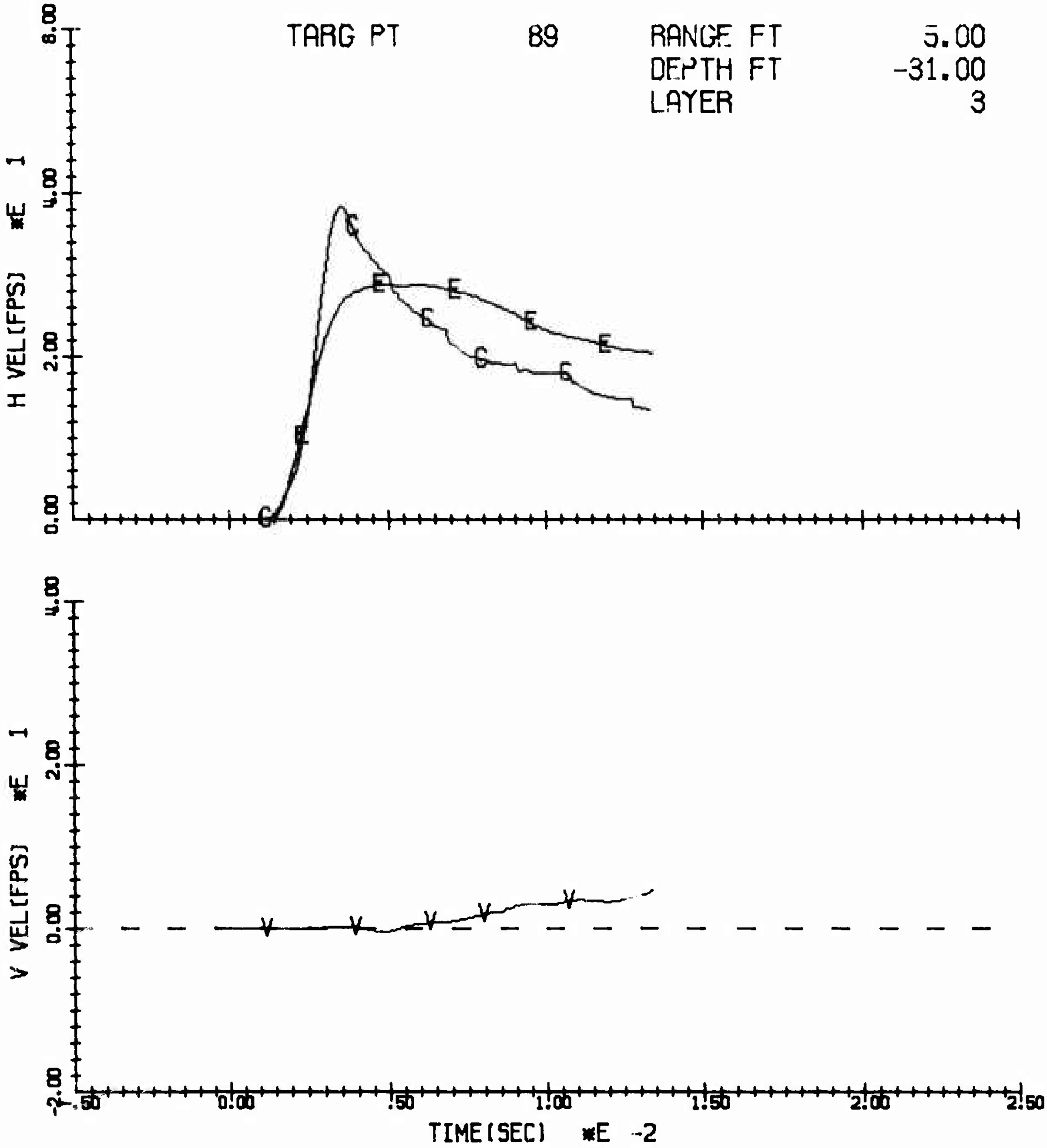

Figure B.8. Comparison of experimental data and AFTON calculation for 5' range and 31' depth for CIST 18D.

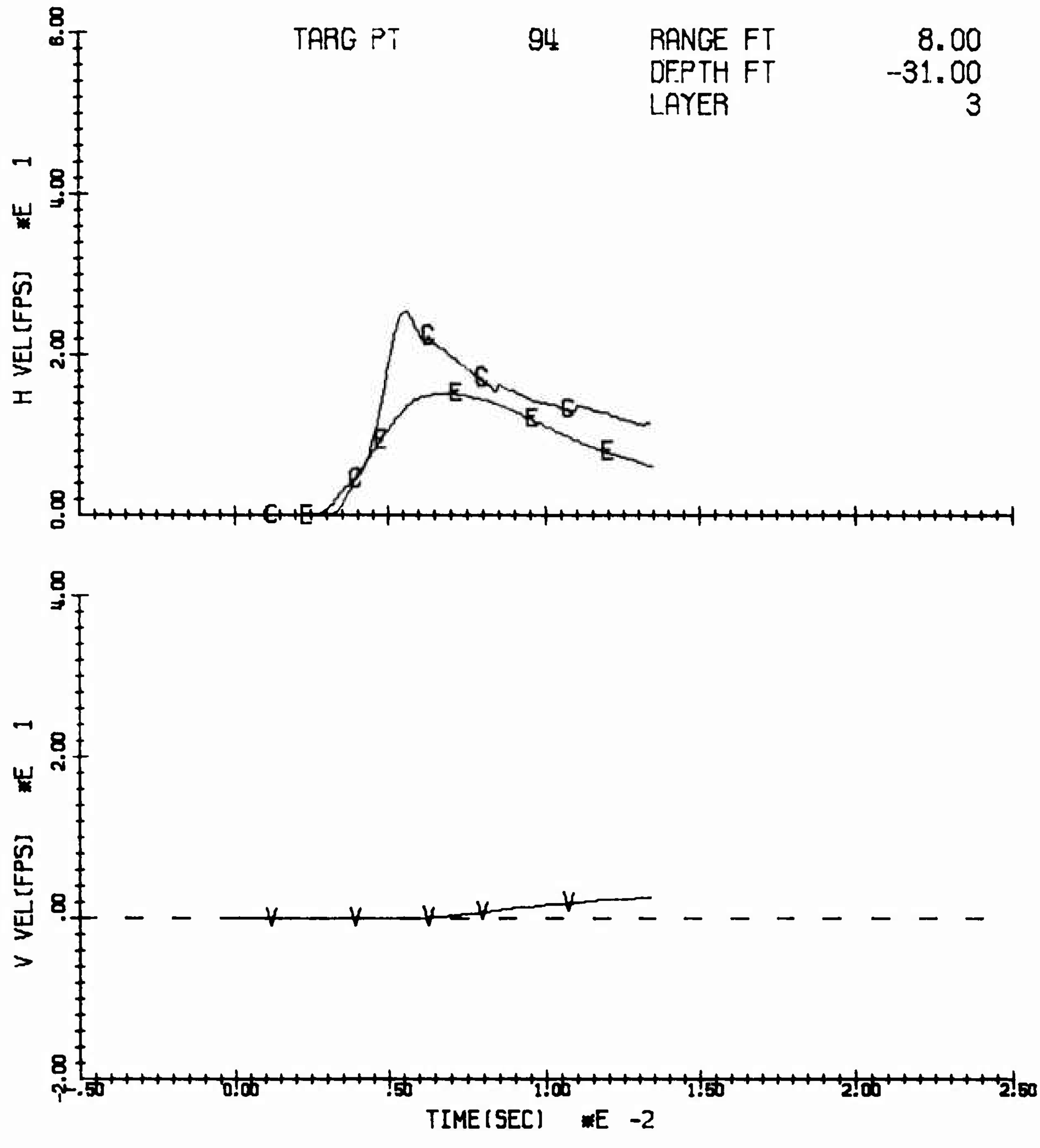

Figure B.9. Comparison of experimental data and AFTON calculation for 8' range and 31' depth in CIST 18D.

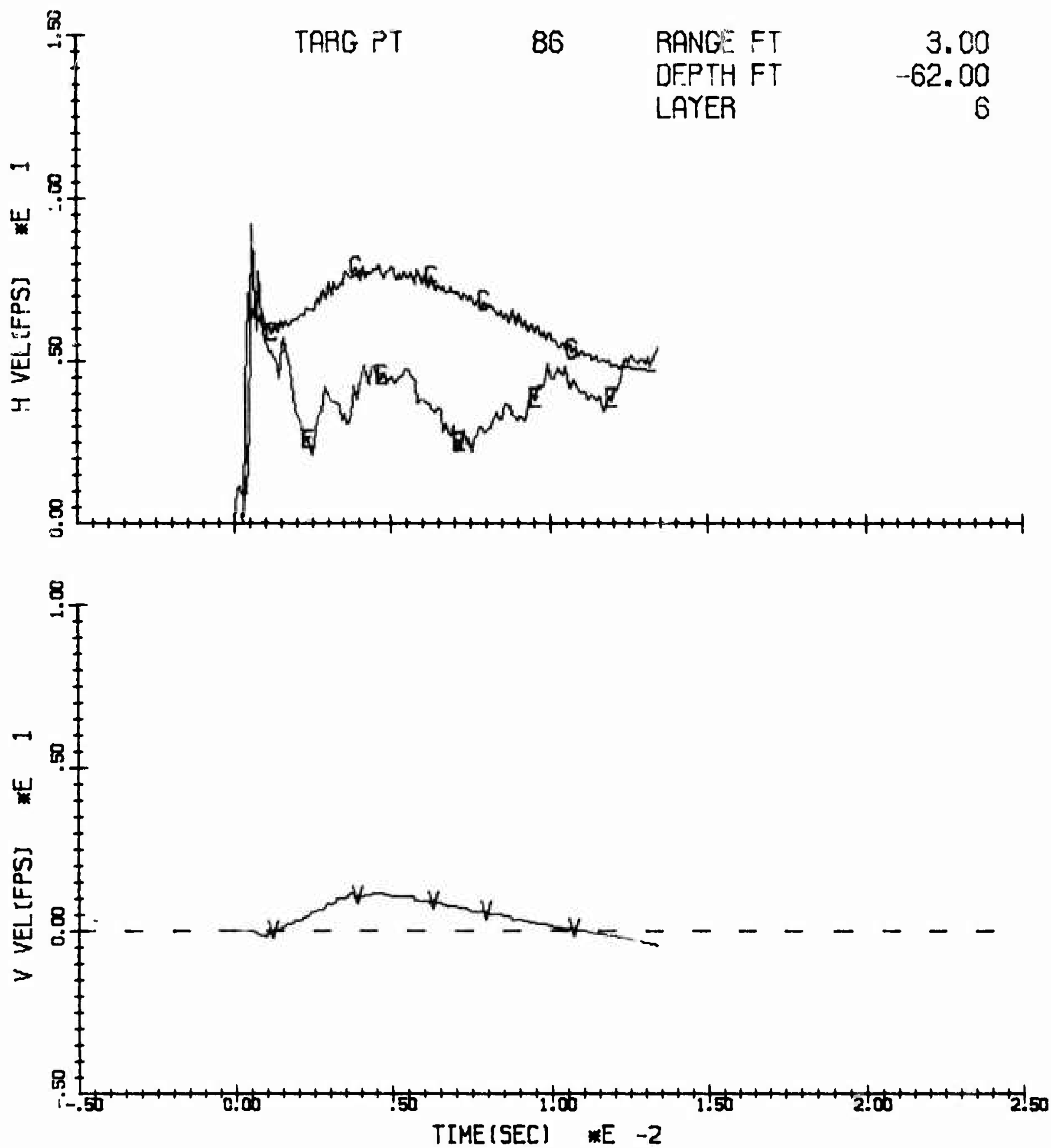

Figure B.10. Comparison of experimental data and AFTON calculation for 3' range and 62' depth for CIST 18D.

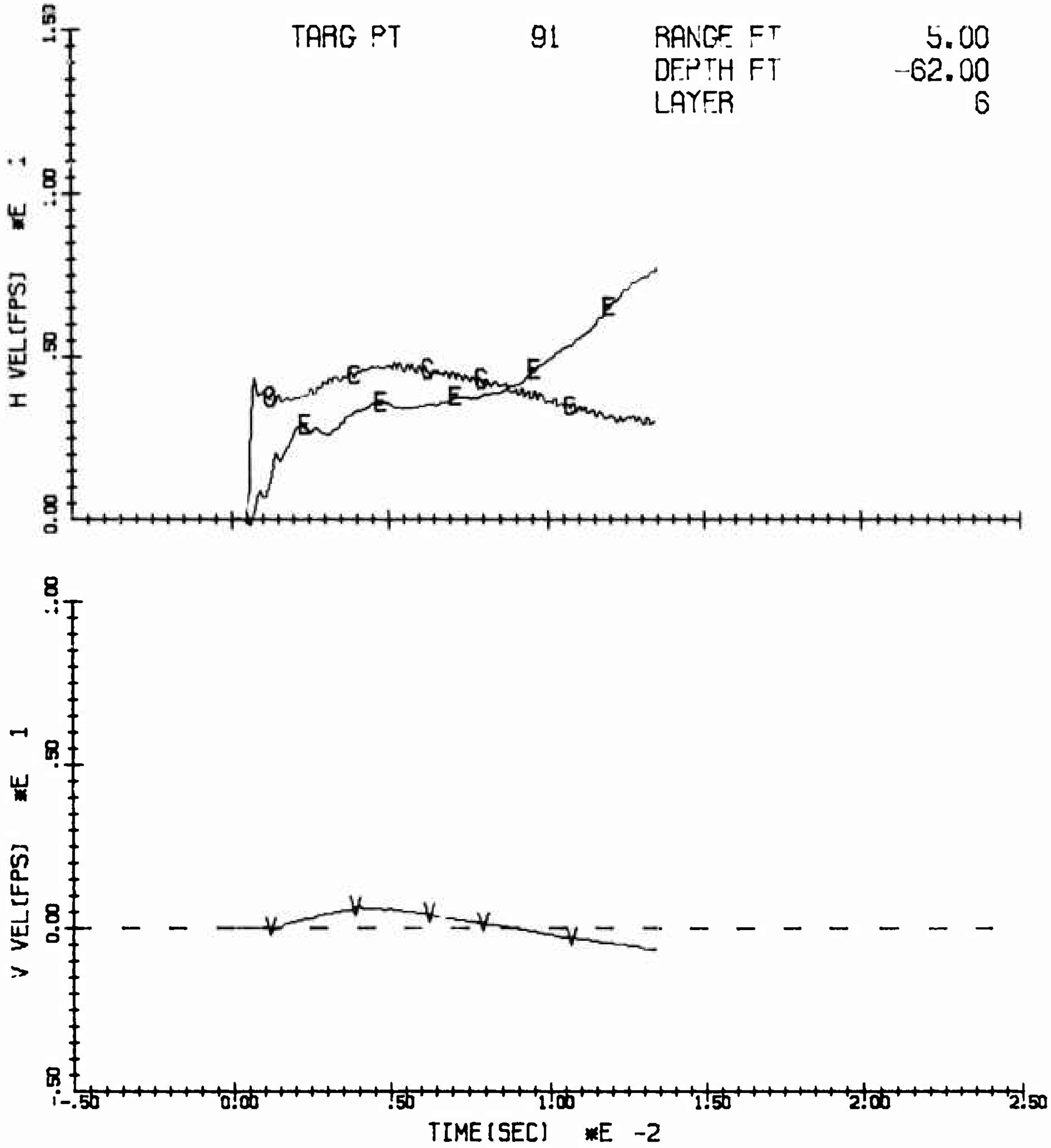

Figure B.11. Comparison of experimental data and AFTON calculation 5' range and 62' depth for CIST 18D.

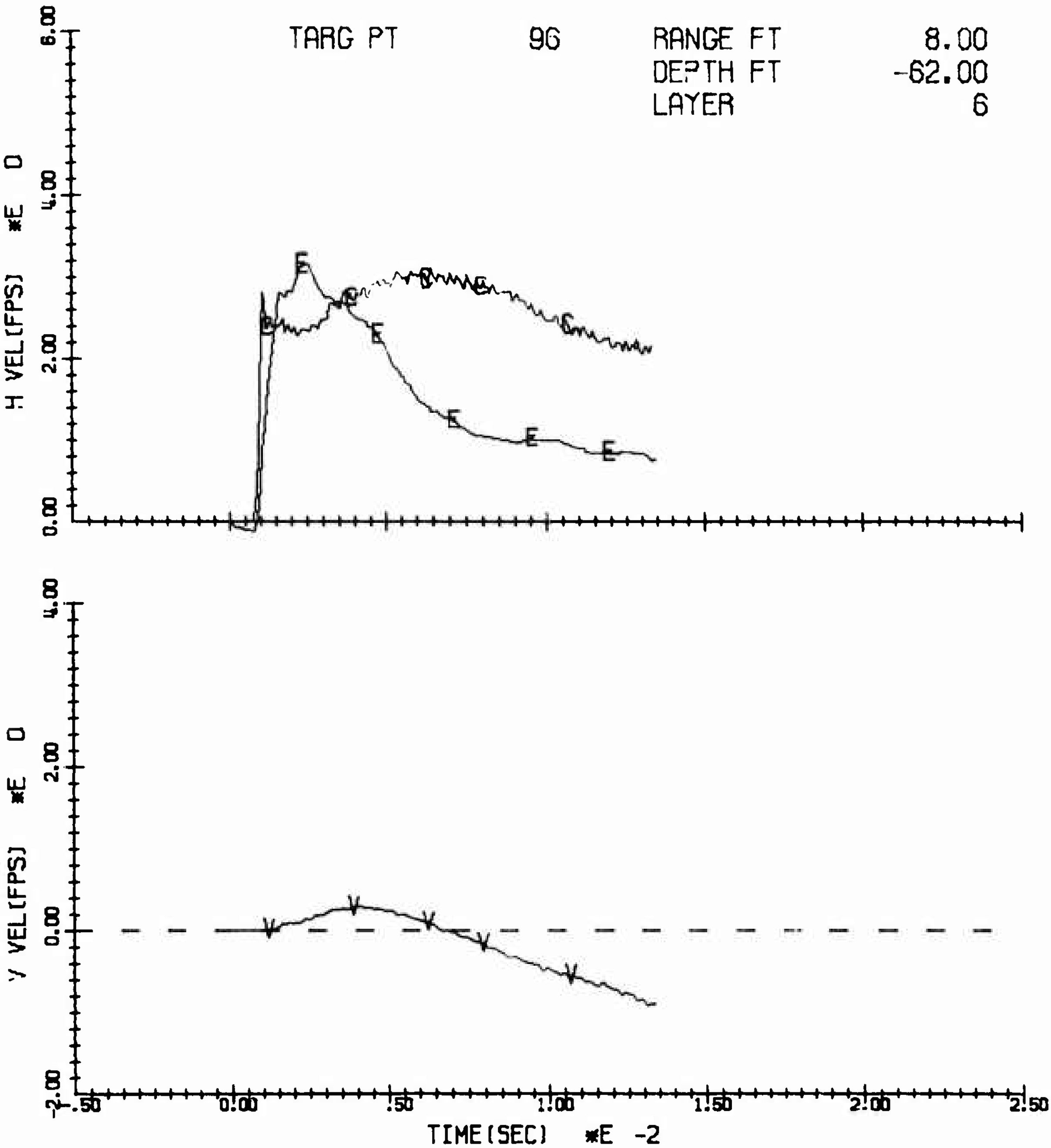

Figure B.12. Comparison of experimental data and AFTON calculation for 8' range and 62' depth for CIST 18D.

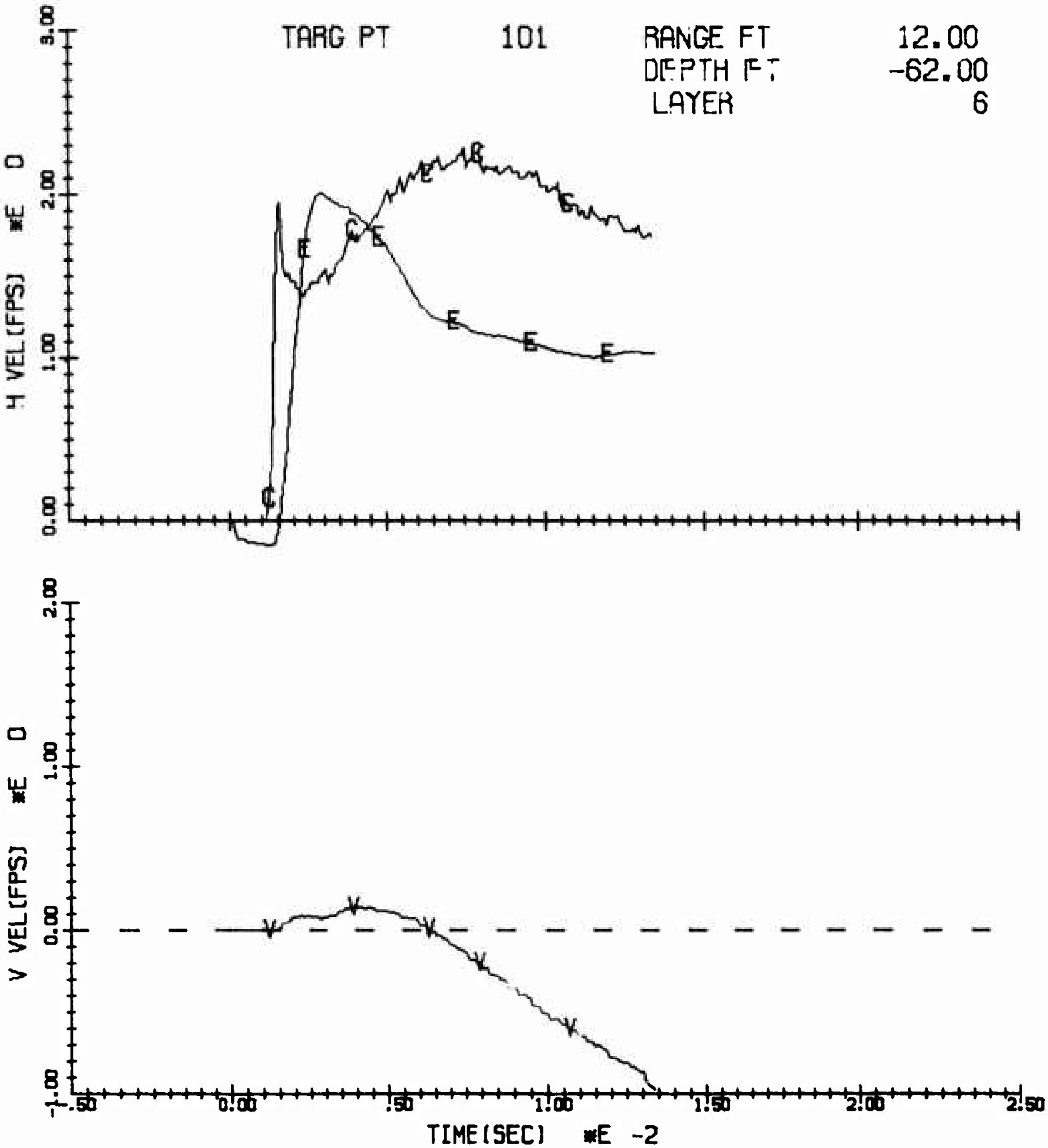

Figure B.13. Comparison of experimental data and AFTON calculation for 12' range and 62' depth.

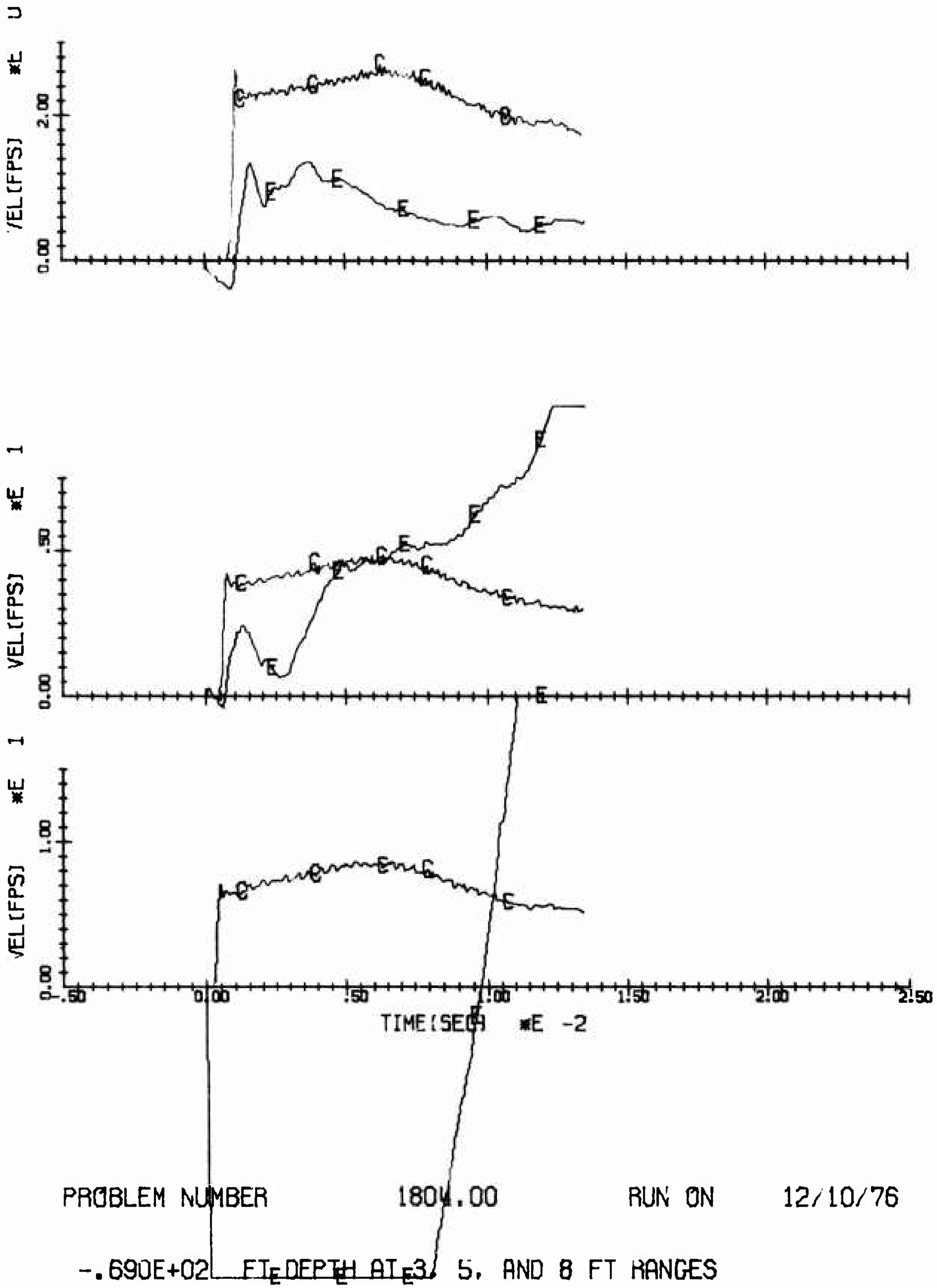

Figure B.14. Comparison of experimental data and AFTON calculation for 3', 5' and 8' ranges and 69' depth in CIST 18D.

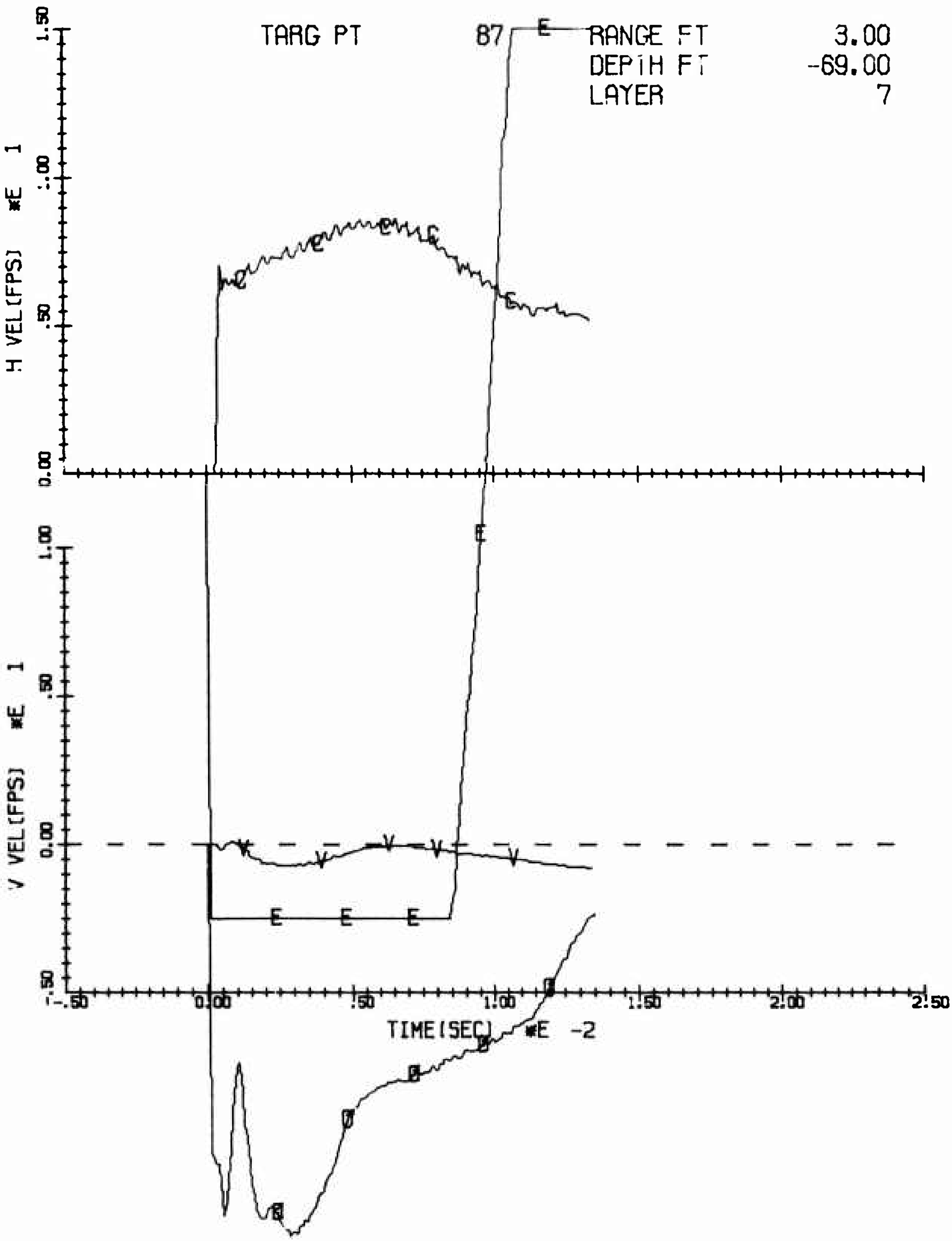

Figure B.15. Comparison of experimental data and AFTON calculation for 3' range and 69' depth in CIST 18D.

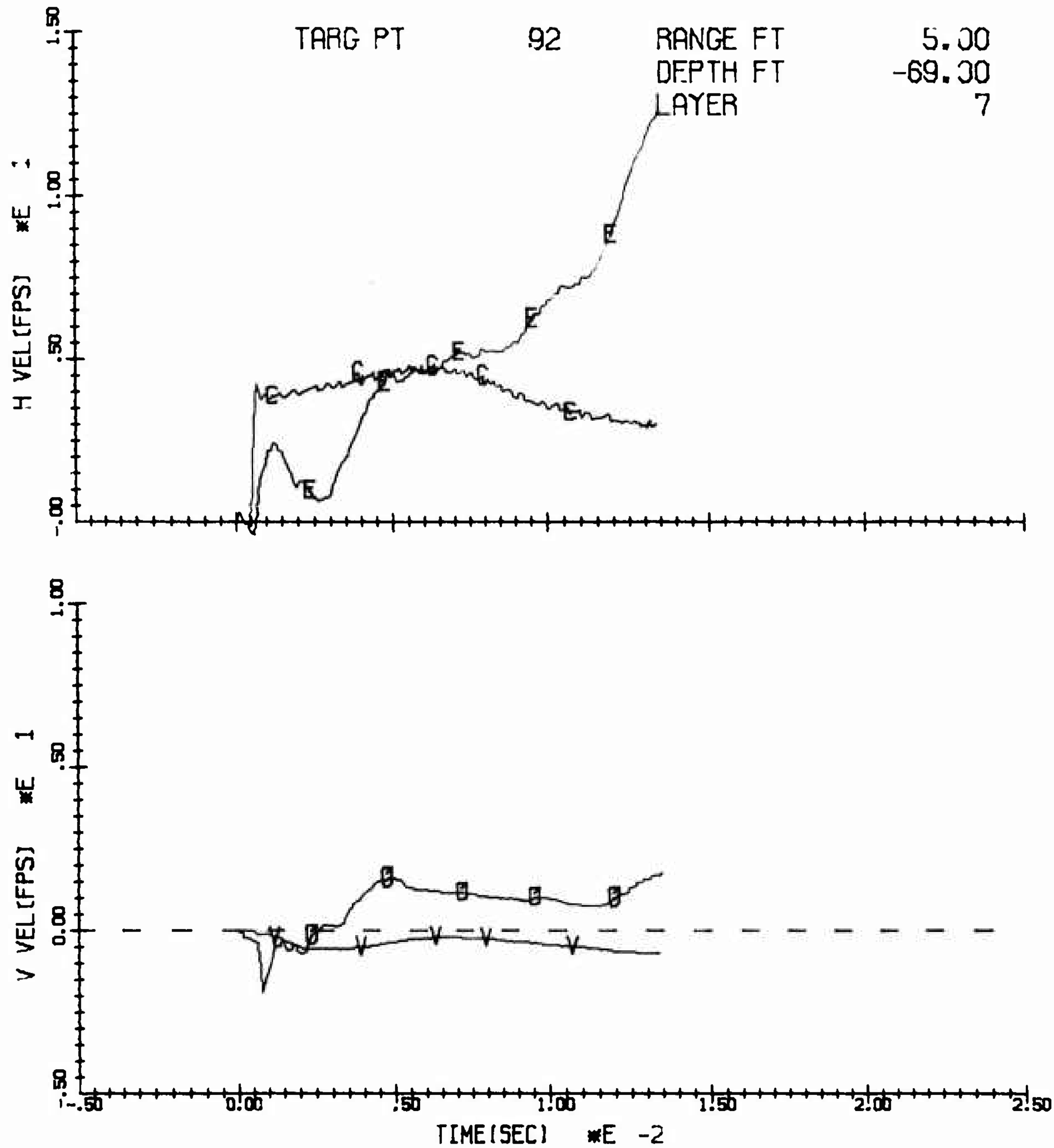

Figure B.16. Comparison of experimental data and AFTON calculation for 5' range and 69' depth in CIST 18D.

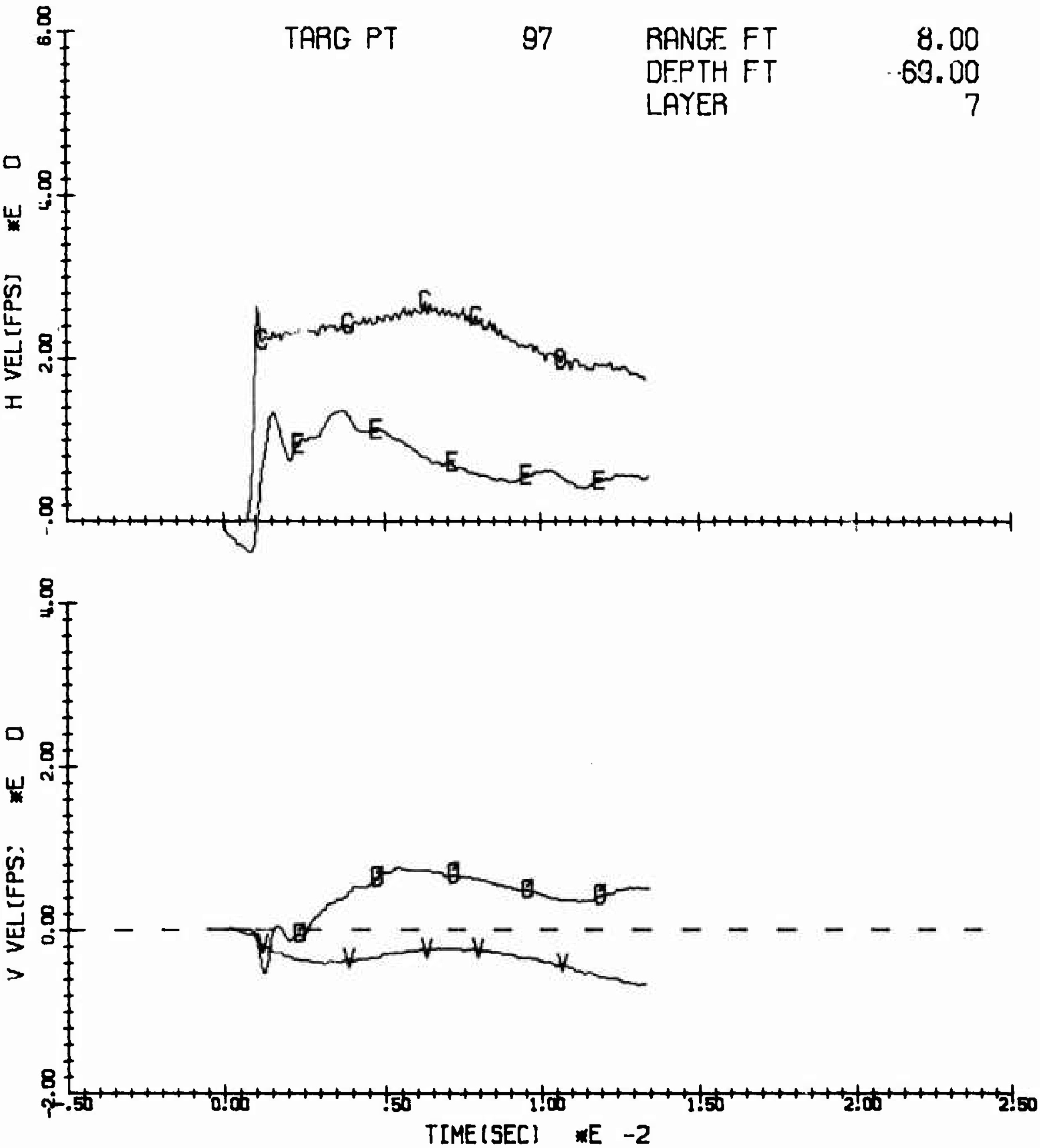

Figure B.17. Comparison of experimental data and AFTON calculation for 8' range and 69' depth in CIST 18D.

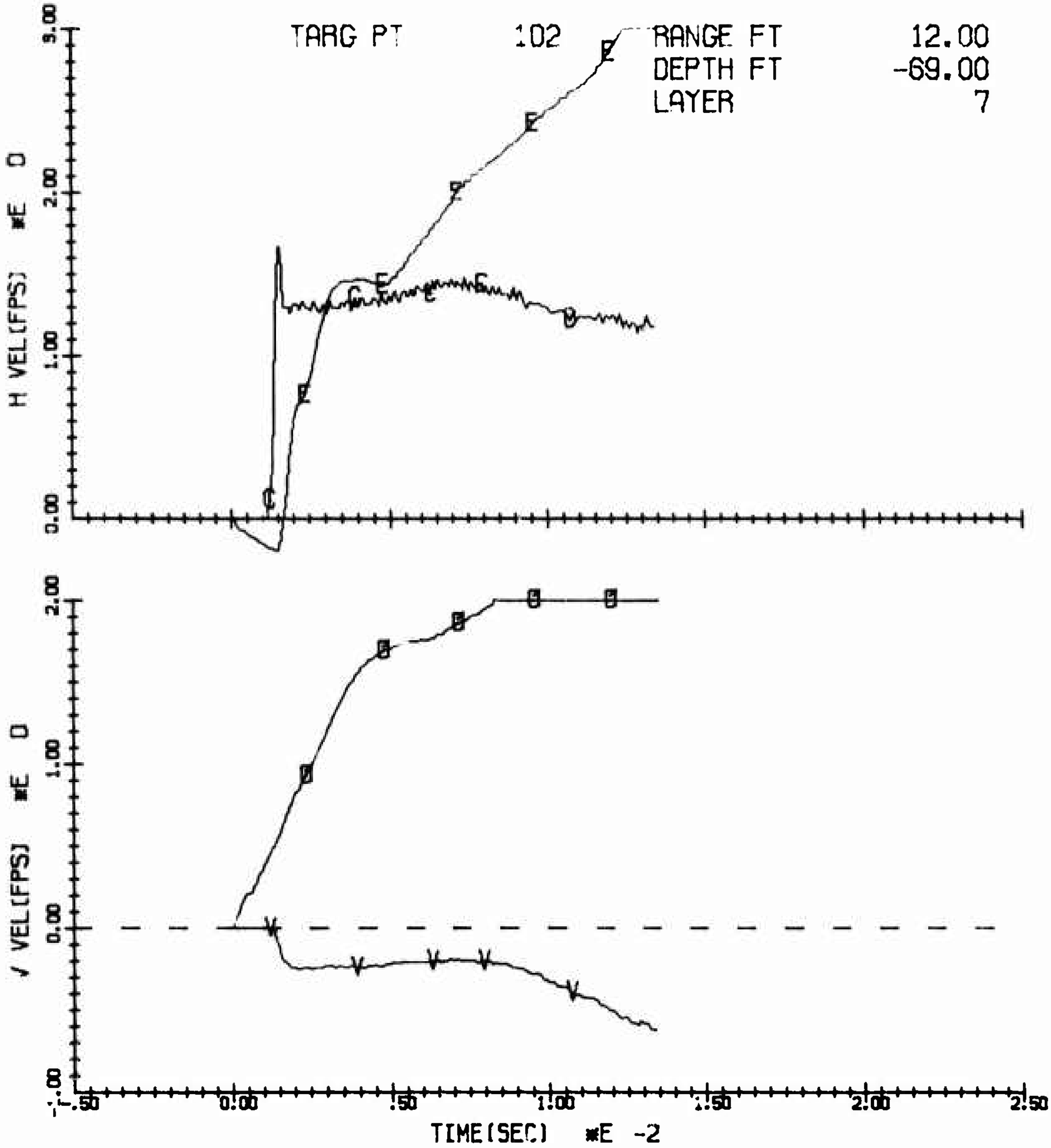

Figure B.18. Comparison of experimental data and AFTON calculation for 12' range and 69' depth in CIST 18D.

DISTRIBUTION LIST

DEPARTMENT OF DEFENSE

Asst. Scy. Def., AE
ATTN: Doc. Control

DDC, Cameron Station
2 cy ATTN: TCA

DDR&E
ATTN: Asst. Dir., Strat. Wpns.

Dir., DIA
ATTN: Lt Col Paul Cavanaugh
ATTN: DIAAP-8B
ATTN: DIAST-3

Director, DNA
ATTN: DDST
2 cy ATTN: TISI
2 cy ATTN: SPSS
3 cy ATTN: TITL

Commander, FCDNA
ATTN: FCPR

OSD, ARPA
ATTN: NMR

DEPARTMENT OF THE ARMY

Director, USA Eng. WW Exp. Station
ATTN: WESRL
ATTN: WESS
ATTN: Dr. J. Zelasko
ATTN: Dr. J. G. Jackson, Jr.
ATTN: Mr. Don Day
ATTN: Mr. Leo Ingram
ATTN: Tech. Library
ATTN: Mr. Paul Hadala
ATTN: Mr. Jim Drake

Dept. Army NIKE-X, Fld. Off.
Bell Tel. Lab
ATTN: AMCPM-NXE-FB

Dept. of the Army
ATTN: Chief of Eng. (ENGMC-EM)

U. S. Army CRREL
ATTN: Scott Blouin

Harry Diamond Laboratories
ATTN: Library

DEPARTMENT OF THE NAVY

NCEL
ATTN: Mr. Jay Algood

Dept. Navy
ATTN: Ofc. Chief Navy Ops.

Dept. Navy (Code 418)
ATTN: Ofc. Navy Rsch.

DEPARTMENT OF THE NAVY (Continued)

Commander, NSWC (Code 730)
ATTN: Naval Research Lab., Tech. Library

NRL (Code 2027)
ATTN: Director

NWO (Code 753)
ATTN: Commander

DEPARTMENT OF THE AIR FORCE

ADC
ATTN: DOA

Air Force Cambridge Rsch. Labs.
ATTN: Dr. Tom Rooney

AFIT, Wright-Patterson AFB
ATTN: Tech. Library, Bldg. 640, Area B
ATTN: DAPD

AFLC, Wright-Patterson AFB
ATTN: DEE

AFSC, Andrews AFB
ATTN: DLSP

AFWL, Kirtland AFB
ATTN: HO
ATTN: DE
ATTN: DY
ATTN: DYC
ATTN: DYP
ATTN: DYE
2 cy ATTN: SUL
2 cy ATTN: DEP
2 cy ATTN: DYM
20 cy ATTN: DES

AU
ATTN: AUL/LDE
ATTN: ED, Dir., Civil Engrg.

HQ USAF
ATTN: RDQSM, 1D425
ATTN: RDQ 5

RADC, Griffis AFB
ATTN: Doc. Library

SAMSO, Norton AFB
ATTN: MNNH, Capt John Kaiser
ATTN: Maj D. Gage

USAF Academy CO
ATTN: DFSLB
ATTN: FJSRL, CC
ATTN: DFCE

OTHER GOVERNMENT AGENCIES

Bureau of Mines, Twin Cities Rsch. Ctr.
ATTN: Dr. T. C. Atchinson

OTHER GOVERNMENT AGENCIES (Continued)

National Aeronautics and Space Administration
AMES Research Center
ATTN: N245-5, Dr. Verne Oberbeck
ATTN: N245-11, Dr. Donald E. Gault

Center of Astrogeology
US Geological Survey
ATTN: R. E. Eggleton
ATTN: H. Masursky
ATTN: J. F. McCauley
ATTN: D. J. Roddy

Department of the Interior, US Geological Survey
ATTN: Daniel J. Milton
ATTN: Richard J. Pike, Jr.
ATTN: Don E. Wilhelms
ATTN: Howard G. Wilshire
ATTN: Cecil B. Raleigh, Earthquake Res. Ctr.
ATTN: John H. Healy

Dept. of Interior
Bureau of Mines
ATTN: Dr. Leonard A. Obert

US Geological Survey, GSA Bldg., Rm. G-26
ATTN: Edward C. T. Chao

DEPARTMENT OF ENERGY

Sandia Laboratories
Livermore Laboratory
ATTN: Doc. Control

Sandia Laboratories
ATTN: Info. Dist. Div.
ATTN: Dr. M. L. Merritt
ATTN: Mr. Carter Broyles
ATTN: Mr. Walt Herrman
ATTN: Mr. Wendel Weart
ATTN: Mr. Al Chabai

Lawrence Livermore Laboratory (Berkeley)
ATTN: Library, Bldg. 50, Rm. 134

University of California
Lawrence Livermore Laboratory
ATTN: Mr. Douglas Stephens
ATTN: Mr. Robert Schock
ATTN: Mark Wilkins

Los Alamos Scientific Laboratory
ATTN: Report Library

Q-51 Los Alamos Scientific Laboratory
University of California (Los Alamos)
ATTN: Thomas R. McGetchin

DEPARTMENT OF DEFENSE CONTRACTORS

Aerospace Corporation
ATTN: Dr. Prem Mather

DEPARTMENT OF DEFENSE CONTRACTORS (Continued)

Aerospace Corporation
ATTN: Mr. Warren Pfefferle
ATTN: Dr. Mason B. Watson

Agbabian Associates
ATTN: Dr. Mike Agbabian

Analytic Services, Inc.
ATTN: George Hesselbacher

Applied Theory, Inc.
ATTN: Dr. J. Trulio

The Boeing Company
ATTN: Mr. Ron Carlson
ATTN: Mr. Bob Pyrdahl

California Institute of Technology
ATTN: Dr. Thomas J. Ahrens
ATTN: Dr. Leon T. Silver

California Research and Technology, Inc.
ATTN: M. Rosenblatt
ATTN: K. Kreyenhagen

Civil Nuclear Systems, Inc.
ATTN: Dr. Robert Crawford

Computer Sciences Corporation
ATTN: Mr. O. A. Israelsen

Merritt CASES, Inc.
ATTN: J. L. Merritt

General American Transportation Corp.
General American Research Division
ATTN: Dr. G. L. Neidhardt, Mgr. of Engr.
ATTN: Dr. Marion J. Balcerzak, Tech. Dir.

IIT Research Institute
ATTN: Tech. Library
ATTN: Peter J. Huck

Institute of Defense Analyses
ATTN: Tech. Info. Off.

Institute of Geophysics and Planetary Physics
ATTN: Orson J. Anderson

Lockheed Missiles and Space Co.
ATTN: Dr. Ronald E. Meyerott, Dept. 50-01, Bldg. 201

Massachusetts Institute of Technology
ATTN: Prof. William F. Brace/ Prof. Eugene Simmons

McDonald Douglas
ATTN: Mr. Ken McClymonds
ATTN: Dr. Joe Logan

Occidental College, Dept. of Geology
ATTN: David Cummings

DEPARTMENT OF DEFENSE CONTRACTORS (Continued)

Pacifica Technology
ATTN: Dr. R. Allen
ATTN: Dr. R. L. Bjork

R & D Associates
ATTN: Dr. Albert Latter
ATTN: Dr. Henry Cooper
ATTN: Dr. Harold L. Brode
ATTN: Mr. Robert Port
ATTN: Mr. John Levesque

Physics International Co.
ATTN: Doc. Control for Dr. Charles Godfrey
ATTN: Doc. Control for Mr. Fred M. Sauer
ATTN: Doc. Control for Mr. Dennis Orphal

Purdue University
ATTN: Mr. William R. Judd

Rand Corporation
ATTN: Dr. C. C. Mow

Research Analysis Corporation
ATTN: Documents Library

Science Applications, Inc.
ATTN: Dr. W. Coleman

Science Applications, Inc.
ATTN: Mr. J. Bratton

Science Applications, Inc.
ATTN: Bill Layson

Science Applications, Inc.
ATTN: Dr. D. Maxwell

Shannon & Wilson, Inc.
ATTN: Mr. Earl Sibley

Southwest Research Institute
ATTN: A. B. Wenzel

Stanford Research Institute
ATTN: Dr. George Abrahamson

Systems, Science, and Software
ATTN: Dr. Ted Cherry
ATTN: Dr. Ronald R. Grine
ATTN: Dr. D. Riney
ATTN: Document Control

DEPARTMENT OF DEFENSE CONTRACTORS (Continued)

Teledyne, Brown Engineering (SETAC)
ATTN: Mr. Manu Patel

Terra Tek, Inc.
ATTN: Dr. H. R. Pratt

TRW Defense and Space Systems Group
ATTN: Mr. Bing Fay
ATTN: Mr. Greg Hulcher

TRW Defense and Space Systems Group
ATTN: Mr. Norm Lipner
ATTN: Dr. Peter K. Dai, R1/2178
ATTN: Dr. Benjamin Sussholtz

University of Illinois
ATTN: Dr. Nathan M. Newmark
ATTN: Dr. Skip Hendron
ATTN: Dr. Bill Hall

University of Oklahoma
Dept. of Info. & Computing Science
ATTN: Dr. John Thompson

University of New Mexico
Civil Engrg. Rsch. Facility
ATTN: Mr. Del Calhoun
ATTN: Mr. D. J. Higgins
ATTN: Dr. Harry Auld

University of Texas
Dept. of Geological Sciences
ATTN: William R. Muehlberger

Virginia Polytechnic Institute
Dept. of Civil Engrg.
ATTN: Dr. C. S. Desai

Weidlinger Associates Consulting Engineers
ATTN: Dr. Melvin L. Baron
ATTN: Ivan Sandler

Weidlinger Associates Consulting Engineers
ATTN: Dr. J. Isenberg

J. H. Wiggins Co.
2 cy ATTN: Dr. Jon Collins

Official Record Copy, DES-G
1 Lt J. D. Shinn